molecules

MDPI

Review

Recent Progress on Low-Temperature Selective Catalytic Reduction of NO_x with Ammonia

Eun Duck Park [1,2]

[1] Department of Energy Systems Research, Ajou University, Suwon 16499, Republic of Korea; edpark@ajou.ac.kr; Tel.: +82-31-219-2384
[2] Department of Chemical Engineering, Ajou University, Suwon 16499, Republic of Korea

Abstract: Selective catalytic reduction of nitrogen oxides (NO_x) with ammonia (NH_3-SCR) has been implemented in response to the regulation of NO_x emissions from stationary and mobile sources above 300 °C. However, the development of NH_3-SCR catalysts active at low temperatures below 200 °C is still needed to improve the energy efficiency and to cope with various fuels. In this review article, recent reports on low-temperature NH_3-SCR catalysts are systematically summarized. The redox property as well as the surface acidity are two main factors that affect the catalytic activity. The strong redox property is beneficial for the low-temperature NH_3-SCR activity but is responsible for N_2O formation. The multiple electron transfer system is more plausible for controlling redox properties. H_2O and SO_x, which are often found with NO_x in flue gas, have a detrimental effect on NH_3-SCR activity, especially at low temperatures. The competitive adsorption of H_2O can be minimized by enhancing the hydrophobic property of the catalyst. Various strategies to improve the resistance to SO_x poisoning are also discussed.

Keywords: low-temperature selective catalytic reduction of NO with NH_3 (NH_3-SCR); catalyst; NO_x reduction; SO_2/H_2O tolerance; transition metal-based catalysts

Citation: Park, E.D. Recent Progress on Low-Temperature Selective Catalytic Reduction of NO_x with Ammonia. *Molecules* **2024**, *29*, 4506. https://doi.org/10.3390/molecules29184506

Academic Editor: György Keglevich

Received: 24 August 2024
Revised: 21 September 2024
Accepted: 21 September 2024
Published: 23 September 2024

1. Introduction

Anthropogenic pollutant emissions increased with human activity until a few decades ago, posing a threat to human well-being. However, over the past few decades, regulations on the emission of these pollutants and the development of technologies to control emissions have had some success in preventing significant pollution. Sulfur oxides (SO_x), nitrogen oxides (NO_x and N_2O), CO, and volatile organic compounds (VOCs) are representative gaseous pollutants that are now strictly regulated [1]. In addition, greenhouse gases, including CO_2 and methane, are currently or will be regulated in the near future, depending on the country.

NO_x, such as nitrogen monoxide (NO) and nitrogen dioxide (NO_2), is formed from a variety of stationary and mobile sources. Fossil fuel-based power plants and internal combustion engine-based transportation vehicles are prime examples of stationary and mobile sources of NO_x emissions, respectively. In any case, thermal NO_x, formed at high temperatures when nitrogen oxidizes with oxygen in the air, is the primary pathway for NO_x emissions. As conventional power plants and internal combustion engine-based vehicles are replaced with renewable energy and electric vehicles, respectively, to cope with the CO_2 emissions problem, the NO_x emissions are expected to continue to decline. Meanwhile, with ammonia gaining much attention as a non-carbon fuel, fuel NO_x, which is formed through the partial oxidation of ammonia, can be another pathway for NO_x emissions in the stationary sources [2–4].

The selective catalytic reduction of NO_x with ammonia (NH_3-SCR) is the most widely adopted method for controlling NO_x emissions from stationary sources among the various

methods developed to date [5,6]. The following reactions occur during NH_3-SCR in the absence of oxygen.

$$6NO + 4NH_3 \rightarrow 5N_2 + 6H_2O \quad (1)$$

$$6NO_2 + 8NH_3 \rightarrow 7N_2 + 12H_2O \quad (2)$$

$$NO + NO_2 + 2NH_3 \rightarrow 2N_2 + 3H_2O \quad (3)$$

In practice, because most flue gases contain varying concentrations of oxygen, the following reactions take place.

$$4NO + 4NH_3 + O_2 \rightarrow 4N_2 + 6H_2O \quad (4)$$

$$2NO + 4NH_3 + 2O_2 \rightarrow 3N_2 + 6H_2O \quad (5)$$

$$2NO_2 + 4NH_3 + O_2 \rightarrow 3N_2 + 6H_2O \quad (6)$$

In addition, ammonia oxidations, shown below, can occur in the presence of oxygen, which is not favorable for NH_3-SCR.

$$4NH_3 + 3O_2 \rightarrow 2N_2 + 6H_2O \quad (7)$$

$$4NH_3 + 5O_2 \rightarrow 4NO + 6H_2O \quad (8)$$

$$4NH_3 + 7O_2 \rightarrow 4NO_2 + 6H_2O \quad (9)$$

$$2NH_3 + 2O_2 \rightarrow N_2O + 3H_2O \quad (10)$$

N_2O can be additionally formed via the following reaction in the presence of the catalyst.

$$4NO + 4NH_3 + 3O_2 \rightarrow 4N_2O + 6H_2O \quad (11)$$

Metal (W and/or Mo) oxides-promoted V_2O_5/TiO_2 is a representative commercial catalyst for NH_3-SCR, achieving high NO_x conversion over a wide operating temperature range of 300–400 °C [7–9]. Because flue gas composition varies depending on the fuel (e.g., coal, biomass, organic wastes, oil, natural gas, etc.), the NH_3-SCR unit is placed in different locations in the flue gas treatment process depending on the process characteristics [10]. Generally, since the flue gas contains fly ash, impurities, and SO_2, the dust removal device (e.g., electrostatic precipitator) and the flue gas desulfurization device can be installed to remove the fly ash and SO_2 in the flue gas, respectively [11]. After these units, additional preheaters are required to raise the flue gas temperature to the proper operating temperature of vanadia-based commercial catalysts because the flue gas temperature is reduced below 200 °C. Therefore, low-temperature NH_3-SCR catalysts need to be developed to eliminate the increased operating cost and an extra capital cost due to these additional preheating units.

To date, a variety of NH_3-SCR catalysts [12–23], including Cu-based [24], Ce-based [25–28], Mn-based [29–31], Ba-based [32], and carbon materials-supported catalysts [33,34], have been studied that are active below 200 °C. Compared with NH_3-SCR catalysts operating at medium and high temperatures, low-temperature NH_3-SCR catalysts are susceptible to poisoning by water vapor and SO_2 in flue gas [19,21]. In particular, SO_2 in flue gas can be catalytically oxidized to form SO_3, which reacts with ammonia and then converts to ammonium salts (NH_4HSO_4 (ABS) and $(NH_4)_2SO_4$ (AS)), which can block the active sites of NH_3-SCR [11,35]. Furthermore, additional side reactions forming N_2O have been observed over these catalysts. Low-temperature NH_3-SCR catalysts capable of solving the above problems have not yet been reported. This review article summarizes recent progress on low-temperature NH_3-SCR catalysis and briefly discusses research directions to address the current obstacles.

2. Low-Temperature NH_3-SCR Catalysts

Vanadia-based catalysts active at moderate temperatures can provide meaningful information about low-temperature NH_3-SCR catalysis. Arnarson et al. [36] proposed a reaction mechanism of 'Standard NH_3-SCR' combining with 'Fast NH_3-SCR' on a $VO_x/TiO_2(001)$ catalyst model (Figure 1). The two cycles shared the same reduction part (A → B → D → E → F → P → R → A in Figure 1) but used NO + O_2 (F → I → M → N → P in Figure 1) and NO_2 (F → G′ → H′ → P in Figure 1) for the re-oxidation process, respectively. They noted that the rate of formation and desorption of H_2O is a decisive factor in the 'Standard NH_3-SCR' reaction at low temperatures and that the reaction of NO_2 with the reduction sites is responsible for accelerating the 'Fast NH_3-SCR' reaction at low temperatures [36].

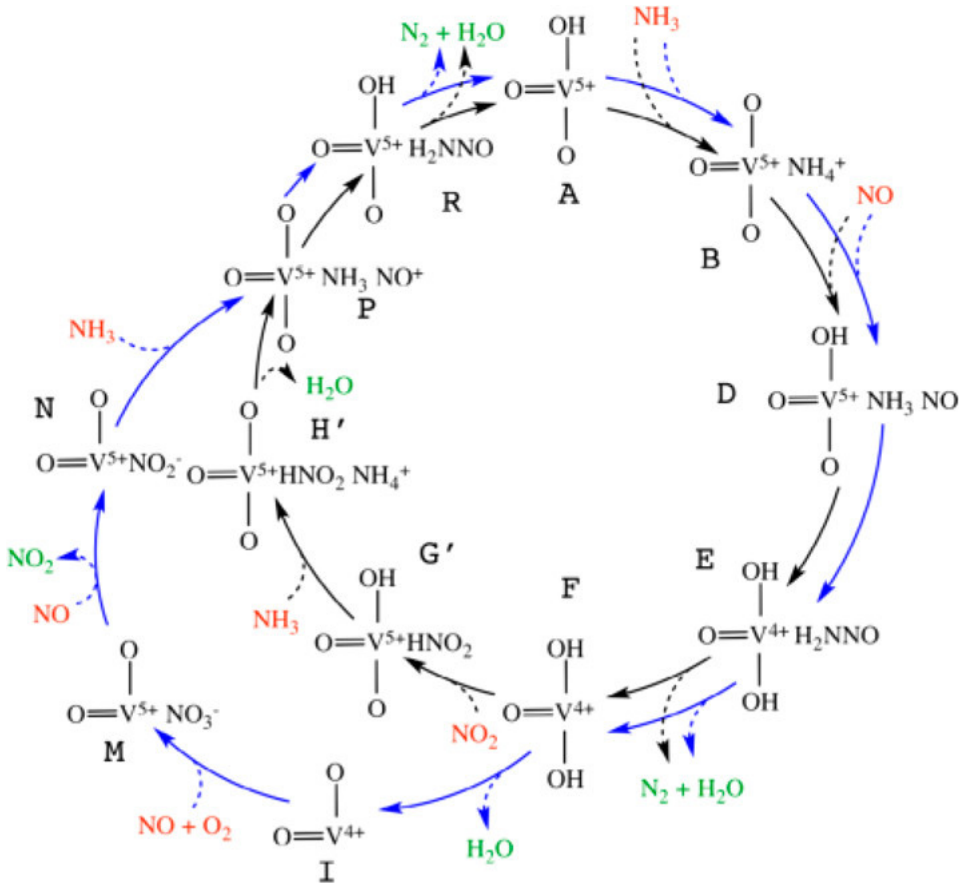

Figure 1. Proposed reaction mechanism over the $VO_x/TiO_2(001)$ model. The black circle represents the 'Fast NH_3-SCR' reaction, and the blue circle represents the NO-activation cycle; the 'Standard NH_3-SCR' reaction is the sum of the black and blue cycles. This schematic diagram is reprinted with permission from ref [36]. Copyright 2017 Elsevier.

The reaction mechanisms [36–38] over V_2O_5/TiO_2 catalyst reveal that NH_3-SCR activity depends on a number of factors, including the redox property of vanadium species between V^{+5} and V^{+4}, Brønsted and Lewis acid sites on the catalyst surface, dispersion of vanadium species, acidic and basic properties of the support, contribution of a support to the redox property of vanadium species, the surface hydrophobicity of the support, the hydrothermal stability of the support, and adsorption property of SO_x. Therefore, these factors should also be considered when designing low-temperature NH_3-SCR catalysts. First of all, the redox properties of the active metal oxides are crucial for this reaction, so Mn, Fe, Co, Cu, and Ce can be selected as promising candidates for the active metal because they have a variety of metal oxides with different oxidation states and are interconvertible under reaction conditions. However, cobalt oxide can be excluded as a promising candidate for this reaction because of its very high activity towards complete oxidation [39].

Therefore, Cu-, Fe-, Mn-, and Ce-based low-temperature NH_3-SCR catalysts are covered in the following sections.

2.1. Cu-Based Catalysts

Cu-containing metal oxides and Cu-based small-pore zeolites have been reported to be active for low- and medium-temperature NH_3-SCR. Various factors, including support, Cu precursor, promoter, crystal structure, preparation method, and interface engineering between Cu and support, have been considered [24]. Research on Cu-based catalysts has been motivated by their high NH_3-SCR activity, especially at low temperatures, but their low SO_2 tolerance is recognized as a significant barrier to field application. Moreover, due to the low hydrothermal stability of Cu-containing metal oxides, recent research has focused on Cu-based small pore zeolites, as shown in Table 1 [40–76]. Among them, low-temperature NH_3-SCR activity was reported over Cu-zeolites such as Cu-LTA [41], Cu-ZSM-5 [42–44], Cu-SSZ-13 [47], Cu-SSZ-16 [49], Cu-SSZ-52 [51], Cu-SAPO-34 [52], Cu-UZM-35 [56], and Cu-ZJM-7 [57], metal-promoted Cu-zeolites such as Ce-Cu-SAPO-18 [59], Fe/Cu-SSZ-13 [62], CuY-SAPO-34 [63], CuNd/SAPO-34, Cu-Ce-La-SSZ-13 [65], and Cu-Ce-USY [68], and other Cu-based oxides such as Cu/ZrO_2 [70] and CuAl layered double oxide (LDO) supported on carbon nanotubes (CNTs) [72].

Table 1. NH_3-SCR activity over some Cu-based catalysts.

Catalysts [1]	Reaction Conditions						NO_x Conversion (%)	Ref.
	NO (ppm)	NH_3 (ppm)	O_2 (vol%)	H_2O (vol%)	Space Velocity	T (°C)		
Cu-LTA	500	500	5	10	100,000 h^{-1}	230–500	>90%	[40]
Cu-LTA	500	500	5	10	100,000 h^{-1}	165–470	>90%	[41]
Cu-ZSM-5	500	575	4	5	30,000 h^{-1}	175–375	>90%	[42]
Cu-ZSM-5	1000	1000	3	-	50,000 h^{-1}	200–375	~100%	[43]
Cu-ZSM-5	500	500	5	10	100,000 h^{-1}	200–400	>90%	[44]
Cu-Beta	1000	1000	6	-	300,000 h^{-1}	250–325	>90%	[45]
Cu/BEA	400	400	8	5	30,300 h^{-1}	225–475	>90%	[46]
Cu-SSZ-13	500	500	10	5	80,000 h^{-1}	160–500	>90%	[47]
Cu-SSZ-13	500	500	5	5	400,000 h^{-1}	210–520	>90%	[48]
Cu-SSZ-16	500	500	10	-	42,500 $mL \cdot h^{-1} \cdot g^{-1}$	190–440	>90%	[49]
Cu-SSZ-39	500	500	5	5	250,000 h^{-1}	225–500	>90%	[50]
Cu-SSZ-52	500	500	5	5	240,000 h^{-1}	200–550	>90%	[51]
Cu-SAPO-34	500	500	6.1	6.4	300,000 h^{-1}	190~500	>90%	[52]
Cu-RTH	500	500	5	10	100,000 h^{-1}	470–750	>90%	[53]
Cu-ERI	300	300	5	3	50,000 h^{-1}	240–500	>90%	[54]
Cu-UZM-9	500	500	5	10	100,000 h^{-1}	250–650	>90%	[55]
Cu-UZM-35	500	500	5	10	100,000 h^{-1}	200–420	>90%	[56]
Cu-ZJM-7	500	500	5	5	80,000 h^{-1}	190~550	>90%	[57]
Cu-SAPO-18	1000	1100	5	10	30,000 h^{-1}	250–500	>90%	[58]
Cu-SAPO-18	500	500	14	5	130,000 h^{-1}	210–540	>80%	[59]
Cu/SSZ-13@SiC	500	500	10	5	80,000 h^{-1}	200–360	>90%	[60]
CuFe/BEA	200	200	10	5	40,000 h^{-1}	225–375	>90%	[61]
Fe/Cu-SSZ-13	500	500	5	-	50,000 h^{-1}	150–500	>90%	[62]
CuY-SAPO-34	350	350	8	5	30,000 h^{-1}	200–310	>90%	[63]
CuNd/SAPO-34	200	200	10	5	40,000 h^{-1}	200–400	>90%	[64]
Cu-Ce-La-SSZ-13	500	500	5	-	150,000 h^{-1}	175–400	>90%	[65]
Ce-Cu-SAPO-18	500	500	14	5	130,000 h^{-1}	250–500	>90%	[66]
La-Cu-SAPO-18	500	500	5	-	20,000 $mL \cdot h^{-1} \cdot g^{-1}$	250~450	>90%	[67]
La-Cu-SAPO-18	500	500	14	5	130,000 h^{-1}	210–580	>80%	[59]
Ce-Cu-SAPO-18	500	500	14	5	130,000 h^{-1}	200–600	>90%	[59]
Nd-Cu-SAPO-18	500	500	14	5	130,000 h^{-1}	250–550	>90%	[59]
Gd-Cu-SAPO-18	500	500	14	5	130,000 h^{-1}	300–460	>90%	[59]

Table 1. *Cont.*

Catalysts [1]	Reaction Conditions						NO_x Conversion (%)	Ref.
	NO (ppm)	NH_3 (ppm)	O_2 (vol%)	H_2O (vol%)	Space Velocity	T (°C)		
Tb-Cu-SAPO-18	500	500	14	5	130,000 h^{-1}	220–570	>90%	[59]
Ho-Cu-SAPO-18	500	500	14	5	130,000 h^{-1}	250–550	>90%	[59]
Lu-Cu-SAPO-18	500	500	14	5	130,000 h^{-1}	250–520	>90%	[59]
Cu-Ce-USY	500	500	5	-	48,000 h^{-1}	180~250	>90%	[68]
CuO(111)/TiO_2	500	500	5	-	45,000 h^{-1}	235–285	>90%	[69]
Cu/ZrO_2	600	600	10	5	58,333 h^{-1}	200–360	>90%	[70]
$LaCuO_{3-x}$/meso-Al_2O_3	500	500	3	10	100,000 h^{-1}	220–275	>50%	[71]
CuAl-(LDO)/(CNTs)	600	600	5	-	45,000 h^{-1}	176–275	>90%	[72]
meso-Cu-SSZ-13@meso-Al-Si	500	500	5	5	400,000 h^{-1}	250–520	>90%	[73]
Cu-SAPO-34@Fe-MOR	500	500	5	-	50,000 h^{-1}	375–525	>90%	[74]
Cu-SSZ13@$Ce_{0.75}Zr_{0.25}O_2$	500	500	5	-	60,000 h^{-1}	220–480	>90%	[75]
Cu-SSZ-13 HN	500	500	3	-	120,000 h^{-1}	200~550	>90%	[76]

[1] LDO: layered double oxide; USY: ultrastable Y; CNTs: carbon nanotubes; meso: mesoporous; Al-Si: aluminosilicate; HN: hollow nanocube.

Only a few reports can be found on Cu-containing metal oxides in the last few years. Chen et al. [69] examined the crystal-plane effects of CuO over CuO/TiO_2 catalysts on NH_3-SCR and reported that the proportion of Cu^+ and surface-adsorbed oxygen (O_α) in CuO(111)/TiO_2 catalyst was higher than that of CuO(001)/TiO_2 catalyst, which could facilitate the NH_3-SCR reactions. Liu et al. [71] reported that $LaCuO_{3-x}$/meso-Al_2O_3 enriched with Cu^{3+} species exhibited significantly higher catalytic activity for NH_3-SCR than CuO/meso-Al_2O_3 counterpart in the low temperature range (100–280 °C), which was attributed to the unique nature of Cu^{3+} species, which had more acid sites and higher redox properties to promote the adsorption and activation of ammonia and NO_x.

Cu-containing zeolites have been intensively studied for NH_3-SCR and/or urea-SCR for their applications to stationary and mobile sources [57,77,78]. The NH_3-SCR performance of Cu-exchanged zeolite catalysts depends on the amount of isolated copper ion sites, SiO_2/Al_2O_3 ratios, and topological structures. The isolated Cu^{2+} species serve as redox sources, the zeolite supplies acidic sites, and the channel structure affects the diffusion of reactants, intermediates, and products. A variety of zeolite catalysts for Fe or Cu ion exchange have been developed, all of which exhibit a wide temperature window, including ZSM-5, SAPO-18, SAPO-34, SSZ-13, SSZ-16, SSZ-39, AFX, BEA, ERI, KFI, LTA, Nu-3, PST-7, RHO, RTH, Sigma-1, UZM-35, etc. [78–83]. In terms of the hydrothermal stability, ion-exchanged small-pore zeolites such as Cu-SSZ-13, Cu-SSZ 16, Cu-SSZ-39, Cu-SAPO-18, Cu-SAPO-34, and Cu-KFI are superior to the medium-pore ZSM-5 zeolite catalysts, and finally, Cu-SSZ-13 catalysts have been commercialized for NO_x control in diesel-powered vehicles owing to their outstanding NO_x removal efficiency and hydrothermal stability [77,79,84]. A comparison of the NH_3-SCR activity of Cu- and Fe-zeolites showed that at low temperatures (below 350 °C), the former was more active than the latter, but above 350 °C, the latter was more active than the former, which was ascribed to the fact that Cu-zeolites had higher adsorption sites for NH_3 than Fe-zeolites [85].

The reaction mechanism over Cu-SSZ-13 is shown in Figure 2 [86]. A mobile NH_3-complex, monomeric Cu ion was identified to be active in the NO_x reduction cycle in the redox mechanism. The Cu^+ ion complexes thus formed subsequently migrate between the zeolite cages to form dimeric species that are important for O_2 activation, which is the rate-limiting step essential for the re-oxidation of Cu^+ to complete the catalytic cycle [87]. Density functional theory (DFT) calculations on a reaction mechanism for low-temperature NH_3-SCR over Cu-CHA reveal that ammonia-solvated Cu cations, $Cu(NH_3)_2^+$, are responsible for O_2 activation as well as the formation of the key intermediates HO-NO and H_2N-NO and that Brønsted acid site is related to decomposition of HO-NO and H_2N-NO to N_2 and H_2O [88]. Oxygen activation requires pairs of $Cu(NH_3)_2^+$ complexes, but HO-NO and H_3N-NO coupling may occur on single complexes [88].

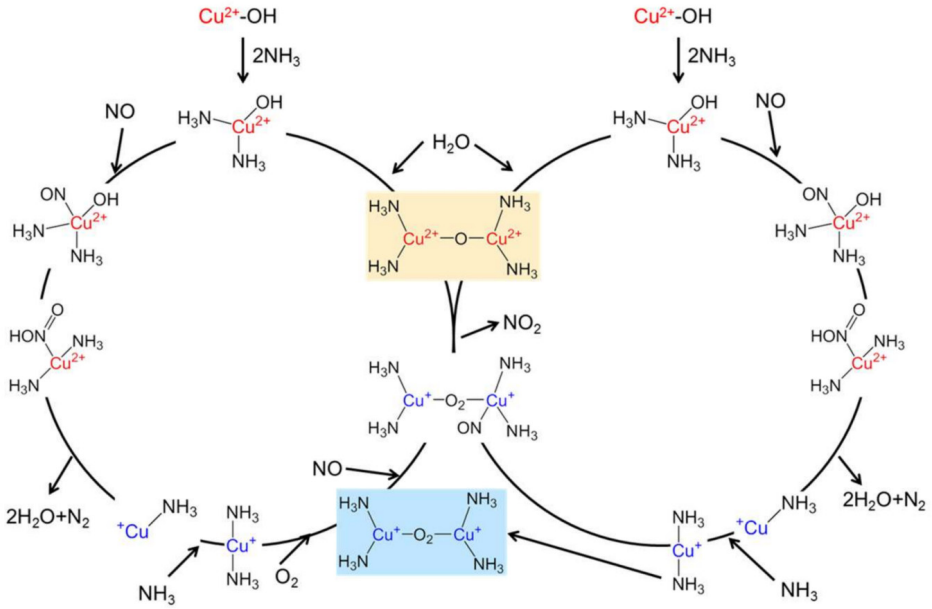

Figure 2. Complete redox cycling mechanism for low-temperature standard NH_3-SCR derived from DFT calculations that involves two Cu(I) centers in the initiation of the oxidation half-cycle [87]. Adapted from permission from [86]. Copyright 2017, American Chemical Society.

Catalyst deactivation in the presence of SO_x in the flue gas can be classified into two categories. One is irreversible deactivation due to the formation of inactive Cu sulfate species through interaction between SO_x and active Cu species [89–95]. The other is reversible deactivation resulting from the deposition of sulfate species (e.g., ABS and AS) [96]. SO_2 poisoning inhibits the oxidation of NO to NO_2, resulting in a lower NH_3-SCR activity below 350 °C [79]. Above this temperature, sulfate compounds are unstable so that the available Cu sites can be sufficient for NH_3-SCR activity [79]. Therefore, sulfur poisoning beyond 350 °C is insignificant. Table 2 summarizes the effects of H_2O and SO_2 on the NH_3-SCR over some Cu-based catalysts [97–109]. Among them, CuO@Cu-metal organic frameworks (MOFs) core-shell catalyst [101] and Cu-doped phosphomolybdic acid catalyst [106] showed a relatively stable catalytic performance even in the presence of H_2O and SO_2 at low temperatures.

Table 2. NH_3-SCR activity in the presence of H_2O and/or SO_2 over some Cu-based catalysts.

Catalysts [1]	Reaction Conditions						NO_x Conversion (%)	Effects of H_2O/SO_2	Ref
	NO (ppm)	NH_3 (ppm)	O_2 (vol%)	H_2O (vol%)	Space Velocity	T (°C)			
Cu-SAPO-18	500	500	14	5	130,000 h^{-1}	200–550	>80%	Reversible inhibition with 5% H_2O and 100 ppm SO_2 at 300 °C	[97]
Cu-Ce-SAPO-18	500	500	14	5	130,000 h^{-1}	200–600	>90%	Reversible inhibition with 5% H_2O and 100 ppm SO_2 at 300 °C	[97]
Cu/TNU-9	500	500	5	10	10,000 h^{-1}	237–400	>90%	Stable NO_x conversion with 10% H_2O and 100 ppm SO_2 at 250 °C	[98]
Cu–Ce/TNU-9	500	500	5	10	10,000 h^{-1}	225–400	>90%	Stable NO_x conversion with 10% H_2O and 100 ppm SO_2 at 250 °C	[98]
Cu–Ce–La/TNU-9	500	500	5	10	10,000 h^{-1}	200–425	>90%	Stable NO_x conversion with 10% H_2O and 100 ppm SO_2 at 250 °C	[98]
Mn-Ce/Cu-SSZ-13	500	500	3	3	50,000 h^{-1}	125–450	>90%	Reversible inhibition with 3% H_2O and 100 ppm SO_2 at 300 °C	[99]

Table 2. *Cont.*

Catalysts [1]	Reaction Conditions						NO_x Conversion (%)	Effects of H_2O/SO_2	Ref
	NO (ppm)	NH_3 (ppm)	O_2 (vol%)	H_2O (vol%)	Space Velocity	T (°C)			
$CuSbTiO_x$	700	700	4	4	60,000 h^{-1}	250–300	>85%	Slowly deactivated with 5% H_2O and 150 ppm SO_2 at 250 °C	[100]
$CuO@Cu_3(BTC)_2$	600	600	4	-	60,000 h^{-1}	180–240	>80%	Stable NO_x conversion with 4% H_2O and 150 ppm SO_2 at 200 °C	[101]
$Cu_{0.5}Ce_{0.5}W_5O_x$	500	500	5	-	36,000 h^{-1}	270–390	~100%	Stable NO_x conversion with 5% H_2O and 50 ppm SO_2 at 240 °C	[102]
$WO_x/Cu\text{-}CeO_2$	500	500	5	-	60,000 h^{-1}	220–400	>90%	Stable NO_x conversion with 10% H_2O and 100 ppm SO_2 at 250 °C	[103]
$Nb_{0.05}CuCeTi$	600	600	3	5	40,000 h^{-1}	160–360	>90%	Reversible inhibition with 5% H_2O and 50 ppm SO_2 at 250 °C	[104]
$CuCeNbO_x$	600	600	5	-	108,000 h^{-1}	185–360	>90%	Stable NO_x conversion with 5% H_2O and 100 ppm SO_2 at 250 °C	[105]
$Cu–HPMo/TiO_2$	500	500	8	-	15,000 h^{-1}	150–350	>80%	100% NO_x conversion with 4% H_2O and 2 00 ppm SO_2 at 200 °C	[106]
Cu–Ce–La/SSZ-13	500	500	5	3	150,000 h^{-1}	210–450	>90%	Stable NO_x conversion with 10% H_2O and 100 ppm SO_2 at 300 °C	[107]
$Cu/(ZSM\text{-}5@CeO_2)$	1000	1000	8	5	50,000 h^{-1}	225–550	>95%	Stable NO_x conversion with 5% H_2O and 200 ppm SO_2 at 275 °C	[108]
Cu–Ce–La/SSZ-13@ZSM-5	500	500	5	3	150,000 h^{-1}	200–450	>80%	Stable NO_x conversion with 10% H_2O and 100 ppm SO_2 at 300 °C	[107]
Cu-SSZ-13@Ce-MnO_x/MS	500	500	5	3	150,000 h^{-1}	175–475	>90%	Relatively stable NO_x conversion with 10% H_2O and 100 ppm SO_2 at 250 °C	[109]

[1] BTC: 1,3,5-Benzenetricarboxylic acid; MS: mesoporous silica.

Hammershøi et al. [89] reported that the NH_3-SCR activity over Cu-SSZ-13 catalysts was significantly inhibited at 160–350 °C after exposure to SO_2, but preserved above 350 °C. Jangjou et al. [110] compared SO_2-induced catalyst deactivation at $[Cu^{II}OH]^+$ and Cu^{2+} sites in Cu-SSZ-13. For Cu^{2+} sites, the NH_3-SCR activity was inhibited due to the formation of ammonium sulfate, which could be fully recovered by regeneration at >380 °C. This implies that Cu^{2+} sites do not adsorb sulfur during the exposure to SO_2 [110]. On the other hand, $[Cu^{II}OH]^+$ sites could adsorb sulfur directly to form Cu bisulfite, causing the irreversible deactivation [110]. Therefore, the sulfur poisoning of $[Cu^{II}OH]^+$ was much more severe than that of Cu^{2+}. H_2SO_4 formed in the presence of SO_2 and H_2O plays an important role in the formation of ammonium sulfate [111,112]. Another route to the formation of Cu bisulfate is the interaction between SO_2 and CuO_x nanoclusters [113].

The effect of SO_2 on Cu-SAPO-34 deactivation was also investigated [91,114]. The NH_3-SCR activity of sulfur-poisoned Cu-SAPO-34 was decreased significantly at 100–500 °C, though sulfur accumulation and zeolite structure collapse were not observed [114]. The deactivation was attributed to the decreased amount of isolated Cu^{2+} ions [91,114]. It was speculated that sulfur poisoning could hinder the copper redox transformation (between Cu^{II} and Cu^{I}) in Cu-SAPO-34, which led to the sulfation of Cu sites [115]. In addition, Cu-SAPO-34 favored the formation of stable $Al_2(SO_4)_3$ species compared with Cu-SSZ-13, resulting in an irrecoverable loss in NH_3-SCR activity [111].

When screening Cu-containing zeolite catalysts, hydrothermal stability has become an important selection criterion in addition to high NO_x conversion over a wide range of reaction temperatures for application in transport vehicles, but this is not as important

for low-temperature NH_3-SCR catalysts for application in stationary sources. Rather, resistance to water and SO_2 at low temperatures is an additional factor to be considered in the development of NH_3-SCR catalysts. In order to improve the low-temperature NH_3-SCR activity of Cu-containing zeolite catalysts, the Cu active sites can be modified by introducing the heteroatoms to facilitate the redox property of Cu and metal oxides to accelerate NO oxidation for 'Fast NH_3-SCR' [116]. Other zeolites with different structures, including AEI and LTA, the small-pore intergrown zeolites, including AFX/CHA and CHA/AEI, and the zeolite morphology can be further examined even though they were excluded because of their poor hydrothermal stability at high temperatures [116]. Additional doping of Y [63] and lanthanides [59–64] to Cu-zeolites was reported to be effective for NH_3-SCR. The composite catalysts such as MnO_2-CeO_2/Cu/SSZ-13 showed excellent NH_3-SCR activity and N_2 selectivity in the temperature ranges of 125 to 450 °C because more active monodentate nitrate was formed on the surface of the composite catalyst compared with Cu/SSZ-13 alone [99].

Chen et al. [107] synthesized a core–shell structure Cu–Ce–La/SSZ-13@ZSM-5 catalyst by a self-assembly method and applied it to NH_3-SCR. They observed that Cu–Ce–La/SSZ-13@ZSM-5 with an appropriate shell thickness presented better NH_3-SCR activity and hydrothermal stability than Cu–Ce–La/SSZ-13 because some metal ions were transferred and redistributed during the assembly of the ZSM-5 shell, resulting in the conversion of $[Cu(OH)]^+$–Z to Cu^{2+}–2Z species and the functionalization of the shell phase, which was beneficial for the adsorption and activation of NH_3. Chen et al. [109] synthesized a multi-functional core-shell catalyst with Cu-SSZ-13 as the core phase and Ce-MnO_x supported mesoporous silica as the shell phase via self-assembly and impregnation. The core-shell catalyst exhibited excellent low-temperature activity, SO_2 tolerance, and hydrothermal stability compared with the Cu-SSZ-13 [109]. The Ce-MnO_x species dispersed in the shell can rapidly activate NO and oxidize it to NO_2, which allows the NH_3-SCR reaction on the core-shell catalyst to be initiated in the shell phase [109]. Meanwhile, Ce-MnO_x species can react preferentially with SO_2 as sacrifice components, effectively avoiding the sulfur inactivation of the copper active sites [109]. This catalyst showed relatively stable NO conversion in the presence of 10% H_2O and 100 ppm SO_2 at 250 °C [109]. It is noteworthy that few low-temperature Cu-based catalysts with high resistance to H_2O and SO_2 poisoning have been reported.

2.2. Fe-Based Catalysts

Various Fe-based catalysts, including single iron oxides, Fe-containing mixed metal oxides, supported iron oxides, supported Fe-containing multicomponent metal oxides, and Fe-containing zeolites, have been reported for NH_3-SCR due to their excellent redox properties and low cost. Another advantage of Fe-based catalysts is their relatively good resistance to water and SO_2, although this has only been reported at temperatures above 200 °C [11].

γ-Fe_2O_3 has been mainly reported for NH_3-SCR among various single-phase Fe_2O_3 with different crystalline structures (e.g., α, β, γ, and ε) [11]. Yu et al. [117] proposed two different reaction mechanisms over γ-Fe_2O_3 (Figure 3). One is the Langmuir–Hinshelwood (L–H) mechanism in which NH_3 and NO are adsorbed on the active sites, Fe^{3+}-OH and Fe^{3+}=O, respectively, and reacted to form N_2 and H_2O, which is prevalent at temperatures below 300 °C [117]. The other is the Eley–Rideal (E–R) mechanism in which NH_3 is first chemisorbed on Fe^{3+}-OH to form Fe^{3+}-$O^{-\cdots}$ H-N^+H_3, which can be further reacted with gaseous NO to produce N_2 and H_2O, which is the main pathway at high temperatures above 300 °C [117]. In any case, this reaction requires the cooperation of acidic sites and redox properties. They also confirmed that the NH_3-SCR activity decreased firstly and then increased slowly after the introduction of SO_2 at temperatures ranging from 225 to 275 °C [117]. This was ascribed to the formation of iron sulfate species inhibiting the adsorption of NO_x, thus interfering with the L–H reaction pathway [117]. On the other

hand, the iron sulfate species formed enhanced the surface acidity, which promoted the E–R reaction pathway and further promoted NH_3-SCR activity [117].

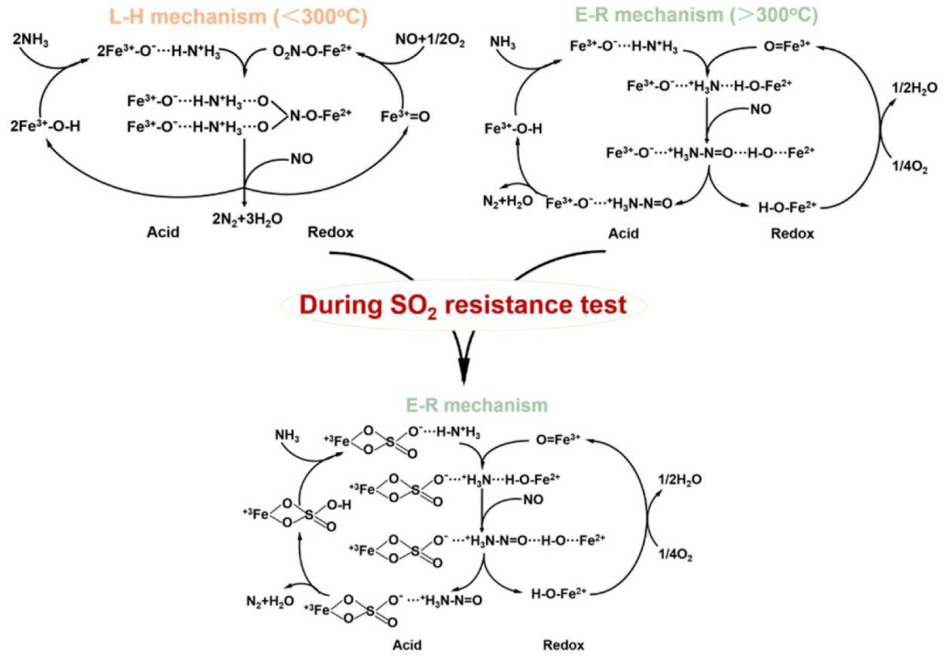

Figure 3. The proposed reaction mechanism before and during the SO_2 resistance test on the γ-Fe_2O_3 catalyst [117]. Adapted from permission from ref [117]. Copyright 2021 Elsevier.

Recent work on single Fe oxides has focused on how to increase the low-temperature NH_3-SCR activity. Qin et al. [118] prepared various Fe_3O_4 nanostructures exposed with different crystal planes from MIL-100(Fe) as the Fe precursor and found that the catalysts with more (1 1 1) had better NH_3-SCR performance than those with (1 0 0) exposure, which they attributed to the preferential exposure of the Fe_3O_4 (1 1 1) crystal faces leading to higher adsorbed oxygen concentration and surface acidity. Yang et al. [119] found through DFT calculations that the 'Fast NH_3-SCR' reaction was the dominant pathway for the NH_3-SCR reaction on Fe_2-N_6 catalysts, with the energy barrier of the rate-determining step (HONO formation) being 1.00 eV, much lower than that of other NH_3-SCR catalysts, enabling excellent low-temperature activity in the temperature window of 300–500 K. Zhang et al. [120] prepared a highly defective α-Fe_2O_3 with enhanced acid (Lewis and Brønsted) and redox properties on homoatomic dinuclear sites comprising more positively charged Fe^{3+} and oxygen vacancy-coupled Fe^{2+} ions. The catalyst showed enhanced NH_3-SCR activity at low temperatures without the addition of other acid transition metals and showed resistance to poisoning of H_2O and SO_2 due to the large amount of Brønsted acid [120].

Various metal oxide-promoted iron oxides have been investigated to enhance the co-operation of surface acidity and redox property to facilitate the low-temperature NH_3-SCR. The positive effects of Mn [121], Nb [122], Mo [123], Ce [124], Sm [125], and W [123,126–128] in promoted iron oxides on the catalytic activity have been reported. Table 3 summarizes the effects of H_2O and SO_2 on the NH_3-SCR over some Fe-based catalysts [120,121,124,125,128–137]. Among them, a relatively stable catalytic performance was observed over Mn-Fe oxides [121] even in the presence of H_2O and SO_2 at low temperatures.

Table 3. NH_3-SCR activity in the presence of H_2O and/or SO_2 over some Fe-based catalysts.

Catalysts	Reaction Conditions						NO_x Conversion (%)	Effects of H_2O/SO_2	Ref.
	NO (ppm)	NH_3 (ppm)	O_2 (vol%)	H_2O (vol%)	Space Velocity	T (°C)			
Defective α-Fe_2O_3	500	500	5.3	-	50,000 h^{-1}	250–300	~100%	100% NO_x conversion with 5% H_2O and 50 ppm SO_2 at 300 °C	[120]
$MnFeO_x$	500	500	5	5	75,000 h^{-1}	75–275	~100%	A rather stable NO_x conversion with 5% H_2O and 50 ppm SO_2 at 100 °C	[121]
Ce/α-Fe_2O_3	500	500	5	5	90,000 h^{-1}	175–325	>95%	Stable NO_x conversion wit 5% H_2O and 200 ppm SO_2 at 250 °C	[124]
Fe–Ce/TiO_2	1000	1000	3	-	30,000 h^{-1}	175–350	>90%	Slowly deactivated with 500 ppm SO_2 at 250 °C	[129]
$Mo_{0.4}Ce_{0.3}FeO_x$	2000	2000	8	-	32,000 h^{-1}	200–350	>95%	Stable NO_x conversion with 10% H_2O and 200 ppm SO_2 at 250 °C	[130]
Fe–Ce–W oxides	450	450	2.5	5	20,000 h^{-1}	250–500	>90%	Relatively stable NO_x conversion with 5% H_2O and 200 ppm SO_2 at 350 °C	[131]
Sm/Fe_2O_3	500	500	5	5	14,400 h^{-1}	175–350	~100%	Stable NO_x conversion with 5% H_2O and 100 ppm SO_2 at 275 °C	[125]
WO_x/Fe_2O_3	500	500	5	-	50,000 h^{-1}	300–425	>90%	Stable NO_x conversion with 100 ppm SO_2 at 300 °C	[128]
$H_3PW_{12}O_{40}$-Fe_2O_3	1000	1100	6	-	13,200 h^{-1}	300–500	>90%	Stable NO_x conversion with 10% H_2O and 200 ppm SO_2 at 280 °C	[132]
Mn-W-Sb modified siderite	500	500	5	-	30,000 h^{-1}	175–375	>90%	Irreversible deactivation with 5% H_2O and 100 ppm SO_2 at 210 °C	[133]
Fe_2O_3-promoted halloysite-supported CeO_2-WO_3	500	500	5	-	40,000 h^{-1}	275–420	>95%	Relatively stable NO_x conversion with 8% H_2O and 100 ppm SO_2 at 300 °C	[134]
Fe_2O_3-CeO_2@Al_2O_3	500	500	5	-	20,000 $mL{\cdot}g^{-1}{\cdot}h^{-1}$	250–430	>90%	Stable NO_x conversion with 10% H_2O and 500 ppm SO_2 at 270 °C	[135]
Fe-ZSM-5@CeO_2	500	500	5	-	177,000 h^{-1}	250–425	>90%	Stable NO_x conversion with 10% H_2O and 100 ppm SO_2 at 350 °C	[136]
Fe-Beta@CeO_2	500	500	3	5	50,000 h^{-1}	225–575	>90%	Stable NO_x conversion with 5% H_2O and 100 ppm SO_2 at 300 °C	[137]

It is noteworthy that, except for catalysts containing additional Mn, few Fe-based catalysts are active for NH_3-SCR at low temperatures (<200 °C) while being resistant to H_2O and SO_2 poisoning. Jiang et al. [138] prepared a phosphotungstic acid (HPW)-promoted Fe-based catalyst from MIL-100(Fe) as the Fe precursor by hydrothermal method and reported that active oxygen species-rich γ-Fe_2O_3 was the main Fe phase, which enhanced NO adsorption and activation, leading to faster NH_3-SCR. The role of HPW was to increase the total acidic sites along with promoting the reactivity of NH_3 adsorbed on Lewis acidic sites at low temperatures. Notably, WO_3-promoted Fe_2O_3 was reported to have a wide temperature window and excellent water and sulfur resistance, showing relatively stable NO conversion in the presence of 100 ppm SO_2 at 300 °C [128]. The roles of WO_3 are known to inhibit the crystallization of the Fe_2O_3 phase and formation of inactive nitrate, instead increasing Lewis acid sites and appropriate redox properties [127,128]. A kind of composite catalyst, HPW-decorated ring-like Fe_2O_3 synthesized via mechanical-chemistry grinding of HPW and Fe_2O_3 nanorings prepared by a microwave-assisted hydrothermal method, showed good NH_3-SCR performance over a wide temperature window of 250–500 °C [139] and an outstanding resistance against SO_2, showing relatively stable NO conversion in the presence of 10% H_2O and 200 ppm SO_2 at 280 °C [132]. Sun et al. [125] reported that Sm modification could weaken the sulfation of active Fe sites in Sm-doped Fe_2O_3,

which was also supported by the DFT calculation results that SO_2 could be more easily adsorbed on the Sm/Fe_2O_3 catalyst with the adsorption sites located at the Sm atom and its neighboring Fe atoms. They observed that more reactive nitrate species were formed on the sulfated Sm/Fe_2O_3 catalyst due to the presence of more un-sulfated Fe sites, which they explained as making the Sm/Fe_2O_3 catalyst resistant to SO_2 poisoning, showing relatively stable NO conversion in the presence of 5% H_2O and 100 ppm SO_2 at 275 °C [125]. Tan et al. [140] reported that the low-temperature (<250 °C) NH_3-SCR activity of $FeTiO_x$ catalyst could be dramatically enhanced by CeO_2 doping, which can be attributed to the presence of a unique Ce-O-Fe structure that contributes to the improvement of redox properties. Chen et al. [124] prepared a single-atom Ce-modified α-Fe_2O_3 catalyst by a citric acid-assisted sol–gel method and reported that a high NO conversion was maintained in the presence of 5% H_2O and 200 ppm SO_2 at 250 °C. They claimed that the atomic dispersion of the Ce species to maximize the amounts of Fe–O–Ce sites in the Ce-doped FeO_x catalyst was critical because the formation of oxygen vacancies in the Fe–O–Ce sites, which could promote the oxidation of NO to NO_2 and decomposition of ABS, was more favorable than that in the Fe–O–Fe sites in the Ce-free α-Fe_2O_3 catalyst [124]. Ma et al. [141] compared a serial of $Cu_{0.02}Fe_{0.2}Ce_yTi_{1-y}O_x$ catalysts prepared by the sol–gel method and found that $Cu_{0.02}Fe_{0.2}Ce_{0.2}Ti_{0.8}O_x$ exhibited superior low-temperature NH_3-SCR performance in the presence and absence of water, which they attributed to the optimal distribution of surface acidity, enhanced surface oxygen content, and surface redox cycle ($Ce^{4+} + Fe^{2+} \rightarrow Ce^{3+} + Fe^{3+}$). Yao et al. [133] prepared Mn-W-Sb modified siderite catalysts by impregnation method and found that the Mn-doping enhanced adsorbed NO_2 formation by synergistic catalysis with Fe^{3+} and that the addition of Sb inhibited sulfate formation on the surface of the catalyst in the presence of SO_2 and H_2O, showing relatively stable NO conversion in the presence of 5% H_2O and 100 ppm SO_2 at 210 °C. Xu et al. [121] prepared various $MnFeO_x$ catalysts with different molar ratios and observed high low-temperature NH_3-SCR activity. The Mn–Fe-0.2 (Mn/Fe = 0.2) catalyst presented excellent SO_2/H_2O tolerance, showing a rather stable NO_x conversion even in the presence of 5% H_2O and 50 ppm SO_2 at 100 °C [121]. Doping Mn not only inhibited the phase transformation of iron oxide (Fe_2O_3) but also strengthened the interaction between MnO_x and Fe_2O_3 due to the electron transfer between them, which led to the formation of Mn–O–Fe [121]. Bai et al. [142] prepared an amorphous metal oxide (FeO_x-$Mn_{0.1}O_y$) with a large surface area, sufficient oxygen vacancies, and excellent redox properties and observed high adsorption and activation capacities for O_2 and NO, which further enhanced the catalytic activity at low temperatures (90–240 °C). The incorporation of Mn into the FeO_x species suppressed the crystallization of hematite, further increasing the surface area and surface acid sites [142]. In addition, the incorporation of manganese increased the number of oxygen vacancies, which decreased the apparent activation energy of hematite and enhanced the redox properties of the amorphous FeO_x-MnO_y catalyst [142].

The mesoporous Fe-doped CeO_2 catalyst after modifying organic sulfate functional groups showed excellent activity in a temperature range of 250–450 °C, which was ascribed to the strong electron interaction between Fe^{3+}-O-Ce^{4+} species and sulfate groups, which modifies the acidity and redox properties of the catalyst [143]. Wang et al. [144] prepared a series of sulfated modified Fe–Ce composite oxide $Fe_{1-x}Ce_xO_\delta$-S catalysts and reported that the $Fe_{0.79}Ce_{0.21}O_\delta$-S catalyst achieved the low-temperature NH_3-SCR activity at temperatures of 175–375 °C. They claimed that sulfation formed a large amount of sulfate on the catalyst surface and provided abundant Brønsted acid sites, which enhances NH_3 adsorption capacity and improves overall NO_x conversion efficiency [144]. The introduction of Ce was the main determinant to control the low-temperature activity of the catalyst by modulating its redox ability, and they found that there was a strong interaction between Fe and Ce in the $Fe_{0.79}Ce_{0.21}O_\delta$-S catalyst, which changed the electron density around the Fe ions, which weakened the strength of the Fe–O bond and improved the lattice oxygen mobility of the catalyst [144]. In addition, during the reaction, the Fe-Ce composite oxide

catalyst showed higher surface lattice oxygen activity and a faster bulk lattice oxygen replenishment rate [144].

The support of the supported iron oxide can increase the dispersion of the iron oxide, providing high surface active sites per mass of iron oxide, provide additional surface acid sites on the support itself and at the interface between the support and the iron oxide, and improve the redox properties of the iron oxide. Different crystal planes of the support (e.g., TiO_2 [145] and CeO_2 [146]) of supported iron oxides were compared. Monolayer Fe_2O_3 supported on TiO_2 nanosheets exhibited a better low-temperature NH_3-SCR activity than that supported on TiO_2 nanospindles because the former had more acidic sites, oxygen defects, and reactive oxygen species [145]. The iron oxides supported on CeO_2 nanorods achieved higher catalytic activity for NH_3-SCR than those supported on CeO_2 nanopolyhedra, which was explained by the DFT calculation results that the Fe_2O_3/CeO_2 {110} catalyst was more reactive to NO and NH_3 than the Fe_2O_3/CeO_2 {110} [146]. The Fe_2O_3{1 1 3}-TiO_2 exhibited superior NO_x removal capacity and a broader temperature operating range than Fe_2O_3{0 1 2}-TiO_2 and Fe_2O_3{0 1 4}-TiO_2, which can be attributed to the improved redox properties, as well as the presence of additional active oxygen species, surface acid sites, and adsorbed nitrate species on the Fe_2O_3{1 1 3}-TiO_2 catalyst [147].

2.3. Mn-Based Catalysts

Mn-based catalysts, including MnO_x, Mn-containing mixed metal oxides, supported MnO_x, and supported Mn-containing multicomponent metal oxides, have been regarded as the promising low-temperature NH_3-SCR catalysts [30,148–150]. A comparison of the low-temperature NH_3-SCR activity between various transition metal oxides supported on TiO_2 showed that it decreased in the following order: Mn > Cu $\geq$ Cr >> Co. > Fe >> V >> Ni [151]. First-principles calculations also revealed that the superior oxidative dehydrogenation performance of Mn-based catalysts to NH_3 lowered the energy barrier for the activation of NH_3 and reduced the formation of the key intermediate NH_2NO, the rate-determining step in NH_3-SCR, over Mn-, Fe-, and Ce-based oxide catalysts [152].

Among various single-phase manganese oxides, including MnO_2, Mn_5O_8, Mn_2O_3, Mn_3O_4, and MnO, MnO_2, and Mn_2O_3 were reported to have the highest low-temperature activity per unit surface area and N_2 selectivity, respectively [153]. The crystallinity and valence state of MnO_x affected by the preparation method and pretreatment conditions have been reported to influence the NH_3-SCR performance [154]. Higher low-temperature NH_3-SCR activity was obtained for the less crystalline MnO_x [155,156]. A comparison of β-MnO_2 and α-Mn_2O_3 showed that the former had a higher NO_x conversion and N_2O production rate per unit surface area than the latter, which was explained by the lower Mn–O bond energy of β-MnO_2, which promoted the activation of NH_3 [157]. The birnessite-type MnO_2 catalyst, prepared from $Mn(NO_3)_2{\cdot}4H_2O$, having the fewest OH groups, was reported to exhibit the best catalytic activity and excellent SO_2 resistance among the same-type catalysts prepared from different Mn precursors [158].

A novel synthetic method was applied to prepare high-surface-area manganese oxide with low crystallinity for this reaction. Mesoporous α-MnO_2 nanosheets prepared by a solvent-free synthetic method had a high surface area and a mesopore size of 4 nm with large oxygen vacancies and showed 100% NO_x conversion under a gas hourly space velocity (GHSV) of 700,000 h^{-1} at 100 °C [159]. Xu et al. [160] prepared MnO_x catalysts with 3D structure by the hard-template method using KIT-6 as a template possessing high reducibility with abundant surface oxygen species and Mn^{4+} species and reported that more Lewis acid sites and Brønsted acid sites on the surface were beneficial for the adsorption and activation of NH_3, leading to the higher NH_3-SCR activity. Chen et al. [161] synthesized a novel MnO_x catalyst with a large surface area, small particle size, and more crystalline defects from MOF-$Mn_3(BTC)_2(H_2O)_6$ using different amounts of polyvinyl pyrrolidone (PVP) and found that this catalyst had abundant acid sites, Mn^{4+}, and surface chemical oxygen, promoting the NH_3-SCR reaction. Moreover, the high SO_2 tolerance was also observed because an irreversible sulfurization rate was reduced and an adsorption

of active bidentate nitrates and NH_4^+ was promoted even in the coexistence of sulfates, showing relatively stable NO conversion in the presence of 50 ppm SO_2 at 175 °C. Zhang et al. [162] also prepared various MnO_x catalysts from MOF-74 under different pretreatment conditions and reported that their redox capability could be controlled by changing the ratio of Mn^{4+}/Mn^{n+} and $O_\alpha/(O_\alpha + O_\beta)$, resulting in the promotion of the adsorption and oxidation of NO to facilitate the 'Fast NH_3-SCR' reaction. Zhou et al. [163] prepared hydrothermally stable MnO_x/Al_2O_3 catalysts with highly dispersed low-coordinated Mn active sites that were originally created with triethanolamine and observed excellent low-temperature NH_3-SCR activity because of active low-coordinated Mn species possessing reactive redox sites and Lewis acid sites.

Li et al. [164] employed DFT calculations for the reaction mechanism of NH_3-SCR over Mn/γ-Al_2O_3 catalyst. NH_3 is mainly adsorbed on the Lewis acid sites and forms coordinated NH_3. Subsequently, an N–H bond in the adsorbed NH_3 can be dissociated to form NH_2*, which can react with the gaseous NO and generate NH_2NO*. NH_2NO* was finally decomposed into N_2* and H_2O* (Figure 4). On the surface of the Mn/γ-Al_2O_3 catalyst, the adsorbed O_2 was decomposed into the active oxygen atoms, which could oxidize NO into NO_2. Among three possible routes for N_2O formation, such as NO decomposition, deep dehydrogenation of NH_3, and two-step dehydrogenation of NH_2NO, the deep dehydrogenation of NH_3 appears to be mainly responsible over the Mn/γ-Al_2O_3 catalyst in both the L–H and E–R reaction mechanisms.

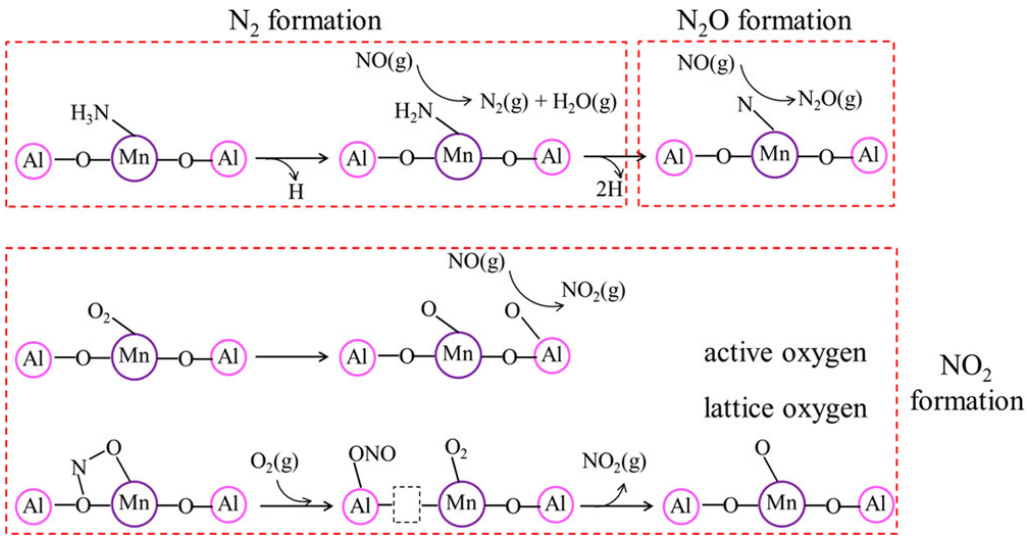

Figure 4. The reaction mechanism of NH_3-SCR on the Mn/γ-Al_2O_3 catalyst calculated by Li et al. [164] Reproduced from ref [164]. Copyright 2019 American Chemical Society.

The formation of N_2O over Mn-based catalysts was systematically examined over MnO_x-TiO_2 catalysts with different Mn/Ti ratios [165]. As the Mn/Ti ratio increased, the MnO_x species layer expanded on TiO_2 support, leading to an increase of redox sites but a decrease of surface acid sites, contributing to the non-selective oxidation of NH_3 on MnO_x species and the over-activation of NH_3 at the Mn-Ti interface and resulting in the formation of N_2O. Yang et al. [166] proposed the scheme for N_2O formation according to the L–H and E–R mechanisms, in which monodentate $–NO_3^-$ (and NH_4NO_3*) and –NH are key intermediates for N_2O formation, respectively (Figure 5). DFT calculations and thermodynamic/kinetic analysis of NH_3-SCR over α-MnO_2 with specific (100), (110) and (310) exposure planes showed that the α-MnO_2 catalyst exposed with the (310) plane exhibited the best NH_3-SCR catalytic performance and the highest N_2 selectivity due to the low energy barrier of NH_3 dehydrogenation and NH_2NO generation and the difficulty of NH_2 dissociation [167].

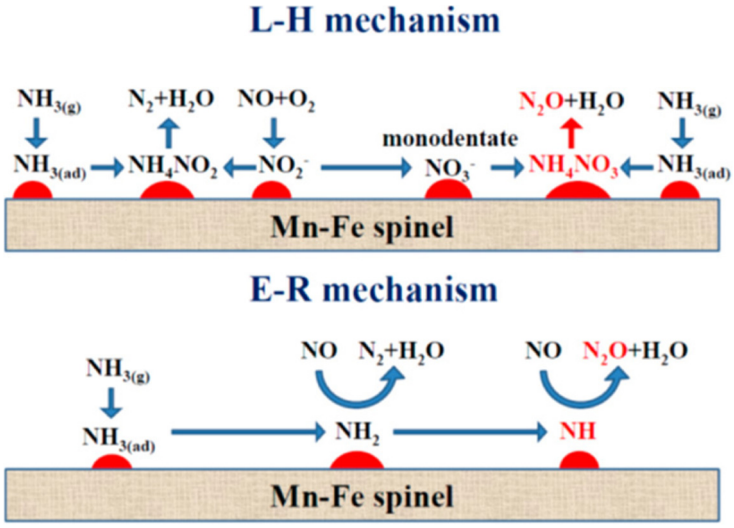

Figure 5. Proposed N_2O formation mechanisms over Mn–Fe spinel. This schematic diagram is reprinted with permission from ref [166]. Copyright 2014 American Chemical Society.

Although manganese oxides exhibit high NH_3-SCR activity at low temperatures, their application in practical processes is limited due to their sensitivity to SO_2 and low N_2 selectivity [21,168]. Therefore, Mn-containing mixed metal oxides and supported Mn-containing metal oxides have been adopted to address these issues. For Mn-containing mixed metal oxides, various second metals including Al [169], Si [170], Ti [171], V [172], Cr [173], Fe [174–178], Co [179–182], Ni [183], Cu [184,185], Y [186], Zr [187], Nb [188], Mo [189–191], Ag [192,193], Sn [194], Sb [195], La [196,197], Ce [197–204], Pr [205], Nd [206], Sm [207–209], Eu [210], Gd [211], Dy [212,213], Ho [214], Er [215], Tm [216], Ta [217], W [218,219], and Bi [220] have been examined. The effects of H_2O and SO_2 on the NH_3-SCR activity over unsupported Mn-based catalysts, supported Mn-based catalysts, and core-shell Mn-based catalysts are summarized in Table 4 [161,173,194,220–262], Table 5 [171,187,189,195,212,215,263–292], and Table 6 [293–308], respectively. Among them, a relatively stable catalytic performance was observed over unsupported Mn-based oxides such as Mn oxides [161], Mn-Cr oxides [173,223], Mn-Fe oxides [224], Mn-Fe-Co oxides [225], Mn-Fe-Mg oxides [226], Mn-Fe-Al oxides [227], Mn-Co oxides [230,232–234], Mn-Co-Ce oxides [235], Mn-Co-V oxides [236], Mn-Ni oxides [235,238,239], Mn-Ni-Al oxides [240], Mn-Ni-Fe oxides [244], Mn-Ni-Ce oxides [235], Mn-Zr-Ti oxides [246], Mn-Ce oxides [248,249], Mn-Ce-Ti oxides [250–252], Mn-Ce-Sn oxides [248], Mn-Sm-Ti oxides [255,256], Mn-Sm-Fe oxides [257], Mn-Sm-Zr-Ti oxides [258], Mn-Sm-Ce-Ti oxides [259], Mn-Nd oxides [206], Mn-Gd oxides [261], Mn-W-Ce oxides [262], and Bi-Mn oxides [220], and supported Mn-based catalysts such as Mn/Fe-Ti spinel [263], Mn/CeO_2-ZrO_2 [266], Mn/CeO_2-ZrO_2-Al_2O_3 [267], TiO_2-MnO_x/CeO_2-ZrO_2 [171], Fe-Mn/TiO_2 [270], Zr-Mn/attapulgite [273], Ce-Mn-V-W/TiO_2 [277], Nd-Mn/TiO_2 [278], Ho-Fe-Mn/TiO_2 [215], Gd-MnO_x/ZSM-5 [212], $NiMnO_x$/activated coke [283], La-Mn-Fe/activated coke [284], Mn/biochar (BC) [285], Zr-Mn/BC [286], MnCe/Granular activated carbon (AC)-carbon nanotubes (CNTs) [291], and MnO_x-CeO_2/graphene [292], and Mn-based core-shell catalysts such as MnO_x@Eu-CeO_x [300], Mn-titanium nanotubes@Ce [303], and Fe_2O_3@MnO_x@carbon nanotube (CNT) [306] even in the presence of H_2O and SO_2 at low temperatures.

Table 4. NH_3-SCR activity in the presence of H_2O and/or SO_2 over some unsupported Mn-based catalysts.

Catalysts [1]	Reaction Conditions						NO_x Conversion (%)	Effects of H_2O/SO_2	Ref.
	NO (ppm)	NH_3 (ppm)	O_2 (vol%)	H_2O (vol%)	Space Velocity	T (°C)			
MnO_x	500	500	5	-	140,000 h^{-1}	125–200	>90%	Relatively stable NO_x conversion with 50 ppm SO_2 at 175 °C	[161]
MnO_x-SiO_2	1000	1000	10	-	24,000 h^{-1}	150–225	>90%	Relatively stable NO_x conversion with 100 ppm SO_2 at 225 °C	[221]
Mn-TiO_x	500	500	5	-	100,000 h^{-1}	160–370	>90%	Relatively stable NO_x conversion with 5% H_2O at 140 °C. Relatively stable NO_x conversion with 100 ppm SO_2 at 260 °C.	[222]
Cr-MnO_x	1000	1000	3	-	30,000 h^{-1}	115–220	>90%	Reversible inhibition with 100 ppm SO_2 at 120 °C	[223]
$CrMn_2O_4$ spinel	500	500	5	-	32,000 h^{-1}	80–225	>90%	Relatively stable NO conversion with 10% H_2O and 150 ppm SO_2 at 200 °C	[173]
MnO_x-Fe	1000	1000	3	5	30,000 h^{-1}	93–220	>90%	Relatively stable NO conversion with 5% H_2O and 100 ppm SO_2 at 200 °C	[224]
MnFeCo-LDO	550	550	5	-	30,600 h^{-1}	63–400	>90%	Stable NO conversion with 5% H_2O and 100 ppm SO_2 at 120 °C	[225]
Mn-Fe-Mg oxides	1000	1000	4	-	30,000 h^{-1}	125–200	>90%	Stable NO_x conversions with 3% H_2O and 100 ppm SO_2 at 150 °C	[226]
Mn-Fe-Al oxides	500	500	5	-	60,000 h^{-1}	110–250	>90%	Stable NO_x conversions with 100 ppm SO_2 at 150 °C	[227]
Mn-Fe-Ce oxides	500	500	11	-	36,000 h^{-1}	180–277	>90%	Stable NO_x conversions with 100 ppm SO_2 at 225 °C	[228]
Mesoporous Mn-Fe-Ce-Ti oxides	600	480	2	-	24,000 h^{-1}	210–395	>90%	Reversible inhibition with 300 ppm SO_2 at 240 °C	[229]
$Mn_2Co_1O_x$	1000	1000	5	-	30,000 h^{-1}	150–325	>90%	Reversible inhibition with 10% H_2O and 100 ppm SO_2 at 200 °C	[230]
Mn-Co oxides	500	500	5	-	23,000 h^{-1}	100–300	>90%	Reversible inhibition with 8% H_2O at 120 °C	[231]
Mn-Co oxides	500	500	3	-	30,000 h^{-1}	100–280	>90%	Stable NO_x conversions with 5% H_2O and 100 ppm SO_2 at 160 °C	[232]
Mn-Co oxides	500	500	5	-	140,000 h^{-1}	80–200	>90%	Stable NO_x conversions with 5% H_2O and 50 ppm SO_2 at 125 °C	[233]
Mn-Co oxides	500	500	5	-	50,000 h^{-1}	60–300	>90%	Reversible inhibition with 5% H_2O and 100 ppm SO_2 at 200 °C	[234]
$Co_1Mn_4Ce_5O_x$	500	500	5	-	48,000 h^{-1}	80–175	>90%	Relatively stable NO_x conversion with 10% H_2O and 150 ppm SO_2 and at 175 °C	[235]
$MnCoVO_x$	500	500	5	-	60,000 $mL \cdot g^{-1} \cdot h^{-1}$	175–425	>90%	Relatively stable NO conversion with 5% H_2O and 100 ppm SO_2 at 200 °C	[236]
Mn-Ni oxides	550	550	5	-	64,000 h^{-1}	105–275	>90%	Stable NO_x conversion with 100 ppm SO_2 at 230 °C	[237]

Table 4. *Cont.*

Catalysts [1]	Reaction Conditions						NO_x Conversion (%)	Effects of H_2O/SO_2	Ref.
	NO (ppm)	NH_3 (ppm)	O_2 (vol%)	H_2O (vol%)	Space Velocity	T (°C)			
$NiMn_2O_4$	500	500	5	-	32,000 h^{-1}	73–250	>98%	Stable NO_x conversions in the presence of 150 ppm SO_2 at 175 °C	[238]
$Ni_1Mn_4O_5$	500	500	5	-	48,000 h^{-1}	125–200	>90%	Relatively stable NO_x conversion with 10% H_2O and 150 ppm SO_2 at 175 °C	[235]
$Ni_1Mn_2O_4$-S	500	500	5	-	68,000 h^{-1}	90–230	>90%	Relatively stable NO_x conversion with 5% H_2O and 100 ppm SO_2 at 150 °C	[239]
$Ni_1Mn_{0.5}Al_{0.5}O_x$	500	500	5	5	60,000 h^{-1}	100–250	>90%	Relatively stable NO conversion with 5% H_2O and 100 ppm SO_2 at 200 °C	[240]
$Ni_{a-x}Mn_xAlO_y$	500	500	6.5	5	45,000 h^{-1}	120–225	>90%	Deactivation with 5% H_2O and 100 ppm SO_2 at 210 °C	[241]
Mn-Ni-Ti oxides	500	500	5	-	40,000 h^{-1}	320–460	>90%	Relatively stable NO_x conversion with 10% H_2O and 100 ppm SO_2 at 400 °C	[242]
Mn-Ni-Ti oxides	1000	1000	3	-	40,000 h^{-1}	190–360	~100%	Relatively stable NO_x conversion with 15% H_2O and 100 ppm SO_2 at 240 °C	[243]
$Ni_{0.5}Mn_{0.5}Fe_{0.5}O_x$	500	500	5	-	60,000 h^{-1}	100–300	>80%	Relatively stable NO_x conversion with 5% H_2O and 100 ppm SO_2 at 200 °C	[244]
Mn-Zr oxides	1000	1000	3	-	30,000 h^{-1}	100–200	~100%	Reversible deactivation with 5% H_2O and 100ppm SO_2 at 150 °C	[245]
Mn-Zr-Ti oxides	650	650	5	-	36,000 h^{-1}	160–300	>90%	Relatively stable NO_x conversion with 3% H_2O and 50 ppm SO_2 at 180 °C	[246]
$Mn_2Nb_1O_x$	500	500	5	-	50,000 h^{-1}	120–200	>90%	Irreversible deactivation with 100 ppm SO_2 at 200 °C	[247]
Mn-Ce oxides	1000	1000	2	-	35,000 h^{-1}	100–300	>80%	Relatively stable NO_x conversion with 12% H_2O and 100 ppm SO_2 at 110 °C	[248]
Mn-Ce oxides	3000	3000	15	-	60,000 $mL{\cdot}g^{-1}{\cdot}h^{-1}$	100–250	>80%	Deactivation with 5% H_2O and 100 ppm SO_2 at 175 °C	[206]
Mn-Ce nanowire aerogel	500	500	5	-	32,000 h^{-1}	100–400	>90%	Stable NO_x conversion with 10% H_2O and 250 ppm SO_2 at 150 °C	[249]
Ce-Ti/MnO_2	600	600	6	-	40,000 h^{-1}	100–225	>95%	Relatively stable NO_x conversion with 10 vol% H_2O and 50 ppm SO_2 at 150 °C	[250]
Mn–Ce–Ti oxides	500	500	5	-	14,400 h^{-1}	170–320	>90%	Stable NO conversion with 5 vol% H_2O and 100 ppm SO_2 at 200 °C	[251]
Mn-Ce-Ti oxides	500	500	5	-	64,000 h^{-1}	150–350	>90%	Stable NO conversion with 5 vol% H_2O and 50 ppm SO_2 at 200 °C	[252]
Mn-Sn-Ce oxides	1000	1000	2	-	35,000 h^{-1}	75–250	>90%	Stable NO conversion with 9% H_2O and 100 ppm SO_2 at 220 °C	[194]
Mn-Sn-Ce oxides	1000	1000	2	-	35,000 h^{-1}	75–225	~100%	Relatively stable NO_x conversion with 12% H_2O and 100 ppm SO_2 at 110 °C	[248]
Mn-Sn−Ce oxides	500	500	5	-	60,000 $mL{\cdot}g^{-1}{\cdot}h^{-1}$	175–275	>60%	Stable NO conversion with 5% H_2O and 100 ppm SO_2 at 250 °C	[253]
Mn-Pr-Ce oxides	600	600	5	-	108,000 h^{-1}	150–400	>80%	Stable NO conversion with 5% H_2O and 100 ppm SO_2 at 250 °C	[205]

Table 4. *Cont.*

Catalysts [1]	Reaction Conditions						NO_x Conversion (%)	Effects of H_2O/SO_2	Ref.
	NO (ppm)	NH_3 (ppm)	O_2 (vol%)	H_2O (vol%)	Space Velocity	T (°C)			
Mn-Sm oxides	500	500	5	-	48,600 h^{-1}	50–250	>90%	Stable NO conversion with 2% H_2O and 100 ppm SO_2 at 250 °C	[254]
Mn-Sm oxides	500	500	5	-	60,000 $mL{\cdot}g^{-1}{\cdot}h^{-1}$	200–325	>80%	Deactivation with 5% H_2O and 100 ppm SO_2 at 175 °C	[206]
Mn-Sm-Ti oxides	500	500	5	-	36,000 h^{-1}	150–300	>90%	Stable NO conversion with 5% H_2O and 100 ppm SO_2 at 200 °C	[255]
Mn-Sm-Ti oxides	500	500	5	-	50,000 h^{-1}	75–230	>90%	Stable NOx conversion with 5% H_2O and 100 ppm SO_2 at 100 °C	[256]
Mn-Sm-Fe oxides	500	500	5	-	60,000 h^{-1}	75–200	~100%	Relatively stable NO_x conversion with 5% H_2O and 100 ppm SO_2 at 200 °C	[257]
Mn-Sm-Zr-Ti oxides	500	500	5	-	30,000 h^{-1}	125–275	~100%	Relatively stable NO_x conversion with 2.5% H_2O and 100 ppm SO_2 at 200 °C	[258]
Mn-Sm-Ce-Ti oxides	500	500	5	-	80,000 h^{-1}	150–400	>90%	Relatively stable NO conversion with 5% H_2O and 200 ppm SO_2 at 200 °C	[259]
Mn-Nd oxides	500	500	5	-	60,000 $mL{\cdot}g^{-1}{\cdot}h^{-1}$	125–230	>90%	Relatively stable NO conversion 5% H_2O and 100 ppm SO_2 at 175 °C	[206]
Mn-Eu oxides	600	600	5	-	108,000 h^{-1}	130–400	~100%	Relatively stable NO conversion with 5% H_2O and 100 ppm SO_2 at 350 °C	[260]
Mn-Eu-Ce oxides	500	500	10	10	60,000 h^{-1}	100–250	>90%	Stable NO_x conversions with 10% H_2O and 50 ppm SO_2 at 230 °C	[210]
Mn-Gd oxides	500	500	5	-	100,000 h^{-1}	120–330	~100%	Stable NO_x conversions with 100 ppm SO_2 at 200 °C	[261]
Mn-W-Ce oxides ($W_{0.1}Mn_{0.4}Ce_{0.5}$)	500	500	5	-	300,000 h^{-1}	150–270	>90%	Stable NO_x conversions with 60 ppm SO_2 at 175 °C	[262]
$BiMnO_3$	1000	1000	5	-	10,000 h^{-1}	160–250	>80%	Relatively stable NO_x conversions with 5% H_2O and 100 ppm SO_2 at 140 °C	[220]

[1] LDO: layered double oxide.

Table 5. NH_3-SCR activity in the presence of H_2O and/or SO_2 over some supported Mn-based catalysts.

Catalysts [1]	Reaction Conditions					NO_x Conversion (%)	Effects of H_2O and SO_2	Ref.
	NO (ppm)	NH_3 (ppm)	O_2 (vol%)	Space Velocity	T (°C)			
Mn/Fe-Ti spinel	500	500	2	24,000 $mL{\cdot}g^{-1}{\cdot}h^{-1}$	150–250	>95%	Stable NO_x conversion with 8% H_2O and 60 ppm SO_2 at 200 °C	[263]
Mn/ZrO_2-TiO_2	500	500	4	35,000 h^{-1}	175–350	>97%	Irreversible deactivation with 10% H_2O and 200 ppm SO_2 at 200 °C	[264]
Mn/CeO_2-TiO_2	200	220	8	60,000 h^{-1}	180–250	>90%	Deactivation with 6% H_2O and 100 ppm SO_2 at 180 °C	[265]
Mn/CeO_2-ZrO_2	600	660	6	45,000 h^{-1}	120–220	>90%	Stable NO_x conversion with 3% H_2O and 100 ppm SO_2 at 180 °C	[266]
Mn/CeO_2-ZrO_2-Al_2O_3	1000	1000	5	10,000 h^{-1}	150–300	>90%	Relatively stable NO_x conversion with 10% H_2O and 100 ppm SO_2 at 200 °C	[267]
$MnO_x(0.25)/CoSn_3Al$-LDO	500	500	5	30,000 h^{-1}	100–350	>95%	Irreversible deactivation with 5% H_2O and 150 ppm SO_2 at 200 °C	[268]

Table 5. *Cont.*

Catalysts [1]	Reaction Conditions					NO_x Conversion (%)	Effects of H_2O and SO_2	Ref.
	NO (ppm)	NH_3 (ppm)	O_2 (vol%)	Space Velocity	T (°C)			
$MnCrO_x$/Sepiolite	1000	1000	5	45,000 h^{-1}	125–340	>90%	Relatively stable NO_x conversion with 200 ppm SO_2 at 220 °C	[269]
TiO_2-MnO_x/CeO_2-ZrO_2	500	500	5	60,000 $mL{\cdot}g^{-1}{\cdot}h^{-1}$	175–225	>90%	Relatively stable NO_x conversion with 5% H_2O and 100 ppm SO_2 at 200 °C	[171]
Fe-Mn/TiO_2	1000	1000	10	30,000 h^{-1}	100–330	>90%	Stable NO_x conversion with 100 ppm SO_2 at 125 °C	[270]
Fe-Mn/Ti-Zr	1000	1000	4	30,000 h^{-1}	80–180	>90%	Deactivation with 6% H_2O and 100 ppm SO_2 at 150 °C	[187]
Fe-Mn-Ce/TiO_2	600	600	3	50,000 h^{-1}	155–260	>90%	Stable NO_x conversion with 3% H_2O at 140/180 °C	[271]
Ni-Mn/TiO_2	400	400	2	50,000 h^{-1}	187–240	>90%	Superior H_2O durability at 200 °C with 10% H_2O	[272]
Zr-Mn/attapulgite	600	600	3	40,000 h^{-1}	153–250	>90%	Stable NO_x conversion with 300 ppm SO_2 at 200 °C	[273]
xSb-4Ce-10Mn/TiO_2	500	500	3	75,000 $mL{\cdot}g^{-1}{\cdot}h^{-1}$	135–325	>95%	Deactivation with 5% H_2O and 100 ppm SO_2 at 200 °C	[195]
Ce-Mn-TNTs	500	500	5	30,000 h^{-1}	150–425	>90%	Stable NO_x conversion with 10% H_2O and 100 ppm SO_2 at 280 °C	[274]
Ce-Mn/TiO_2	800	800	3	40,000 h^{-1}			Deactivation with 3% H_2O and 100 ppm SO_2 at 150 °C	[275]
Ce-Mn/TiO_2	720	800	3	30,000 h^{-1}	120–200	>90%	Deactivation with 100 ppm SO_2 at 180 °C	[276]
Ce-Mn-V-W/TiO_2	1500	1500	3	40,000 h^{-1}	150–400	>90%	Stable NO_x conversion with 5% H_2O and 100 ppm SO_2 at 250 °C	[277]
Nd-Mn/TiO_2	600	600	3	40,000 h^{-1}	100–320	100%	Stable NO_x conversion with 3% H_2O and 50 ppm SO_2 at 120 °C	[278]
Eu-Mn/TiO_2	600	600	5	108,000 h^{-1}	175–400	>90%	Deactivation with 100 ppm SO_2 at 150 °C	[279]
Ho-Mn-Ce/TiO_2	800	800	5	10,000 h^{-1}	140–220	>90%	Deactivation with 10% H_2O and 300 ppm SO_2 at 180 °C	[280]
Ho-Fe-Mn/TiO_2	800	800	5	20,000 h^{-1}			Stable NO_x conversion with 15% H_2O and 200 ppm SO_2 at 120 °C	[215]
Gd-MnO_x/ZSM-5	800	800	5	40,000 h^{-1}	110–240	>90%	Relatively stable NO conversion with 100 ppm SO_2 at 180 °C	[212]
$Ce_{0.5}$/$Co_1Mn_{0.5}Al_{0.5}O_x$	500	500	5		100–250	>90%	Deactivation with 100 ppm SO_2 at 200 °C	[281]
Mn-Ce-V/AC	500	500	5	18,000 h^{-1}	125–300	>95%	Deactivation with 10% H_2O and 100 ppm SO_2 at 200 °C	[282]
Nb_2O_5-Zn-Ce-Mn/AC	500	500	11	14,500 h^{-1}	150–250	>90%	Deactivation with 100 ppm SO_2 at 200 °C	[189]
$NiMnO_x$/activated coke	500	500	10	30,000 h^{-1}	125–250	>80%	Stable NO_x conversion with 200 ppm SO_2 at 200 °C	[283]
La-Mn-Fe/activated coke	500	500	5	6000 h^{-1}	150–300	>90%	Reversible deactivation with 5% H_2O and 200 ppm SO_2 at 150 °C	[284]

Table 5. *Cont.*

Catalysts [1]	Reaction Conditions					NO_x Conversion (%)	Effects of H_2O and SO_2	Ref.
	NO (ppm)	NH_3 (ppm)	O_2 (vol%)	Space Velocity	T (°C)			
Mn/BC	600	600	11	12,000 h^{-1}	160–240	>80%	Reversible deactivation with 100 ppm SO_2 at 180 °C	[285]
Zr-Mn/BC	500	500	5	36,000 h^{-1}	125–250	>75%	Stable NO_x conversion with 5% H_2O and 100 ppm SO_2 at 200 °C	[286]
MnO_x@CNTs	500	500	3	30,000 h^{-1}	165–325	>90%	100% NO_x conversion with 4% H_2O at 225 °C	[287]
MnO_x/Functionalized multi-walled CNTs	900	900	5	30,000 h^{-1}	150–300	>80%	Deactivation with 2.5% H_2O and 100 ppm SO_2 at 200 °C	[288]
MnO_x-CeO_x/CNTs	400	400	3	12,000 h^{-1}	200–260	>90%	Stable NO_x conversion with 100 ppm SO_2 at 220 °C	[289]
MnO_x-CeO_x@CNTs	500	500	3	10,000 h^{-1}	200–350	>90%	Stable NO_x conversion with 4% H_2O and 100 ppm SO_2 at 300 °C	[290]
MnCe/granular AC-CNTs	500	550	5	10,000 h^{-1}	125–200	>80%	Stable NO_x conversion with 5% H_2O and 50 ppm SO_2 at 150 °C	[291]
MnO_x-CeO_2(8:1)/graphene	500	500	5	24,000 h^{-1}	80–140	>99%	Reversible deactivation with 10% H_2O and 200 ppm SO_2 at 140 °C	[292]

[1] LDO: layered double oxide; TNTs: titanium nanotubes; AC: active carbon; BC: biochar; CNTs: carbon nanotubes.

Table 6. NH_3-SCR activity in the presence of H_2O and/or SO_2 over some Mn-based core-shell catalysts.

Catalysts [1]	Reaction Conditions					NO_x Conversion (%)	Effects of H_2O/SO_2/	Ref.
	NO (ppm)	NH_3 (ppm)	O_2 (vol%)	Space Velocity	T (°C)			
MnO_x@TiO_2	500	500	5	24,000 h^{-1}	110–260	>90%	Deactivation with 10% H_2O and 200 ppm SO_2 at 160 °C	[293]
MnO_x@TiO_2	500	500	5	30,000 h^{-1}	130–375	>90%	Reversible inhibition with 5% H_2O at 180 °C	[294]
MnO_x–CeO_2@TiO_2	500	500	5	24,000 h^{-1}	150–210	>90%	Reversible inhibition with 200 ppm SO_2 at 180 °C	[295]
MnO_x@PrO_x	800	800	5	40,000 h^{-1}	93–240	>90%	Irreversible inhibition with 10% H_2O and 100 ppm SO_2 at 160 °C	[296]
MnO_x@CeO_2	800	800	5	40,000 h^{-1}	114–220	>90%	Deactivation with 100 ppm SO_2 at 220 °C	[297]
α-MnO_2@CeO_2	500	500	3	100,000 $mL \cdot g^{-1} \cdot h^{-1}$	125–250	>90%	Deactivation with 200 ppm SO_2 at 220 °C	[298]
MnFe@CeO_x	500	500	5	30,000 h^{-1}	160–240	>90%	Reversible inhibition with 5% H_2O at 160 °C	[299]
MnO_x@Eu-CeO_x	600	600	2.5	90,000 h^{-1}	100–210	>90%	Reversible inhibition with 100 ppm SO_2 at 200 °C	[300]
MnO_x@Fe_2O_3/TNT	500	500	5	40,000 h^{-1}	180–360	~100%	Deactivation with 150 ppm SO_2 at 240 °C	[301]
Ho-TNT@Mn	500	500	5	30,000 h^{-1}	110–300	>90%	Slowly deactivated with 100 ppm SO_2 at 180 °C	[302]
Mn-TNTs@Ce	500	500	5	30,000 h^{-1}	130–375	>90%	Relatively stable NO conversion with 5 % H_2O and 100 ppm SO_2 at 200 °C	[303]

Table 6. *Cont.*

Catalysts [1]	Reaction Conditions					NO_x Conversion (%)	Effects of H_2O/SO_2/	Ref.
	NO (ppm)	NH_3 (ppm)	O_2 (vol%)	Space Velocity	T (°C)			
H-MnO_2@TiO_2@HL	500	500	5	30,000 h^{-1}	175–260	>90%	Reversible inhibition with 5% H_2O at 180 °C	[294]
Ce@Mn@TiO_x	1000	1000	5	30,000 h^{-1}	140–230	>90%	Inhibition with 5% H_2O at low temperature	[304]
$MnCeO_x$@ZSM-5	500	500	5	960,000 $mL{\cdot}g^{-1}{\cdot}h^{-1}$	220–380	>90%	Relatively stable NO conversion with 5% H_2O and 100 ppm SO_2 at 300 °C	[305]
Fe_2O_3@MnO_x@CNT	550	550	5	20,000 h^{-1}	120–300	>90%	Reversible inhibition with 10% H_2O and 100 ppm SO_2 at 180 °C	[306]
mesoTiO_2@MnCe/CNTs	500	500	3	10,000 h^{-1}	225–400	>90%	Relatively stable NO conversion with 200 ppm SO_2 at 300 °C	[307]
$Co_{(3-x)}Mn_xO_4$@TiO_2	500	500	5	24,000 h^{-1}	125–275	>80%	Relatively stable NO conversion with 10% H_2O and 100 ppm SO_2 at 225 °C	[308]

[1] TNT: titanium nanotube; TNTs: titanium nanotubes; layered double oxide; HL: hydrophobic layer; CNT: carbon nanotube; CNTs: carbon nanotubes.

Liang et al. [221] reported that the MnO_x-SiO_2 mixed oxide catalyst synthesized by the co-precipitation method showed high NH_3-SCR activity with high N_2 selectivity and sulfur resistance because doping SiO_2 increased the specific surface area of the catalyst, surface acidity, and NH_3 adsorption. Doping with SiO_2 inhibited the adsorption of SO_2 for surface deposition of sulfate, effectively protecting the redox properties of the catalyst so that the MnO_x-SiO_2 catalyst showed relatively stable NO conversion in the presence of 100 ppm SO_2 at 225 °C [221]. Zhu et al. [222] synthesized mesoporous Mn-TiO_x with a three-dimensional structure by a solvent-free self-assembling strategy and observed an outstanding sulfur poisoning tolerance. The hierarchical cross-linked structure with a large specific surface area appeared to be favorable for enhancing the synergy between Mn and Ti, exposing more active sites, and dispersing the poisoning species [222]. Wang et al. [309] synthesized a series of $Mn_xCe_yTi_z$ catalysts with three-dimensionally ordered macroporous (3DOM) structure by a soft template method and reported that after adding Ti, the redox capacity of the 3DOM-$Mn_3Ce_1Ti_1$ catalyst decreased and the N_2 selectivity was enhanced due to the strong adsorption of NH_3 on the acid sites, widening the temperature window. Yao et al. [171] found that the TiO_2-modified MnO_x/CeO_2-ZrO_2 nanorod exhibited higher catalytic activity than the MnO_x/CeO_2-ZrO_2 nanorod due to the larger amount of oxygen vacancy, the higher ratio of Mn^{4+} among Mn species, the higher proportion of surface adsorbed oxygen species among oxygen species, and the improvement of surface acidity. Furthermore, the TiO_2 modification appropriately weakened the redox properties of the MnO_x/CeO_2-ZrO_2 nanorods, effectively inhibiting the nonselective oxidation of NH_3 to N_2O [171]. Finally, TiO_2-modified MnO_x/CeO_2-ZrO_2 nanorod exhibited excellent H_2O + SO_2 tolerance, showing relatively stable NO conversion in the presence of 5% H_2O and 100 ppm SO_2 at 200 °C [171]. Xu et al. [256] reported that over a wide operating temperature range (60–225 °C), Ti-doped Sm–Mn mixed oxide showed a superior NH_3-SCR performance, especially excellent SO_2/H_2O resistance. Stable NO_x conversion was achieved even in the presence of 5% H_2O and 100 ppm SO_2 at 100 °C [256]. The inclusion of Ti can inhibit MnO_x crystallization to increase the high specific surface area and the amount of acid sites, while Sm doping can modulate the redox properties to promote NO oxidation and inhibit NH_3 nonselective oxidation [256].

Jiang et al. [282] reported that doping V_2O_5 to Mn-Ce/AC enhanced the NO conversion, N_2 selectivity, and SO_2 tolerance than Mn-Ce/AC because doping with V_2O_5 enhanced surface acidity and enriched surface chemisorbed oxygen. The stronger surface acidity of Mn-Ce-V/AC inhibited the competitive adsorption of SO_2 and suppressed the reaction between adsorbed SO_2 and NH_3 species [282]. In addition, the cluster of vanadium

oxide species partially prevented the dispersed Mn-Ce solid solution from being sulfated by SO_2 [282]. This catalyst showed relatively stable NO conversion in the presence of 10% H_2O and 100 ppm SO_2 at 200 °C [282]. Li et al. [236] reported that the $Mn_{0.50}Co_{0.49}V_{0.01}O_x$ catalyst exhibited superior catalytic performance over a wide temperature window (162–508 °C) among ternary $MnCoVO_x$ catalysts and also displayed enhanced SO_2 tolerance, showing relatively stable NO conversion in the presence of 5% H_2O and 100 ppm SO_2 at 200 °C.

Gao et al. [173] prepared Cr-Mn mixed-oxide catalysts by citric acid method and observed good low-temperature NH_3-SCR performance at 100–225 °C owing to their high specific surface area, more active sites (Mn^{3+} and Mn^{4+}), and effective electron transfer ($Cr^{5+} + 2Mn^{3+} \rightarrow Cr^{3+} + 2Mn^{4+}$). The stronger Mn–O binding energy and weaker dehydrogenation ability in $CrMn_2O_4$ spinel were the main reasons for the lower N_2O by-product than Mn_3O_4 [173]. The $CrMn_2O_4$ spinel showed relatively stable NO conversion in the presence of 10% H_2O and 150 ppm SO_2 at 200 °C [173]. The formation of Cr(III) sulfate could protect Mn active sites from sulfating. Furthermore, the transformation of -HSO_3 and SO_4^{2-} to ($H\cdots SO_4^{2-}$) can provide new Brønsted acid sites for ionic NH_4^+, enhancing the NH_3-SCR activity via 'Fast-NH_3-SCR' ($NO_2 + NH_4^+ \rightarrow NH_4NO_2 \rightarrow N_2 + 2H_2O$) [173].

The DFT calculation results indicated that Fe doping promoted the adsorption of NH_3 on the Mn sites over the β-MnO_2 (110) surface, weakened SO_2 adsorption capacity, and limited the oxidation of SO_2, which promoted the decomposition of ammonium sulfate and relieved the catalytic site blockage on the catalyst surface [310]. DFT calculation demonstrated that the thermodynamically most favored structure after Fe doping was MnO_{2-x}, and the structure remained stable as the doping amount increased [311]. The adsorption behavior of gas molecules on MnO_{2-x} showed that NH_3 and H_2O preferred to adsorb on the Mn Lewis acid sites, while NO and SO_2 preferred to adsorb on the O sites. MnO_{2-x} with enhanced acidity after Fe doping showed good SO_2 tolerance [311]. Wu et al. [312] prepared various Mn/TiO_2 catalysts promoted with different transition metals, including Fe, Cu, Ni, and Cr, by the sol–gel method and found that more NO could be oxidized to NO_2 and nitrate and then reacted with NH_3, thus leading to the enhanced NH_3-SCR activity at low temperatures. The promoting effect of Fe on Mn-Fe composite oxide catalysts was explained by the fact that Fe promoted NO oxidation and generated more monodentate and bidentate nitrate adsorption species on the catalyst surface [312]. It was also reported that the addition of Fe enhanced the amount and intensity of Brønsted and Lewis acid sites, which promoted the absorption of NH_3 to form active intermediates, thereby improving the low-temperature NH_3-SCR performance [313].

Jiang et al. [232] prepared MnO_2–CoO_x catalysts with different Mn/Co ratios using PVP as an assistant to control the morphology and exposed crystal faces of composite oxides. The best Mn–Co oxide showed stable NO_x conversions in the presence of 5% H_2O and 100 ppm SO_2 at 160 °C [232]. Feng et al. [314] prepared a series of Mn-Co mixed metal oxides, $Mn_yCo_{3-y}O_x$, by an ultrasonic technology followed by a hydrothermal treatment and found that they exhibited much better NH_3-SCR performance than single metal oxides (MnO_x or CoO_x). This can be attributed to the strong interaction between MnO_x and CoO_x, which reduces the crystallinity of the $Mn_yCo_{3-y}O_x$ catalyst, increases the specific surface area, establishes the redox cycle of $Co^{3+} + Mn^{3+} \rightarrow Co^{2+} + Mn^{4+}$, improves the reducibility, enhances the surface acid sites, and accelerates the reaction between adsorbed NO_x species and coordinated NH_3 bound to Lewis acid sites [314]. Chen et al. [233] prepared a $MnCoO_x$ catalyst using glucose as the forming pore agent and urea as the structural direction reagent and found that it exhibited higher low-temperature activity and SO_2 resistance than pure MnO_x catalysts. They revealed that the high surface area, abundant chemisorbed oxygen species, and the redox cycle ($Co^{3+} + Mn^{3+} \rightarrow Mn^{4+} + Co^{2+}$) collectively account for the enhanced catalytic activity of $MnCoO_x$ catalysts [233]. The $Mn(5)Co(5)O_x$ catalyst showed stable NO_x conversions even in the presence of 5% H_2O and 50 ppm SO_2 at 125 °C [233]. Zhang et al. [281] prepared a highly active Ce/CoMnAl from layered double hydroxides (LDHs), which showed low-temperature NH_3-SCR with good thermal stability and SO_2/H_2O resistance. The $Ce_{0.5}/Co_1Mn_{0.5}Al_{0.5}O_x$-layered double

oxide (LDO) showed relatively stable NO_x conversion at 200 °C for 10 h with 100 ppm SO_2 in the feed stream [281].

Gao et al. [238] reported that the Mn-Ni spinel nanosheet ($NiMn_2O_4$) prepared by the urea hydrolysis hydrothermal synthesis exhibited excellent resistance to H_2O and SO_2 in the low temperature range at 150–300 °C. This catalyst showed stable NO_x conversions even in the presence of 150 ppm SO_2 at 175 °C [238]. Ni-doped MnO_x catalysts prepared by the solvent-free doping method maintained excellent low temperature (100–200 °C) NH_3-SCR activity, which was attributed to the fact that the appropriate nickel loading could effectively adjust the surface lattice oxygen activity and acidity of the catalyst, ensuring its ability to activate NH_3 at low temperatures [315]. Liu et al. [316] reported that $NiMn_2O_4$ catalysts prepared via the solvothermal method exhibited excellent NH_3-SCR performance in the temperature range of 85 to 285 °C due to their large specific surface area, high Mn^{4+}/Mn^{n+} ratio, sufficient O_α, appropriate acidity, and redox ability. Yan et al. [240] reported that the $Ni_1Mn_{0.5}Al_{0.5}O_x$ showed the highest NH_3-SCR activity at 100–250 °C among LDHs-derived $NiMnAlO_x$ catalysts because of more active species, abundant surface oxygen, moderate acidic sites, and redox properties. This catalyst also exhibited better resistance to SO_2 with fewer sulfate species deposited on the surface, showing relatively stable NO conversion in the presence of 5% H_2O and 100 ppm SO_2 at 200 °C [240]. Hou et al. [241] prepared a series of highly dispersed $Ni_{4-x}Mn_xAlO_y$ catalysts derived from LDHs and reported that the optimal $Ni_{4-x}Mn_xAlO_y$ catalyst exhibited high NH_3-SCR performance at a low temperature range of 120~210 °C but was deactivated in the presence of 5% H_2O and 100 ppm SO_2 at 210 °C. Yan et al. [244] prepared $NiMnFeO_x$ catalysts by the LDH-derived oxide method and reported that the optimized $Ni_{0.5}Mn_{0.5}Fe_{0.5}O_x$ catalyst had the best NH_3-SCR activity, excellent N_2 selectivity, a wider active temperature range (100–250 °C), higher thermal stability, and better H_2O and/or SO_2 resistance. This catalyst showed relatively stable NO conversion even in the presence of 5% H_2O and 100 ppm SO_2 at 200 °C [244]. Wang et al. [283] reported that $NiMnO_x$ supported on active coke prepared by deposition-precipitation method showed the high NH_3-SCR activity because of the higher content of (Mn^{3+} + Mn^{4+}), the high ratio of Mn^{3+}/Mn^{4+}, and Ni^{3+}/Ni^{2+}. This catalyst showed a stable NO conversion even in the presence of 200 ppm SO_2 at 200 °C [283].

Doping MnO_x and $CeMnO_x$ with Y did not improve NO conversion, but it broadened the range of high N_2 selectivity compared with the undoped case [186]. The addition of Zr to Fe-Mn-Ti oxide catalysts was reported to decrease the deactivation rate in the presence of 100 ppm SO_2 at 150 °C [187]. Chen et al. [285] prepared several metal (Zr, Ni, and Co) oxide-doped BC-supported Mn oxide (MnO_x) catalysts by the impregnation method and found that the Zr-Mn/BC catalyst exhibited the best NH_3-SCR activity among them because of the high concentration of Mn^{4+}, more surface oxygen (O_α), excellent redox property, and more Lewis acid sites and Brønsted acid sites. Furthermore, the Zr-Mn/BC catalyst showed stable NO conversion in the presence of 5 vol% H_2O and 100 ppm SO_2 at 200 °C [285]. Che et al. [317] reported that the highly dispersed active MnO_x species supported on the amorphous structure of $ZrTiO_x$ had a uniquely bridged Mn^{3+} bonded with the support through oxygen linked to Ti^{4+} and Zr^{4+}, respectively, which regulated the optimal oxidizability of the MnO_x species, leading to high NH_3-SCR activity and N_2 selectivity.

Zhou et al. [188] found that doping Nb_2O_5 could effectively enhance the NH_3-SCR performance and N_2 selectivity of the Zn-Mn-Ce/AC catalyst. Meanwhile, Nb_2O_5 could significantly improve the SO_2 poisoning resistance of the Zn-Mn-Ce/AC catalyst, showing relatively stable NO conversion in the presence of 100 ppm SO_2 at 225 °C because Nb_2O_5 could react with SO_2 in a preferential way to restrain the sulfuration of manganese and cerium oxides on the catalyst [188]. More importantly, Nb_2O_5 reacted with SO_2 to form Nb sulfate and then formed a new acidic site on the Zn-Mn-Ce/AC catalyst surface, which promoted the adsorption of NH_3 and inhibited the adsorption of SO_2, then restricted the reaction between NH_3 and SO_2 and hindered the formation of ammonium sulfate channels [188]. The promotional effect of Mo in Mo-MnO_x catalyst was reported to be

due to its higher Mn^{4+} content, abundant surface adsorbed oxygen (O_α), and more acid sites [189]. Li et al. [318] employed Mo and V to simultaneously fine-tune the acid and redox sites of MnO_x and found that the adjusted $Mn_{0.90}Mo_{0.09}V_{0.01}O_x$ catalyst demonstrated excellent low-temperature activity and a significantly broader active temperature window.

Chang et al. [194] reported that SnO_2–MnO_x–CeO_2 catalysts prepared by a co-precipitation method showed remarkably high activity, N_2 selectivity, and SO_2 resistance at temperatures in the range of 200–500 °C, which can be due to the significant enhancement of Lewis acid sites generated by surface sulfation during the SO_2-containing NH_3-SCR reaction. They also explained that the high SO_2 tolerance can be ascribed to the inhibited formation of $MnSO_4$ [194]. This catalyst showed stable NO_x conversions in the presence of 12% H_2O and 100 ppm SO_2 at 110 °C [194]. Wang et al. [268] synthesized Sn-doped modified CoAl-LDH by a hydrothermal method and used it as a support for the preparation of the active hexagonal sheet structure of the $MnO_x(0.25)/CoSn_3Al$-LDO catalyst, which also showed relatively stable NO conversion at 200 °C after the introduction of 150 ppm SO_2. Sn doping increased the ratios of Mn^{4+}/Mn^{3+} and Co^{3+}/Co^{2+} as well as the adsorbed oxygen amount on the catalyst surface, improved the redox capacity of the catalyst, and increased the number of acid sites, resulting in the excellent low-temperature NH_3-SCR performance [268].

Xie et al. [195] prepared a series of xSb-4Ce-10Mn/TiO_2 (x = 0, 2, 3, 4, 5, 6) catalysts by a reverse co-precipitation method and observed that the addition of Sb^{5+}/Sb^{3+} slightly decreased the catalytic activity but helped improve the H_2O/SO_2 resistance. They found that the Sb^{5+}/Sb^{3+} addition decreased the Mn^{4+} and Ti^{4+} content but increased the Ce^{3+}, surface adsorbed oxygen content, and the surface area, which promoted the decomposition of AS and inhibited the formation of $MnSO_4$ [195]. However, stable NOx conversion was not achieved in the presence of 5% H_2O and 100 ppm SO_2 at 200 °C [195].

Li et al. [319] reported that the addition of Mn to ceria greatly promotes the formation of surface oxygen vacancies that readily capture O_2 from the air and form surface reactive oxygen species (superoxide and peroxide), which efficiently oxidize NO to NO_2 and then promote the 'Fast NH_3-SCR' reaction. Rong et al. [206] prepared the $MnXO_x$ catalysts (i.e., $MnSmO_x$, $MnNdO_x$, and $MnCeO_x$) by the reverse co-precipitation method and found that the $MnCeO_x$ catalyst showed the best low-temperature catalytic activity and excellent $H_2O + SO_2$ resistance because of the largest amount of acid sites and the best reducibility among these $MnXO_x$ catalysts. However, stable NO_x conversion was not achieved over these catalysts in the presence of 5% H_2O and 100 ppm SO_2 at 175 °C [206]. Fang et al. [320] reported enhanced NH_3-SCR activity and SO_2 tolerance of Ce-modified birnessite-MnO_2 and attributed it to the preferential adsorption and oxidation of SO_2 onto Ce species to form a new adsorption site for NH_4^+, $Ce_2(SO_4)_3$, which protects the Mn active site from sulfidation and deactivation.

It is generally accepted that homogeneous metal doping into the MnO_x matrix is beneficial for NH_3-SCR activity. However, Cheng et al. [321] claimed that the presence of crystalline Mn_3O_4 and its interfacial interaction with CeO_2 played a significant role in boosting the NH_3-SCR performance, suggesting the great synergy between CeO_2 and the crystalline phase of Mn_3O_4, which were responsible for NO_x adsorption and the formation of NH_2 species through the activation of NH_3, respectively. Zhu et al. [322] prepared a series of Ce_x-Mn-Ti_y catalysts by the co-precipitation method and found that the best NH_3-SCR activity was obtained over the $Ce_{0.1}$-Mn-$Ti_{0.1}$ catalyst with the proper redox ability, abundant acid sites, high content of Mn^{4+} and Ce^{3+}, and surface-adsorbed oxygen. Wei et al. [251] prepared Mn–Ce–Ti–O composite aerogels with large mesopore size and reported that the Mn–Ce–Ti–O catalyst calcined at 600 °C showed stable NO conversion in the presence of 5 vol% H_2O and 100 ppm SO_2 at 200 °C, which they attributed to its large pore size, averaging 32 nm, and abundant Lewis acid sites, as the former promoted the decomposition of ABS and the latter reduced the vapor pressure of NH_3. Teng et al. [323] prepared a series of rare-earth (Ce, La, Nd, and Y) oxide-doped Mn/Al_2O_3 catalysts by the impregnation method and found that rare earth oxide addition significantly enhanced

the NH_3-SCR catalytic activity of Mn/Al_2O_3, with $CeMn/Al_2O_3$ obtaining the highest activity at 125–300 °C. Except for Y_2O_3, the rare earth oxide additives promoted the surface distribution of Mn elements and enhanced the ratio of chemisorbed oxygen and Mn^{4+} on the surface of Mn/Al_2O_3 [323]. In addition, the introduction of rare earth oxides enhanced the reducibility of MnO_2 species and obtained a larger amount of weak acid sites [323]. Contrary to some reports on the promotional effect of Ce in Ce-MnO_x catalysts, Gevers et al. [324] reported that the intrinsic NH_3-SCR activity of the Mn active sites is not positively affected by Ce species at low temperatures based on the fact that the surface-area normalized activity did not increase by Ce addition. They concluded that Ce decreased the average oxidation state and activity of Mn active species and was just a structural promotor, increasing catalyst surface area, and that addition of Ce suppressed second-step oxidation reactions and thus N_2O formation by structurally diluting MnO_x [324]. The diffuse reflectance infrared Fourier transform spectroscopy (DRIFTS) analysis showed that N_2O was mainly generated by the reaction between NO and excessive hydrogen abstraction of NH_3 (i.e., forming NH species) and that Ca addition inhibited the formation of NH species on the catalyst surface, thereby reducing the formation of N_2O [325]. Ca addition could also lead to a decreased formation of NO_2, which could react with NH_3 to form N_2O, contributing to the promoted selectivity of N_2 over Ca-modified Ce-Mn/TiO_2 [325].

Wu et al. [205] reported that the Pr modification could boost the $MnCeO_x$ catalysts' NH_3-SCR activity and SO_2 resistance because of the expanded specific surface area, the improved dispersion of active components, the enhanced surface acidity and redox ability, and the generated more chemisorbed oxygen (O_{ads}) species. The $MnCePrO_x$-0.3 catalyst exhibited stable NO conversion even in the presence of 5 vol% H_2O and 100 ppm SO_2 at 250 °C [205]. Wang et al. [259] reported that the $MnCeSmTiO_x$ catalyst preserved higher catalytic performance after introducing H_2O and SO_2 compared with the catalysts without adding Sm. They claimed that the synergistic effect of the Lewis acid sites and oxidation catalytic sites of mixed oxides was responsible for NH_3-SCR by following the L–H mechanism [261]. Doping Sm into $MnCeSmTiO_x$ was reported to be able to increase oxygen vacancies and transfer electrons to Mn^{4+} and Ce^{4+}, promoting the formation of active adsorbed NO_2, bidentate nitrate, and bridging nitrate intermediates and suppressing SO_2 poisoning by inhibiting the oxidation of SO_2 by Mn^{4+} and Ce^{4+} [259]. The $MnCeSmTiO_x$ catalyst exhibited a rather stable NO conversion even in the presence of 5% H_2O and 200 ppm SO_2 at 200 °C [259]. Kim et al. [326] reported that the addition of Sm to MnO_x/TiO_2 increased the redox properties and the proportion of Mn^{4+} in MnO_x catalysts, and the addition of Ce further improved the redox properties of Sm-MnO_x/TiO_2 catalysts. They also reported that when exposed to SO_2/O_2, Sm and Ce-modified MnO_x/TiO_2 not only inhibited the degradation but also increased the N_2 selectivity by inhibiting the formation of N_2O_4 intermediate species, thereby inhibiting the formation of N_2O [326].

The addition of Eu to MnO_x/TiO_2 was reported to be effective against the resistance of SO_2 (i.e., NO_x conversion gradually decreased but reached a steady-state value in the presence of 100 ppm SO_2 at 150 °C) [279]. Wang et al. [210] prepared a series of $MEuMnO_x$ ternary oxides (M = Ce, Ni, Co, Sb, Sn, Mo) by one-pot co-precipitation method and observed that $CeEuMnO_x$ ternary oxide catalysts showed a high NH_3-SCR activity at 100–250 °C and stable NO_x conversions in the presence of 10 vol% H_2O and 50 ppm SO_2 at 230 °C. The facile electron transfer through the redox cycle of $Mn^{3+} + Ce^{4+} \rightarrow Mn^{4+} + Ce^{3+}$ and enhanced oxygen mobility can promote the formation of more Mn species in high oxidation states and chemisorbed oxygen, accelerating oxidation of NO, and the adsorbed NO_2 formed can facilitate the 'Fast NH_3-SCR' reaction to improve low-temperature activity [210]. The addition of Ce to the $EuMnO_x$ catalyst boosts adsorption of NH_3 and NO_x species. NH_3 species are activated as crucial intermediates (NH_2) to promote the NH_3-SCR reaction [210]. Guan et al. [211] synthesized a series of Gd-modified MnO_x/ZSM-5 catalysts via a citric acid–ethanol dispersion method and found that the Gd-modified MnO_x/ZSM-5 catalyst presented the higher catalytic activity and better SO_2 resistance than MnO_x/ZSM-5 in the presence of 100 ppm SO_2. The high catalytic performance was mainly owing to the

large surface area, enriched Mn^{4+} and surface chemisorbed oxygen species, strong redox properties, and the proper acidity of the catalyst [211]. The addition of Gd inhibited the reaction between the SO_2 and MnO_x active sites to form inactive bulk manganese sulfate, resulting in high SO_2 resistance [211]. The GdMn/Z-0.3 catalyst showed a rather stable NO conversion in the presence of 10% H_2O and 100 ppm SO_2 at 180 °C [211]. Gao et al. [212] synthesized Dy-doped MnFe oxides with the morphology of one-dimensional nanowire by using the electrospinning method and found that the doping of Dy with an appropriate amount enhanced the surface Mn^{4+} concentration and surface chemical adsorption of oxygen and increased adsorption capacity for NH_3 and NO. Zhuang et al. [214] investigated the effect of SO_2 on the low-temperature NH_3-SCR activity for Ho-modified Fe-Mn/TiO_2 catalyst. The $Fe_{0.3}Ho_{0.1}Mn_{0.4}/TiO_2$ catalyst showed excellent SO_2 durability at 120 °C when the concentration of SO_2 was lower than 400 ppm, and the catalytic activity could recover considerably after the SO_2 supply was interrupted [214]. When the concentration of SO_2 was increased to 1000 ppm, the deactivation behavior was irreversible, but the deactivated catalyst could be regenerated after thermal reduction (350 °C) with 5% NH_3 [214]. Zhao et al. [304] synthesized the Ho-modified titanium nanotubes (TNTs)@MnO_x, where the manganese oxide active species was confined in a Ho-modified TNTs, and observed the improved SO_2 resistance and N_2 selectivity during NH_3-SCR at low temperatures, showing NO conversion, which decreased slowly over time in the presence of 100 ppm SO_2 at 180 °C. They claimed that the pore confinement effect of Ho-TNTs on Mn increased the dispersion of Mn, thereby promoting the interfacial effect between Mn and Ho, and the electron synergy between Mn and Ho inhibited the electron transfer between SO_2 and Mn, thus preventing the poisoning of SO_2 [302]. They also found that the interaction between Ho and Mn contributed to the proper redox ability to induce electron transfer to inhibit the generation of Mn^{4+}, thereby achieving high N_2 selectivity [302].

Zha et al. [218] found that the addition of tungsten created more Brønsted acid sites and reduced the energy barrier for NO_x species adsorbed on the surface. They also claimed that the formed NH_3 species and NO_x species of MnCeW/m-TiO_2 were more reactive due to the promotional effects of W than those of MnCe/m-TiO_2 [218]. Liu et al. [327] reported the promotional effect of W-doping on the $CoMn_2O_4/TiO_2$ catalyst on the resistance to H_2O at low temperature. The superior performance of the $CoMn_2O_4$/W-TiO_2 catalyst was ascribed to its unique spinel structure, mesoporous structure, highly dispersed tungsten species, and larger surface acidity [327]. The electron cycle among Mn, Co, W, and Ti helped to keep the Mn^{3+}/Mn^{4+} and Co^{3+} at high concentrations and improve lattice oxygen mobility [327]. Both Lewis and Brønsted acid sites were generated by the incorporation of tungsten in the presence of H_2O, which enhanced NH_3 adsorption and thus promoted the E–R reaction pathway [327]. In addition, the N_2 selectivity was significantly enhanced by H_2O, which could be attributed to the decreased redox activity [327].

Yan et al. [305] assembled a confined $MnCeO_x$ catalyst using a mesoporous zeolite (ZSM-5) as the shell and Mn-Ce oxides as the active core ($MnCeO_x$@ ZSM-5) with a simple one-pot method and found that the novel $MnCeO_x$@ ZSM-5 catalyst displayed enhanced water and SO_2 resistance as compared with the $MnCeO_x$ supported on ZSM-5 ($MnCeO_x$/ZSM-5) and its precursor ($MnCeO_x$@Al-SiO_2), which was ascribed to the zeolite shell's shielding effect and the synergy between the alumina-silica zeolite shell's acidic properties and the mixed oxide cores' redox properties. This catalyst showed relatively stable NO conversion in the presence of 5% H_2O and 100 ppm SO_2 at 300 °C [305]. Cai et al. [328] fabricated MnFe@CeO_x@TiO_x nanocage with a yolk-shell structure, where the CeO_2 shell could effectively increase the oxygen vacancy defect sites and the TiO_2 shell could remarkably improve the surface acid sites, which exhibited excellent NH_3-SCR performance in the temperature range of 120–240 °C, which was ascribed to the increased proportion of active species (Mn^{4+}, Fe^{3+}, Ce^{3+}, and O_{ads}) and enhanced interaction between metal oxides. Huang et al. [304] prepared a series of yolk-shell-structured Ce@Mn@TiO_x, where the TiO_2 shell could provide more surface acid sites to promote the adsorption and activation of ammonia (Figure 6). The Ce@Mn@TiO_x exhibited excellent NH_3-SCR

performance at low temperature and H_2O and SO_2 tolerance, showing relatively stable NO conversion in the presence of 100 ppm SO_2 at 200 °C [304]. Qiao et al. [329] prepared various MnO_x-ZSM-5 catalysts with different MnO_x locations and found that MnO_x clusters dispersed on the outside of ZSM-5 exhibited higher catalytic activity at low temperature than MnO_x nanoparticles encapsulated in the channels of the support because the excellent redox ability and the dominant Mn^{3+} species over the former one improved the oxidation of NO to NO_2 and the formation of unstable NO_x intermediates, enhancing the low-temperature NH_3-SCR activity. Ran et al. [330] synthesized a series of MnO_x-CeO_x confined in the mesopores of SBA-15 and found that they displayed enhanced resistance to SO_2. Guo et al. [331] reported that the catalyst with larger mesopores exhibited much improved sulfur resistance. Zhang et al. [307] synthesized a core-shell structural catalyst, carbon nanotube (CNT)-supported MnO_x and CeO_x nanoparticles coated with mesoporous TiO_2 sheaths (mesoTiO_2@MnCe/CNTs), in which the meso–TiO_2 sheaths could prevent the generation of ammonium/manganese sulfate species from blocking the active sites, resulting in a higher SO_2-tolerance during NH_3-SCR. The reversible deactivation was observed over this catalyst due to the presence of 200 ppm SO_2 at 300 °C [307]. Yan et al. [305] prepared the core-shell $MnCeO_x$@mesorporus ZSM-5 catalysts, in which a mesoporous zeolite (ZSM-5) covers the active core Mn-Ce oxides as the shell, and observed enhanced water and SO_2 resistance during NH_3-SCR owing to the zeolite shell's shielding effect, which hinders the formation of sulfate species, and the synergy between the alumina-silica zeolite shell's acidic properties and the mixed oxide cores' redox properties. Zhao et al. [303] constructed a Mn-TNTs@Ce catalyst, where MnO_x was confined in TNT via in situ introduction following Ce ion exchange into the skeleton of TNTs. The nanotube-confined structure improved the surface acidity to restrain SO_2 adsorption, and Ce species acted as a protective site protecting Mn from SO_2 attacking [303]. Furthermore, the short-range structure Ce-O-Ti promoted the electron transformation between Mn and Ce to suppress the formation of -NH and NH_4NO_3, resulting in inhibiting the generation of N_2O [303]. It is remarkably that the Mn-TNTs@Ce catalyst showed a relatively stable NO conversion even in the presence of 5 vol% H_2O and 100 ppm SO_2 at 200 °C [303].

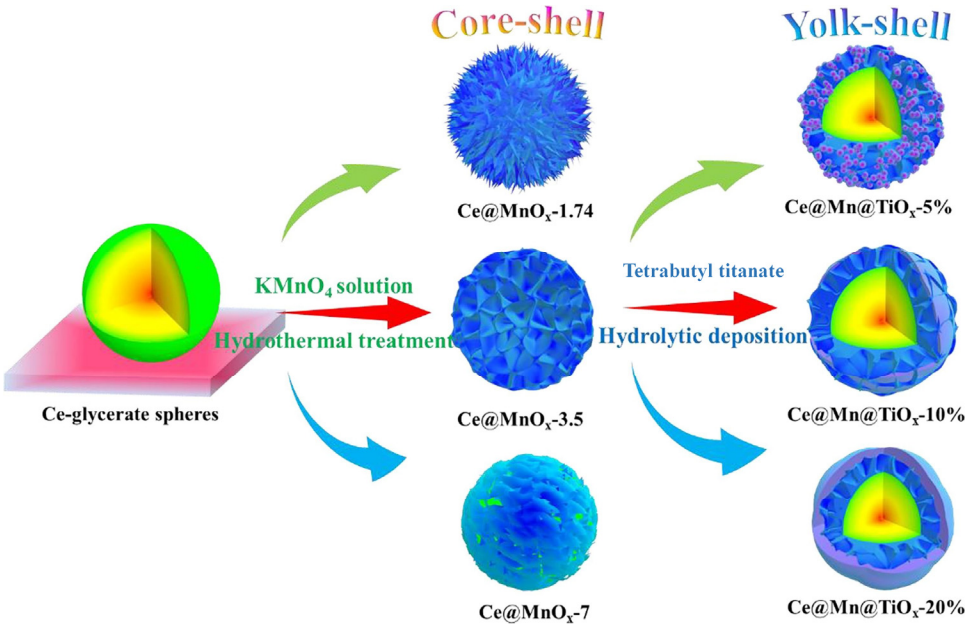

Figure 6. The schematic illustration of the construction for yolk-shell Ce@Mn@TiO_x [306]. Adapted from permission from ref [306]. Copyright 2021 Elsevier.

It is noteworthy that several promising Mn-based catalysts capable of performing NH_3-SCR at low temperatures, even in the presence of H_2O and SO_2, have been reported; however, most of them have only been shown to be stable for short reaction times, and

catalyst analysis of post-reaction samples has been limited. For previously reported promising catalysts, long-term lifetime tests should be performed at low temperatures using flue gases containing H_2O and SO_2 to observe deactivation phenomena, and real-time analysis should be performed to identify and validate detailed mechanisms of resistance to H_2O and SO_2.

2.4. Ce-Based Catalysts

Since cerium-exchanged sodium-type mordenite (CeNa-MOR) was first reported to be active for NH_3-SCR over a wide temperature range of 250–560 °C [332], unsupported and supported ceria, metal-doped ceria, and multicomponent Ce-containing mixed metal oxides [333–335] have been applied to NH_3-SCR [336]. While NH_3-SCR activity was reported to be dependent on ceria morphology (i.e., nanosphere is better than nanocube), unsupported ceria showed relatively low catalytic activity at low temperatures, even after sulfation to provide surface acidic sites [337]. Therefore, metal-doped ceria and multicomponent Ce-containing mixed metal oxide catalysts have received much attention for application in low-temperature NH_3-SCR. Since Cu-, Fe-, and Mn-containing Ce-based catalysts have already been covered in the previous sections, this section mainly introduces Ce-based catalysts with other metals. The effects of H_2O and SO_2 on the NH_3-SCR activity over Ce-based catalysts are summarized in Table 7 [338–376]. Among them, a relatively stable catalytic performance was observed over CO-pretreated CeO_2 [338], F-Ce-Ti oxides [345], P-CeO_2/TiO_2 [346], Ti-Sn-Ce-O_x [352], and CeBi/TiO_2 [353] even in the presence of H_2O and SO_2 at low temperatures.

Table 7. NH_3-SCR activity in the presence of H_2O and/or SO_2 over some Ce-based catalysts.

Catalysts [1]	Reaction Conditions						NO_x Conversion (%)	Effects of H_2O/SO_2	Ref.
	NO (ppm)	NH_3 (ppm)	O_2 (vol%)	H_2O (vol%)	GHSV	T (°C)			
CO-pretreated CeO_2	600	600	5	-	108,000 h^{-1}	250–350	>90%	Stable NO conversion with 5% H_2O and 100 ppm SO_2 at 200 °C	[338]
H_2SO_4-pretreated CeO_2	500	500	5	-	60,000 $mL \cdot g^{-1} \cdot h^{-1}$	350–475	>90%	Stable NO conversion with 5% H_2O and 100 ppm SO_2 at 400 °C	[339]
CeO_2/HAT	500	500	5	-	177,000 h^{-1}	250–400	>90%	Stable NO conversion with 5% H_2O and 50 ppm SO_2 at 300 °C	[340]
TiO_x/CeO_2	500	500	5	-	90,000 h^{-1}	250–450	>80%	Irreversible deactivation with 5% H_2O and 200 ppm SO_2 at 300 °C	[341]
CeO_x/TiO_2	500	500	5	-	90,000 h^{-1}	250–450	>80%	Irreversible deactivation with 5% H_2O and 200 ppm SO_2 at 300 °C	[341]
$CeTiO_x$ Hollow nanotube	1000	1000	3	-	40,000 h^{-1}	180–390	>98%	Stable NO conversion with 6% H_2O and 100 ppm SO_2 at 240 °C	[342]
CeO_2-TiO_2/P25	500	500	5	5	60,000 $mL \cdot g^{-1} \cdot h^{-1}$	300–450	>80%	Stable NO conversion with 5% H_2O and 100 ppm SO_2 at 400 °C	[343]
$CeTiO_x$	600	600	3	-	150,000 h^{-1}	180–300	>80%	Slowly deactivated with 5% H_2O and 100 ppm SO_2 at 225 °C	[344]
F-Ce-Ti oxides	500	600	5	-	41,000 h^{-1}	180–240	>90%	Reversible deactivation with 100 ppm SO_2 at 150 °C	[345]
P-CeO_2/TiO_2	500	500	5	-	60,000 h^{-1}	200–430	>80%	Relatively stable NO conversion with 5% H_2O and 500 ppm SO_2 at 200 °C	[346]

Table 7. *Cont.*

Catalysts [1]	Reaction Conditions						NO_x Conversion (%)	Effects of H_2O/SO_2	Ref.
	NO (ppm)	NH_3 (ppm)	O_2 (vol%)	H_2O (vol%)	GHSV	T (°C)			
Ce/Ti-Si-Al oxides	500	500	5	-	65,000 h^{-1}	215–465	>80%	Reversible deactivation with 10% H_2O and 100 ppm SO_2 at 320 °C	[347]
Ce/TiO_2-SiO_2	500	500	3	-	28,000 h^{-1}	250–450	>90%	100% NO_x conversion for 24 h with 10% H_2O and 200 ppm SO_2 at 300 °C	[348]
$Ce/Mo\text{-}TiO_2$	500	500	5	-	60,000 $mL{\cdot}g^{-1}{\cdot}h^{-1}$	200–350	~100%	Stable NO conversion with 2% H_2O and 100 ppm SO_2 at 250 °C	[349]
WO_3/CeO_2	500	500	3.5	-	60,000 $mL{\cdot}g^{-1}{\cdot}h^{-1}$	250–450	~100%	Slowly deactivated with 4% H_2O and 300 ppm SO_2 at 200 °C	[350]
Ce-W/UiO-66	300	300	3	-	10,000 h^{-1}	200–350	>90%	Stable NO conversion with 5% H_2O and 200 ppm SO_2 at 250 °C	[351]
Ti-Sn-Ce-O_x	600	600	6	-	20,000 h^{-1}	200–375	>90%	Stable NO conversion with 10% H_2O and 300 ppm SO_2 at 200 °C	[352]
$CeBi/TiO_2$	600	600	5	-	108,000 h^{-1}	250–400	>95%	Relatively stable NO conversion with 5% H_2O and 100 ppm SO_2 at 150 °C	[353]
$CeSnO_x/TiO_2$	500	500	5	-	30,000 h^{-1}	200–420	>90%	Relatively stable NO conversion with 5% H_2O and 100 ppm SO_2 at 220 °C	[354]
Sn-Ce-Ti oxides	500	500	5	-	30,000 h^{-1}	180–460	>90%	Stable NO conversion with 300 ppm SO_2 at 240 °C	[355]
$CuSO_4$-$CeSnTiO_x$	500	500	5	-	30,000 h^{-1}	240–340	>90%	Relatively stable NO conversion with of 5% H_2O and 100 ppm SO_2 at 240 °C	[356]
Co-Ce-Ti oxides	500	500	5	-	30,000 h^{-1}	200–440	~100%	Slowly deactivated with 5% H_2O and 100 ppm SO_2 at 180 °C	[357]
Ge-Ce-W oxides	1000	1000	2	-	50,000 h^{-1}	200–470	>95%	Deactivation with 100 ppm SO_2 at 220 °C	[358]
Ce–Nb oxides	650	650	5	-	120,000 $mL{\cdot}g^{-1}{\cdot}h^{-1}$	220–400	~100%	Stable NO conversion with 5% H_2O and 50 ppm SO_2 at 280 °C	[359]
$Ce_{0.4}Nb_{0.6}$ nanospheres	500	500	5	-	30,000 h^{-1}	250–450	>98%	Reversible deactivation with 200 ppm SO_2 at 300 °C	[360]
$Ce_{20}Nb_{20}Ti$ oxides	1000	1000	3	-	90,000 h^{-1}	250–460	>95%	Deactivated with 10% H_2O and 200 ppm SO_2 at 350 °C	[361]
Ce-Nb-Ti oxides	1000	1000	3	-	90,000 h^{-1}	250–500	>90%	Irreversible deactivation with 500 ppm SO_2	[362]
$Nb/CeSi_2$	500	500	4	-	60,000 h^{-1}	215–450	>80%	Relatively stable NO conversion with 5% H_2O and 200 ppm SO_2 at 250 °C	[363]
Ni-Ce-La oxides	1000	1000	5	-	20,000 h^{-1}	270–390	>90%	Stable NO conversion with 10% H_2O and 500 ppm SO_2 at 300 °C	[364]
$Mo\text{-}CeO_2/TiO_2$	500	500	5	-	128,000 h^{-1}	275–400	>90%	Relatively stable NO conversion with 5% H_2O and 50 ppm SO_2 at 300 °C	[365]
$Mo_{0.1}CeSi_2$	500	500	5	-	90,000 h^{-1}	215–400	>90%	100% NO_x conversion for10 h with 5% H_2O and 200 ppm SO_2 at 250 °C	[366]
Cr-Ce-Ti oxides	500	500	5	-	40,000 h^{-1}	182–405	>90%	Slowly deactivated with 5% H_2O and 100 ppm SO_2 at 250 °C	[367]
$Cr_1CeZr_2O_x$	600	600	5	5	108,000 h^{-1}	200–350	>90%	Stable NO conversion with 5% H_2O and 100 ppm SO_2 at 250 °C	[368]

Table 7. *Cont.*

Catalysts [1]	Reaction Conditions						NO_x Conversion (%)	Effects of H_2O/SO_2	Ref.
	NO (ppm)	NH_3 (ppm)	O_2 (vol%)	H_2O (vol%)	GHSV	T (°C)			
Zr-$CeTiO_x$	500	500	5	-	60,000 h^{-1}	200–375	>95%	Stable NO conversion with 5% H_2O and 50 ppm SO_2 at 225 °C	[369]
P-Ce-Zr-Ti oxides	800	720	3	-	30,000 h^{-1}	180–400	>80%	Relatively stable NO conversion with 5% H_2O and 200 ppm SO_2 at 300 °C	[370]
Ce-Sn-W-Ba oxides/TiO_2	930	930	10	-	8000 h^{-1}	235–470	>90%	Relatively stable NO conversion with 5% H_2O and 200 ppm SO_2 at 350 °C	[371]
CeO_2-WO_3-palygorskite/TiO_2	500	500	5	-	30,000 h^{-1}	240–400	>80%	Relatively stable NO_x conversion with 100 ppm SO_2 at 360 °C	[372]
Sulfated CeO_2-Rod	500	500	3	-	150,000 $mL \cdot g^{-1} \cdot h^{-1}$	300–450	~100%	Stable NO_x conversion with 5% H_2O and 100 ppm SO_2 at 250 °C	[373]
Sulfated CeO_2-ZrO_2	250	250	2.5	-	90,000 h^{-1}	250	90%	Relatively stable NO_x conversion with 200 ppm SO_2 at 250 °C	[374]
CeO_2@TiO_2 Core-shell	500	500	5	-	24,000 h^{-1}	200–450	>80%	Irreversible deactivation with 200 ppm SO_2 at 280 °C	[375]
CeO_2@TiO_2	500	500	5	-	36,000 h^{-1}	225–400	>95%	Relatively stable with 5% H_2O and 100 ppm SO_2 resistance at 350 °C	[376]

[1] HAT: halloysite.

Zhou et al. [344] utilized bimetallic MOFs to prepare $CeMO_x$ (M=Ti, Cu) catalysts, allowing the homogeneous distribution of promoters. The $CeTiO_x$ catalyst with high acidity and good redox properties with abundant Ce^{3+} and Ti^{4+} showed high NH_3-SCR activity from 180 to 300 °C and maintained stable performance in SO_2/H_2O at 225 °C [344]. Meanwhile, the aliovalent substitution of ceria by Cu^{2+} in $CeCuO_x$ formed oxygen vacancies and enhanced its redox properties but led to poor N_2 selectivity due to NH_3 over-oxidation [344]. Guo et al. [353] used Bi as the modifier to boost the performance of the Ce/TiO_2 catalyst for NH_3-SCR. The $CeBi/TiO_2$ catalyst with a proper Bi content showed a rather stable NO conversion in the presence of 5% H_2O and 100 ppm SO_2 at 150 °C because the addition of Bi could generate more Ce^{3+} and chemisorbed surface oxygen species, along with enhanced redox capability and surface acidity [353].

Jin et al. [371] investigated the role of each metal component in Ce-Sn-W-Ba-O_x/TiO_2 and found that TiO_2 provided sufficient acid sites, CeO_2 enhanced redox properties, weakened acid strength, and increased chemisorbed oxygen concentration, which helped to promote the activation and desorption of NH_3. They also reported that SnO_2 increased chemisorbed oxygen concentration, enhanced redox properties, and improved the activation rate of NH_3, WO_3 increased the amount of acid, and BaO enhanced resistance to water vapor and SO_2 [371]. A rather stable NO conversion was achieved at 350 °C in the presence of 5% H_2O and 200 ppm SO_2 [371].

Zeng et al. [346] prepared a P-doped CeO_2/TiO_2 catalyst by dispersing CeO_2 on strongly acidic and highly stable mesoporous P-doped TiO_2. The P-doped CeO_2/TiO_2 catalyst exhibited much higher catalytic activity than the CeO_2/TiO_2 catalyst at temperatures of 200–450 °C and a rather stable NO conversion even in the presence of 5% H_2O and 500 ppm SO_2 at 200 °C [346]. Mu et al. [354] synthesized an ordered mesoporous $CeSnO_x/TiO_2$ catalyst through a classical evaporation-induced self-assembly (EISA) strategy and ascribed the low-temperature NH_3-SCR activity to abundant reactive oxygen species (O_α), improving the surface acidity and redox capacity of the catalyst. This catalyst also showed a rather stable NO conversion even in the presence of 5% H_2O and 100 ppm SO_2 at 220 °C [354]. Mu et al. [356] prepared an ordered mesoporous catalyst, $CeSnTiO_x$, modified with copper sulfate and revealed that the copper sulfate-modified one increased the reaction sites (redox

site and acid site). They reported that Cu species can interfere with the electron cycle of the catalyst and reduce the strong redox performance of the Ce active site, which can effectively inhibit the adsorption of SO_2, while S-species (from SO_4^{2-}) can change the distribution of acid sites on the catalyst surface and the total acid content to realize a 'Fast NH_3-SCR' reaction [356]. This catalyst also showed a rather stable NO conversion even in the presence of 5% H_2O and 100 ppm SO_2 at 240 °C [356]. Liu et al. [377] prepared a series of W-modified Ce-Sn catalysts by the co-precipitation method and reported that the W species regulated the structure by promoting the formation of the Ce-doped tetragonal SnO_2 (*t*-Sn(Ce)O_2) active phase while preventing the generation of the Sn-doped cubic CeO_2 (*c*-Ce(Sn)O_2) phase. In addition, the highly dispersed W species on the surface of the $Ce_1W_{0.24}Sn_2O_x$ catalyst also coupled with Ce species to form new Ce-O-W active sites [377]. The W modification also promoted the ability of the catalysts to oxidize NO to NO_2 at 150–300 °C [377]. Liu et al. [378] reported the promotional effect of Ti in Ti-doped Ce–Sn mixed oxide (Ce–Sn–Ti) catalysts on the low-temperature NH_3-SCR. The appropriate doping Ti formed Sn–O-Ti, Sn–O-Ce and Ti–O-Ce structures, which could increase the content of Ce^{3+} through electron transfer from Sn or Ti to Ce ($Ce^{3+} + Ti^{4+} \rightarrow Ce^{4+} + Ti^{3+}$ and $2Ce^{4+} + Sn^{2+} \rightarrow 2Ce^{3+} + Sn^{4+}$) [378]. The solid solution structure increased specific surface areas, active sites (Ce^{3+}), and Lewis acid sites over the $Ce_{0.6}Sn_{2.4}Ti_2$ catalysts [378].

Yang et al. [379] reported that the emergence of Ce^{3+}–O–Ce^{3+} structural units induced by Mo doping in Mo-doped CeO_2 catalysts led to much better NH_3-SCR performance by achieving low-energy barrier activation of NH_3 molecules, thereby changing the dominant reaction mechanism in the catalytic reaction. They also observed the same trend in (W)-doped CeO_2 catalysts, further confirming the pivotal role of Ce^{3+}–O–Ce^{3+} structural units [379]. The addition of MoO_3 improved the activity of the CeO_2/TiO_2 catalyst for NH_3-SCR irrespective of the presence of H_2O and SO_2 because the introduction of Mo to the CeO_2/TiO_2 catalyst can suppress the adsorption of H_2O and SO_2 and the formation of surface sulfate species [365]. The MoO_3-promoted CeO_2/TiO_2 exhibited higher activity than CeO_2/TiO_2 even in the co-presence of H_2O and SO_2, showing relatively stable NO conversion in the presence of 5% H_2O and 50 ppm SO_2 at 300 °C [365]. Liu et al. [380] reported the enhanced NH_3-SCR performance of MoO_3/CeO_2 catalyst by introducing Cu to induce the generation of active Mo=O structure because the adding of Cu into MoO_3/CeO_2 catalyst could create unsaturated sites on CeO_2 for Mo anchor, and the enhanced electron transfer from Mo to Cu would cause the formation of a new terminal Mo=O with highly distorted octahedral geometry, which is a new Lewis acid site for coordinated NH_3 production. Meanwhile, the added Cu creates the adsorbed site for gaseous NO, and the formed Mo-O-Cu pair center facilitates the transformation of ionic NO_2^- generated from NO adsorption to NO_2, which is conducive to the 'Fast NH_3-SCR reaction' process [380]. Mo doping to CeO_2-SiO_2 mixed-oxide NH_3-SCR catalyst exhibited high low-temperature NH_3-SCR activity and superior N_2 selectivity and resistance to SO_2/H_2O poisoning [366]. The Mo-doped CeO_2-SiO_2 catalyst showed a rather stable NO conversion even in the presence of 5% H_2O and 200 ppm SO_2 at 250 °C [366]. Two elements (Mo and Cu) could be selected for doping into CeO_2 to promote the NH_3 adsorption of CeO_2-based materials by means of DFT calculations [381].

A comparison of NH_3-SCR activity among CeO_x supported on WO_3 nanorods (WO_3-NR) and WO_3 microspheres self-assembled by nanorods (WO_3-MP), and WO_3 nanoparticles (WO_3-NP) revealed that WO_3-NP enclosed with (0 0 1) facets of the hexagonal WO_3 showed the best redox ability due to the largest molar ratio of $W^{5+}/(W^{5+} + W^{6+})$, the highest concentration of Ce^{4+} on the surface of Ce/WO_3-NP, the strongest surface redox properties, and the largest molar ratio of $O_\alpha/(O_\alpha + O_\beta)$, which was beneficial for NH_3-SCR activity in the temperature range of 250–400 °C [382]. Hao et al. [103] designed a novel WO_x/Cu-CeO_2 oxide catalyst in which the WO_x species are highly dispersed on the {111}/{100}-terminated surface of Cu-doped CeO_2 nanospheres, which exhibits excellent NH_3-SCR performance over a wide operating temperature window (200–400 °C), as well as good sulfur resistance and N_2 selectivity. The stable NO conversion was obtained in the

presence of 5% H_2O and 100 ppm SO_2 at 250 °C [103]. They found that the Cu introduction into the lattice of CeO_2 not only increased the surface Ce^{3+} and oxygen vacancy concentration but also provided more sites for capture and dispersion of WO_x species, thus mediating and improving the Lewis and Brønsted acid sites and reducibility of catalyst [103]. They also found that electronic interaction between WO_x and Cu-doped CeO_2 was enhanced due to the existence of interactions of short-range Ce-O-Cu and Ce-O-W [103]. Fang et al. [383] designed a Ce_1–W_1/TiO_2 model catalyst by anchoring Ce_1–W_1 atom pairs on anatase TiO_2(001) to investigate the synergy between Ce and W in NH_3-SCR and found that the Ce_1–W_1 synergy not only shifted down the lowest unoccupied states of Ce_1 near the Fermi level, thus enhancing the abilities in adsorbing and oxidizing NH_3 but also makes the frontier orbital electrons of W_1 delocalized, thus accelerating the activation of O_2.

The promotional effect of Nb doping to CeO_2/TiO_2 in terms of the resistance to high GHSV, H_2O, and SO_2 was ascribed to the better dispersion of Ce, more chemisorbed oxygen species, and Ce^{3+}/Ce^{4+} redox pairs on the catalyst surface [361]. The $Ce_{20}Nb_{20}Ti$ catalyst was slowly deactivated in the presence of 10% H_2O and 200 ppm SO_2 at 300 °C [361]. Zhu et al. [360] prepared a series of porous Ce_xNb_{1-x} (x = 0, 0.2, 0.4, 0.6, 1) hollow nanospheres by a modified seed-mediated growth approach and found that a strong interaction between Nb_2O_5 and CeO_2 affected the oxygen defects, valence, reducibility, and the number of acid sites. The porous $Ce_{0.4}Nb_{0.6}$ nanospheres with more acid sites and excellent reducibility exhibited superior catalytic activity in the temperature range of 250–450 °C and high catalytic stability for H_2O and SO_2, showing reversible deactivation in the presence of 200 ppm SO_2 at 300 °C, which can be attributed to the porous double-shell structure and the strong interaction of Nb_2O_5 and CeO_2 species [360]. Jiang et al. [362] synthesized Ce-Nb-Ti metal oxide catalysts (CeNbTi) and found that CeNbTi prepared with the impregnation method possessed superior NH_3-SCR performance in the temperature range of 250–450 °C and better resistance to SO_2 and potassium, showing irreversible deactivation in the presence of 500 ppm SO_2. The best catalyst had relatively high concentrations of Ce^{3+} and chemisorbed oxygen, a strong synergistic effect among different components, and well-dispersed active species [362]. More importantly, the catalyst had stronger reduction capacity and a large number of Lewis acid sites, which contributed to its excellent catalytic performance [362]. Zhang et al. [359] synthesized CeO_2, Ce–Nb–O_x and Nb_2O_5 catalysts by the citric acid method and found that the mixed oxide Ce–Nb–O_x presented a higher NH_3-SCR activity than the single oxide CeO_2 or Nb_2O_5 catalyst. In addition, the Ce–Nb–O_x catalyst showed high resistance towards H_2O and SO_2 at 280 °C [359]. The incorporation of Nb provides abundant oxygen vacancies for capturing more surface adsorbed oxygen, which provides a superior redox capability and accelerates the renewal of active sites. Niobium pentoxide shows high surface acidity, which is partly retained in the Ce–Nb–O_x catalyst possessing a high content of Lewis and Brønsted acid sites [359]. Ding et al. [363] synthesized a set of catalysts for the $Nb/CeSi_2$ with different loadings of niobium and found that a catalyst for $20Nb/CeSi_2$ exhibited the best low-temperature NH_3-SCR performance while maintaining excellent SO_2/H_2O resistance, showing relatively stable NO conversion in the presence of 5% H_2O and 200 ppm SO_2 at 250 °C.

Since the redox properties of ceria can operate at medium and high temperatures, in order to achieve low-temperature NH_3-SCR activity, catalysts containing ceria should include Cu, Fe, and Mn together in the catalyst composition. Among them, Mn is the most promising metal component for this purpose according to the literature.

2.5. Other Catalysts

Generally, the surface concentration of vanadium is an important factor to determine the surface vanadium species such as monomeric vanadyl without V–O–V bonds, oligomeric vanadyl with V–O–V bridge, and crystallized V_2O_5 nanoparticles, which can be found at a low surface concentration (<2 V atoms/nm^2), moderate surface concentration (2–8 V atoms/nm^2), and high surface density (>8 V atoms/nm^2), respectively [7]. The polymeric vanadyl species have been reported to have a higher NH_3-SCR activity than the

monomeric vanadyl species because the coupling effect of the polymeric structure shortens the reaction pathway for the regeneration of redox sites [38]. Inomata et al. [384] reported that defective bulk vanadium oxide (V(V) + V(IV)) catalysts, synthesized by the calcination of vanadium(IV)-oxalate at 270 °C, showed NH_3-SCR activity at a low temperature below 150 °C. The transformation of crystalline V_2O_5 on low-vanadium-loading catalysts into an active polymeric vanadyl species under NH_3-SCR reaction conditions was reported to explain a remarkably enhanced catalytic performance of the vanadia-based catalyst at low temperatures [385]. Highly active supported oligomeric surface vanadia sites, which can provide exclusive centers for adsorbed bridging and bidentate nitrates and assist in NH_3 activation to generate amide intermediates, could be fabricated by transformation from monomeric surface VO_x sites from a classic supported V_2O_5–WO_3/TiO_2 catalyst via a H_2 plasma treatment [386]. Lin et al. [387] prepared vanadia supported on defective TiO_2 nanosheets, which demonstrated excellent NH_3-SCR performance over a wide temperature range of 140–380 °C. This catalyst was also resistant to H_2O and SO_2 poisoning, maintaining an NO conversion at 180 °C [387]. Hwang et al. [388] mechanochemically localized vanadia on the surface of WO_3-TiO_2 by physically grinding high-vanadia-loading V_2O_5/WO_3-TiO_2 with WO_3-TiO_2. They found that clustered vanadia sites exhibited enhanced activity for low-temperature (<250 °C) NH_3-SCR [388]. This catalyst also exhibited superior sulfur resistance at 220 °C because the exposed TiO_2 sites absorbed ABS from the clustered vanadia sites, preventing the blockage of the catalytic active sites [388].

A comparison of NH_3-SCR activity among V_2O_5, $Na_{0.33}V_2O_5$, and $Na_{1.2}V_3O_8$ synthesized by the oxalate method revealed that the reaction rate of $Na_{0.33}V_2O_5$ was 6.1-times higher than that of V_2O_5, indicating that Na intercalation accelerates NH_3-SCR cycles [389]. Bulk W-substituted vanadium oxide catalysts with the high redox ability and reactivity of Brønsted acid sites were reported to be active for NH_3-SCR at a low temperature (100–150 °C) and in the presence of water (~20 %). Lewis acid sites of W-substituted vanadium oxide are converted to Brønsted acid sites in the presence of water vapor, and NH_4^+ species adsorbed on Brønsted acid sites react with NO with the reduction of V^{5+} sites at 150 °C [390]. Zr-doped $CeVO_4$ solid solution catalysts showed excellent NH_3-SCR performance from 150 to 375 °C because of the increased Brønsted/Lewis acid sites and facilitated electron transfer among Ce, Zr, and V [391]. The $Ce_{0.85}Zr_{0.15}VO_4$ catalyst was slowly deactivated at 190 °C in the presence of 8% H_2O and 200 ppm SO_2 [391]. Furthermore, TiO_2 nanosheets promoted the activity and H_2O/SO_2 tolerance compared with TiO_2 nanoparticles for Zr–$CeVO_4/TiO_2$ catalysts [392]. However, TiO_2 nanosheets were slowly deactivated at 225 °C in the presence of 8% H_2O and 200 ppm SO_2 [392]. $FeVO_4/TiO_2$ was reported to show stable NO conversion in the presence of 200 ppm SO_2 at 190 °C and reversible deactivation due to 5% H_2O at 240 °C [393]. Kim et al. [394] prepared various $Ce_{0.5}RM_{0.5}V_1O_4$ catalysts in which half of Ce in TiO_2-supported $Ce_1V_1O_4$ was replaced by RM (Tb, Er, or Yb) and observed the promotive effect anticipated by RM substitution for $Ce_{0.5}RM_{0.5}V_1O_4$ only at high temperatures. $Ce_{0.5}Er_{0.5}V_1O_4$ possessed the greatest Lewis acidity/redox feature, thus revealing the best performance at elevated temperatures [394].

Liu et al. [395] prepared a serial of $W_aCo_{0.4}TiO_x$ catalysts (a = 0.04, 0.06, 0.08, 0.10) by the sol–gel method, and the $W_{0.08}Co_{0.4}TiO_x$ catalyst achieved the best NH_3-SCR activity at 190–430 °C and good resistance to H_2O/SO_2. However, the $W_{0.08}Co_{0.4}TiO_x$ catalyst was slowly deactivated at 280 °C in the presence of 100 ppm SO_2 [395]. The doping of W enhanced the acidity and weakened the oxidation capacity of $W_aCo_{0.4}TiO_x$, but the high surface acidity, especially the large number of Brønsted acid sites, can compensate for the effect of the reduced oxidation capacity on the low-temperature activity [395].

Phosphates are used in a variety of catalytic reactions due to their excellent thermal stability, proton conductivity, ion exchange, and acidity, and in P-doped CeO_2/TiO_2 catalysts, the amorphous $CePO_4$ species has been demonstrated to promote NH_3-SCR activity by activating the NH_4^+ species at the Brønsted acid site of the phosphate radical while generating NH_2 species that react with gaseous NO via the E–R mechanism [12]. The phosphorus is the acid site for NH_3 adsorption, and CeO_2 is the redox site. The NH_3-SCR proceeded

according to the L–H mechanism, and the excellent redox properties promoted the 'Fast NH_3-SCR' reaction after the introduction of 3% H_2O + 100 ppm SO_2 at 240 °C [396]. The Ce-O-P catalysts prepared with a sol–gel method exhibited enhanced NH_3-SCR activity due to increased surface acidity and redox capacity and improved SO_2 tolerance in the presence of 5% H_2O and 100 ppm SO_2 at 250 °C due to the effect of SO_2 capture by abundant reactive oxygen species [397]. Zhao et al. [398] synthesized a series of cerium phosphate catalysts with different crystal phases by hydrothermal method and co-precipitation method. Hexagonal cerium phosphate ($CePO_4$-H) showed better NH_3-SCR activity in the temperature range of 300–500 °C than monoclinic cerium phosphate ($CePO_4$-M) and mixed phases of $CePO_4$-H and $CePO_4$-M because $CePO_4$-H had much stronger surface acidity and more surface adsorbed oxygen species [398].

Fe- and Cu-based catalysts have been demonstrated to have enhanced high-temperature NH_3-SCR activity in the presence of SO_2 due to the increased acidity derived from the sulfate formed. However, supported sulfate catalysts have the disadvantage of exhibiting low-temperature NH_3-SCR activity due to their poor redox properties. Therefore, it is necessary to enhance the redox ability of the catalyst to improve its low-temperature NH_3-SCR activity. The active ingredient, sulfate, can prevent the formation of metal sulfates, but the deposition of AS/ABS with decreasing temperature is the main cause of catalyst deactivation. Therefore, future research on sulfate-based catalysts should focus on improving their redox capacity while promoting the degradation of AS/ABS [399]. NO_x reduction conversions and N_2 selectivity of sulfated CeO_2 cubes prepared by the impregnation of CeO_2 cubes by ammonium sulfates could be significantly improved compared with pure CeO_2 cubes. Sulfation treatment could create and strengthen Brønsted acid sites originated from the protons on surface sulfates, further facilitating ammonia adsorption and activation [400]. Yu et al. [401] prepared $CuSO_4/TiO_2$, $Fe_2(SO_4)_3/TiO_2$, $MnSO_4/TiO_2$, $Ce(SO_4)_2/TiO_2$, and $CoSO_4/TiO_2$ catalysts via a sol–gel protocol. The presence of SO_2 had little influence on the activity of all metal sulfate catalyst samples [401]. $CuSO_4/TiO_2$ showed the highest NH_3-SCR activity and apparent activation energy among the metal sulfate catalysts following the sequence of $CuSO_4/TiO_2$ < $Fe_2(SO_4)_3/TiO_2$ < $MnSO_4/TiO_2$ < $Ce(SO_4)_2/TiO_2$ < $CoSO_4/TiO_2$ [401]. The amount of acid sites was the main factor that influenced the catalytic activity of the metal sulfate catalysts [401].

3. Strategies to Improve the Low-Temperature NH_3-SCR Activity

The reaction mechanism for NH_3-SCR indicates that both surface acid site and redox property are required to complete the catalytic cycle. Two representative reaction mechanisms have been proposed for this reaction: The L–H and E–R mechanisms, which predominate at low and medium/high temperatures, respectively. In any case, adsorption of NH_3 on the surface acid sites followed by oxidative dehydrogenation is an important step in this reaction. Therefore, the NH_3-SCR catalyst surfaces must have specific acid sites that are required for the adsorption of NH_3 onto the catalyst surface. Lewis and Brønsted acidic sites enable the adsorption of NH_3 and conversion of NH_3 to NH_4^+, respectively, which is a prerequisite for the generation of the -NH_2 active species, and its subsequent interaction with NO_2 and NO species is an essential component of this reaction. The key to broadening the active temperature window of NH_3-SCR catalysts, including the low-temperature region, is to activate the N-H bond in the adsorbed NH_3. The oxidative activation of adsorbed NH_3 is very important. Dehydrogenation of NH_3 produces the active NH_2 species, and -NH_2 can react with gaseous NO or adsorbed NO/NO_2/nitrate, nitrite, and other species to form N_2. The oxidation capability of the catalyst surface determines the efficiency of NH_3 dehydrogenation; therefore, the surface redox sites of the catalyst play an important role. At low temperatures, the adsorption of NH_3 is not a significant obstacle; rather, the oxidation capacity of the catalyst itself becomes particularly important at low temperatures. However, it is important to note that the surface oxidation of the catalyst should not be too strong, as too much surface oxidation will result in the over-oxidation of NH_3 to NH or -N, resulting in the consumption of NH_3 and the production of significant amounts of N_2O

(Figure 7). The over-oxidation of NO_2 to NO_3^- also adversely affects NH_3-SCR activity and N_2 selectivity, since the formation of N_2O is usually due to the reaction of adsorbed -NH with gas-phase NO or surface-bound NH_4^+ with NO_3^- (Figure 7). Therefore, the oxidizing power of the catalyst should be 'just right,' meaning that it should have enough oxidizing power to remove the first H from NH_3, but not over-oxidize NH_3 to -NH.

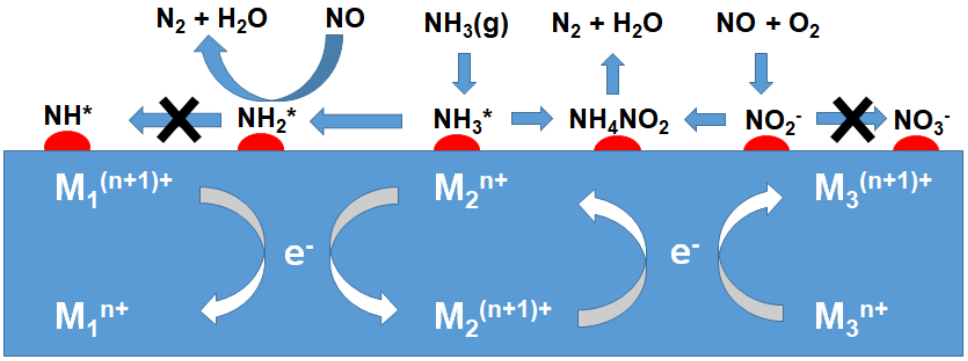

Figure 7. The schematic illustration of the plausible surface reactions during NH_3-SCR over multicomponent mixed metal oxide catalysts with multiple redox circles to avoid over-oxidation of NH_3 [12,166].

Many researchers have observed that low-temperature NH_3-SCR reactions occur primarily through the L–H mechanism. NO_2, nitrite, and nitrate species are important intermediates in the L–H mechanism, and the activation of NO to NO_2 (gas phase or adsorption) is very important. The importance of NO_2 generation by NO oxidation can also be seen from the fact that NO_2 contributes to the occurrence of the 'Fast NH_3-SCR' pathway. It is widely recognized that when a certain amount of NO_2 coexists with NO, the reaction rate increases significantly, resulting in 'Fast NH_3-SCR', which significantly improves NH_3-SCR performance. Koebel et al. [402,403] first discovered that partial conversion of NO to NO_2 with the help of an oxidizing catalyst greatly improved the catalytic performance of the NH_3-SCR, especially at low temperatures. The optimal NO_2:NO ratio is 1:1, which allows all NO_x to react through a 'Fast NH_3-SCR' reaction. The evolution of NO_2 into nitrate and nitrite after adsorption is also important. Nitrite/nitrate bonding can occur to form monodentate nitrate, linear nitrite, bridging nitrate, and bidentate nitrate. These nitrates/nitrites have specific reactivity at certain temperatures; the level of reactivity depends on the catalyst system. In general, low-stability nitrates/nitrites react with NH_4^+ at low temperatures and contribute to enhanced low-temperature activity, whereas high-stability nitrates/nitrites are detrimental to low-temperature activity because they are too stable to react with NH_x species and thus poison the active site.

Some promising strategies to improve the acidity and redox properties of metal oxide catalysts have been proposed, such as modification or doping of transition and rare earth metals, optimization of preparation methods, generation of new nanostructures, morphology modification, exposure of specific crystal faces, etc. [12]. As shown in the previous sections, MnO_x-based catalysts exhibit very good low-temperature NH_3-SCR activity but always produce a large amount of by-product N_2O. In order to regulate the redox property and surface acidity of MnO_x catalysts, multicomponent Mn-based composite oxides have been reported. They generally contain VO_x, Fe_2O_3, or CuO as the main active metal oxides and Al_2O_3, SiO_2, TiO_2, CrO_x, CoO_x, NiO, Y_2O_3, ZrO_2, NbO_x, MoO_x, AgO_x, SnO_2, SbO_x, LaO_x, CeO_x, PrO_x, NdO_x, SmO_x, EuO_x, GdO_x, DyO_x, HoO_x, ErO_x, TmO_x, TaO_x, and WO_3 as promoters. The creation of a multi redox cycle over a multicomponent oxide catalyst effectively promotes electron transfer and facilitates the adsorption/activation of NO/NH_3 (Figure 7).

Highly dispersed metal oxide composites can be prepared by utilizing MOF [375,404–406] or LDH [216,407–409] as precursors and constructing solid solution catalysts. Designing specific nanostructures such as nanoneedles, nanospheres, nanotubes, or core-shell

structures can increase the amount of acid sites/reactive oxygen species and promote the formation of active species. Selective exposure of certain facets of the active ingredient, such as MnO_x and Fe_2O_3, as well as TiO_2 and CeO_2 support, can improve redox/acidic properties and metal-support interactions. Additionally, acidification or functionalization of the support with specific acids or oxygen/nitrogen-containing groups can significantly improve acidity and the interaction between the active ingredient and support.

4. Strategies to Improve the H_2O/SO_2 Tolerance at Low Temperatures

Since water vapor is an unavoidable part of real flue gas, its effect on NH_3-SCR activity has been an important issue. Positive or negative effects have been reported depending on the reaction conditions (e.g., reaction temperature), catalyst, and reducing agent [410,411]. Although the negative effect of water vapor on NH_3-SCR activity over low-temperature catalysts has been frequently reported due to its competitive adsorption of NH_3 and/or NO onto the active sites, regardless of the L–H and E–R mechanisms, irreversible deactivation was seldom reported and reversible deactivation was commonly observed, where initial catalytic activity could be recovered after stopping the introduction of water vapor into the feed [412]. Controlling the surface hydrophobicity of the catalyst by incorporating hydrophobic metal oxide shells into the active site [293] or using hydrophobic supports [33,34] can be effective in minimizing the adverse effects of water at low temperatures.

In contrast to the effect of water vapor, SO_2 has been reported to have a negative effect on NH_3-SCR catalytic activity and is known to cause irreversible deactivation, especially for low-temperature catalysts [19,31,412–415], which limits the practical application of low-temperature catalysts.

There are several strategies to improve the SO_2 tolerance of catalysts: (1) reducing the adsorption of SO_2 and its subsequent oxidation; (2) improving the adsorption of NH_3 and NO to form active intermediates in the presence of surface sulfate species; (3) building sacrificial sites to protect active sites; (4) promoting the decomposition of sulfate; and (5) searching for SO_2-tolerant compounds with good NH_3-SCR activity [12].

(1) Reducing the adsorption of SO_2 and its subsequent oxidation. Inhibiting the adsorption and oxidation of SO_2 can significantly reduce the deposition of sulfates. Increasing the acidity of the catalyst can reduce SO_2 adsorption to some extent. However, on the other hand, more NH_3 can also be adsorbed on the surface acidic sites, promoting the formation of ammonium sulfate. Therefore, it is important to fine-tune the surface acidity to reduce the adsorption of SO_2 and NH_3 simultaneously. The introduction of SiO_2, Al_2O_3, and TiO_2 to the low-temperature NH_3-SCR catalysts might be effective for this purpose. Inactive metal sulfates and ammonium sulfates (i.e., AS and ABS) are derived from the reaction of SO_3 with metal oxides and NH_3, respectively, so it is necessary to inhibit the oxidation of SO_2 to SO_3 by decreasing the oxidation ability of active sites via adding electron-donating promoters [282,310]. Since NO_2, which can form under 'Fast NH_3-SCR' conditions at low temperatures, can promote the oxidation of SO_2 to SO_3, designing a catalyst that can follow the 'Fast NH_3-SCR' while inhibiting the oxidation of SO_2 to SO_3 is challenging but necessary to achieve high low-temperature NH_3-SCR activity as well as SO_2 tolerance (Figure 8).

(2) Improving the adsorption of NH_3 and NO to form active intermediates in the presence of surface sulfate species. When the active sites begin to be sulfated by SO_x, the redox capacity of the active sites is reduced, and this leads to a decrease in NH_3-SCR activity, especially at low temperatures. Active NO_x species are adsorbed competitively with SO_x, but the adsorption of NH_4^+ species is generally enhanced by new Brønsted acid sites derived from the deposited sulfate. Therefore, improving the adsorption of active nitrite/nitrate and gaseous NO_2 species in the presence of sulfate species is important to achieve SO_2 durability in NH_3-SCR reactions that follow the L–H mechanism. Compared with un-doped catalysts, more NH_4^+, nitrates, and NO_2 were formed on Eu-modified Mn/TiO_2 [278] and Zr-modified $Fe–Mn/TiO_2$ [187] catalysts following the L–H mechanism, leading to improved SO_2 tolerance. If the catalyst

follows the E–R mechanism, where the active NH_3 and NH_4^+ species react directly with gaseous NO, this can lead to high SO_2 tolerance as NO does not need to be competitively adsorbed onto the catalyst surface as nitrate or nitrite. However, the E–R mechanism is not prevalent at low temperatures.

(3) Building sacrificial sites to protect active sites. A rather simple strategy in which H-Y zeolite was physically mixed with V_2O_5/TiO_2 to trap ABS was reported to be effective to protect vanadium active sites, maintaining stable performance in the presence of 10% H_2O and 30 ppm SO_2 at a low temperature of 220 °C [416]. Ceria is well known to interact with SO_2 to form $CeSO_4$ or $Ce_2(SO_4)_3$, which can be used as a sacrificial site to protect the main active phase from sulfation, thereby improving the SO_2 tolerance of the catalyst [417]. Cr [173] and Nb [188] were also reported to react with SO_2 preferentially to prevent the sulfuration of active metal oxides (Figure 8). Designing a core–shell structure with outer sacrificial sites for SO_x adsorption and ammonium sulfate deposition and inner active sites for NH_3-SCR can effectively protect active sites from sulfate deposition [17,22,23,216,418,419].

(4) Promoting the decomposition of sulfates. Ammonium sulfate and metal sulfate are two common sulfates observed during NH_3-SCR in the presence of SO_2. The former can be deposited on the catalyst and block surface active sites, but can be removed by water washing and heat treatment. However, the thermally stable metal sulfates formed through sulfation of active sites irreversibly deactivate the catalysts. Compared with metal sulfates, ammonium sulfates (AS and ABS) can decompose at lower temperatures. Therefore, reducing the decomposition temperature of ammonium sulfates can improve the SO_2 tolerance at lower temperatures. It was found that ABS decomposed more easily on SBA-15 with larger pores [330]. Therefore, it can be said that the decomposition of ammonia sulfate can be facilitated via constructing some mesoporous structure. Since metal sulfates are very difficult to decompose at low temperatures, it is desirable to interfere with their formation by adding suitable electrophilic or nucleophilic additives that can interact strongly with SO_4^{2-} and metal cations [12]. Chen et al. [420] proposed to place a single Mo atom on TiO_2 to form a Mo-Ti acid-base double site on Mo and Ti that can adsorb NH_4^+ and HSO_4^- from ABS, respectively. When NH_4^+ is oxidized by surface lattice oxygen on the Mo site, the electrons left on the dual site will transfer to the adsorbed HSO_4^- on the Ti site, releasing SO_2 at low temperatures. Fe doping [310] and Sb addition [195] were also reported to promote the decomposition of ammonium sulfate and inhibit the formation of $MnSO_4$.

(5) Searching for SO_2-resistant compounds. Some metal sulfates, including $CuSO_4$ and $FeSO_4$, are known to have improved SO_2 tolerance, but due to their poor redox properties, they can exhibit NH_3-SCR activity only at moderate and/or high temperatures. Therefore, it is necessary to improve the redox properties of the catalyst to enhance its low-temperature activity. Nevertheless, the removal of deposited ammonia sulfate is not easy at low temperatures, and the resulting catalyst deactivation is inevitable. Therefore, future research should focus on preventing the deposition of ammonia sulfate at low temperatures or promoting its decomposition even if it is deposited while enhancing its redox ability.

The strategies mentioned above may seem different, but they are closely related. Considering all the above strategies, a promising low-temperature NH_3-SCR catalyst could have the following properties:

(1) The active site must be composed of a multi-component metal oxide with moderate oxidation capacity not to oxidize SO_2 to SO_3, but still retain the oxidation capacity to oxidize NO to NO_2 and follow the 'Fast NH_3-SCR' pathway. Different catalyst compositions can be screened by DFT calculations that allow for the comparison of competing oxidation reactions, including SO_2 oxidation and NO oxidation, on the proposed catalyst surface [421–423]. The other type of active site is the promoted metal sulfate, which has both a high oxidation capacity to activate adsorbed NO species to

follow the L–H reaction mechanism and the ability to decompose ammonium sulfate at low temperatures.

(2) The active site mentioned above should be protected from the adsorption of SO_x and/or the ammonium sulfate produced by introducing some kind of sacrificial and/or protective component on or near the surface of the active site. The surface acidity, pore structure, and surface composition of the protective layer must be fine-tuned to take into account the adsorption property of SO_x and the decomposition of ammonium sulfate.

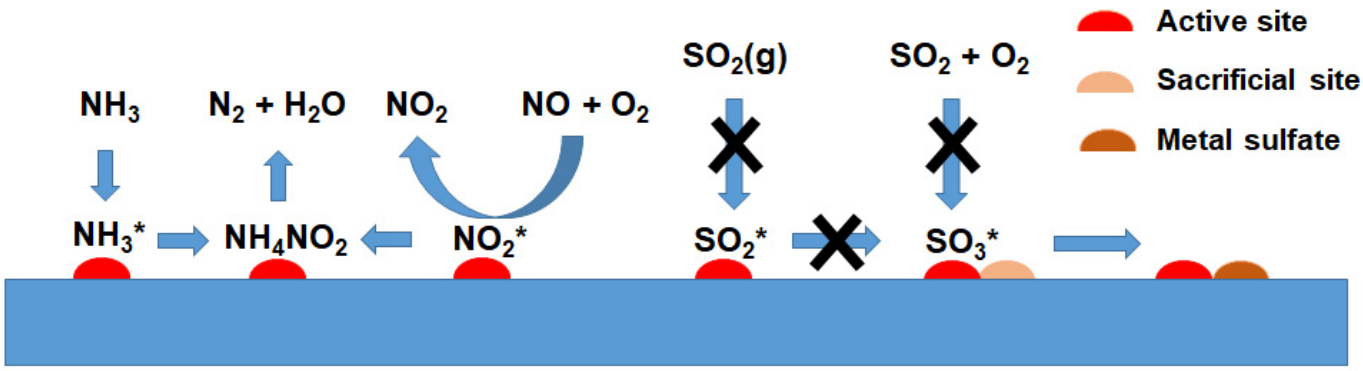

Figure 8. The schematic illustration of the plausible surface reactions during low-temperature NH_3-SCR in the presence of SO_2.

5. Summary

The redox properties and surface acidity are important factors affecting the catalytic activity of NH_3-SCR. Ammonia is adsorbed on the Lewis and Brønsted acid sites in the form of NH_3 and NH_4^+, respectively, and is oxidatively dehydrogenated to form active intermediates. NO can react directly with adsorbed intermediates derived from NH_3 in the E–R mechanism, or in the L–H mechanism prevalent at low temperatures, NO can be adsorbed as is or oxidized to NO_2 and then adsorbed and react with adsorbed ammonia or ammonia derivatives. Moderate redox properties are very important for low-temperature NH_3-SCR catalysts, as strong redox properties can reduce N_2 selectivity due to the formation of unwanted N_2O, and weak redox properties can reduce the overall denitrification rate.

Water vapor and SO_x are often found in flue gas along with NO_x, and their effect on NH_3-SCR activity is particularly important at low temperatures. Water vapor in flue gas can cause reversible deactivation because it adsorbs competitively with NO_x and ammonia for active sites. SO_2 in flue gas can adsorb strongly to the active site or oxidize to SO_3 and further react with ammonia in the presence of water vapor to form ammonium bisulfate and/or ammonium sulfate, which irreversibly blocks the active site. SO_3 can react directly with active metal oxides to form metal sulfates with weak redox properties, resulting in low NH_3-SCR activity at low temperatures.

Among Cu-, Fe-, Mn-, and Ce-based catalysts, Mn-containing multivalent metal oxides can be promising candidates for low-temperature NH_3-SCR. The redox properties of MnO_x can be tuned by the incorporation of other multivalent metal oxides. The electronic properties of the active metal can be fine-tuned by adding appropriate promoters. The reduction of NH_3-SCR activity by water vapor can be overcome by increasing the surface hydrophobicity, which can be accomplished by using a hydrophobic support or by applying a hydrophobic sheath to the outside of the active metal oxide. When selecting the active metal oxide, DFT calculations should be performed to compare SO_2 adsorption, NO oxidation, and SO_2 oxidation to ensure that the oxidation of NO occurs without the adsorption of SO_2 and the oxidation of SO_2, allowing 'Fast NH_3-SCR' to proceed. The mesoporous shell will not only help to remove ammonium sulfate at the reaction temperature but also prevent SO_2 poisoning. Metal sulfate catalysts with strong redox properties and V-based

catalysts containing oligomeric vanadyl species with sulfur-resistant properties still need to be further investigated for application in NH_3-SCR at low temperatures.

Funding: This research was supported by the Ministry of Trade, Industry and Energy (MOTIE), and the Korea Evaluation Institute of Industrial Technology (KEIT) (No. 20026357).

Data Availability Statement: The original contributions presented in the study are included in the article; further inquiries can be directed to the corresponding author.

Acknowledgments: E.D.P. would like to thank Seohyeon Park, Eunyeong Yang, Jung Hun Maeng, and Bohyeon Hwang for their editorial assistance.

Conflicts of Interest: The author declare no conflicts of interest.

References

1. Asghar, U.; Rafiq, S.; Anwar, A.; Iqbal, T.; Ahmed, A.; Jamil, F.; Khurram, M.S.; Albar, M.M.; Farooq, A.; Shah, N.S.; et al. Review on the progress in emission control technologies for the abatement of CO_2, SO_x and NO_x from fuel combustion. *J. Environ. Chem. Eng.* **2021**, *9*, 106064. [CrossRef]
2. Zhu, X.; Du, J.; Yu, Z.; Cheng, Y.B.; Wang, Y. NO_x Emission and control in ammonia combustion: State-of-the-art review and future perspectives. *Energy Fuels* **2023**, *38*, 43–60. [CrossRef]
3. Yao, N.; Pan, W.; Zhang, J.; Wei, L. The advancement on carbon-free ammonia fuels for gas turbine: A review. *Energy Convers Manag.* **2024**, *315*, 118745. [CrossRef]
4. Park, Y.K.; Kim, B.S. Catalytic removal of nitrogen oxides (NO, NO_2, N_2O) from ammonia-fueled combustion exhaust: A review of applicable technologies. *Chem. Eng. J.* **2023**, *461*, 141958. [CrossRef]
5. Liu, Y.; Zhang, W.; Chen, W. Denitrification technology and the catalysts: A review and recent advances. *ChemCatChem* **2024**, *16*, e202301662. [CrossRef]
6. Elkaee, S.; Phule, A.D.; Yang, J.H. Advancements in selective catalytic reduction (SCR) technologies for NO_x reduction: A comprehensive review of reducing agents. *Process Saf. Environ. Prot.* **2024**, *184*, 854–880. [CrossRef]
7. Lai, J.K.; Wachs, I.E. A perspective on the selective catalytic reduction (SCR) of NO with NH_3 by supported V_2O_5–WO_3/TiO_2 catalysts. *ACS Catal.* **2018**, *8*, 6537–6551. [CrossRef]
8. Li, Y.; Zhang, T.; Niu, X.; Zhu, Y. Vanadium-based catalysts for selective catalytic reduction of NO_x with ammonia: Synthesis, poisoning mechanism, regeneration methods and research prospects. *Fuel* **2024**, *365*, 131184. [CrossRef]
9. Ye, B.; Jeong, B.; Lee, M.J.; Kim, T.H.; Park, S.S.; Jung, J.; Lee, S.; Kim, H.D. Recent trends in vanadium-based SCR catalysts for NO_x reduction in industrial applications: Stationary sources. *Nano Converg.* **2022**, *9*, 51. [CrossRef]
10. Schreifels, J.J.; Wang, S.; Hao, J. Design and operational considerations for selective catalytic reduction technologies at coal-fired boilers. *Front. Energy* **2012**, *6*, 98–105. [CrossRef]
11. Lin, D.; Zhang, L.; Liu, Z.; Wang, B.; Han, Y. Progress of selective catalytic reduction denitrification catalysts at wide temperature in carbon neutralization. *Front. Chem.* **2022**, *10*, 946133. [CrossRef] [PubMed]
12. Han, L.; Cai, S.; Gao, M.; Hasegawa, J.Y.; Wang, P.; Zhang, J.; Shi, L.; Zhang, D. Selective catalytic reduction of NO_x with NH_3 by using novel catalysts: State of the art and future prospects. *Chem. Rev.* **2019**, *119*, 10916–10976. [CrossRef] [PubMed]
13. Chen, W.; Zou, R.; Wang, X. Toward an atomic-level understanding of the catalytic mechanism of selective catalytic reduction of NO_x with NH_3. *ACS Catal.* **2022**, *12*, 14347–14375. [CrossRef]
14. Chen, J.; Guan, B.; Liu, Z.; Wu, X.; Guo, J.; Zheng, C.; Zhou, J.; Su, T.; Han, P.; Yang, C.; et al. Review on advances in structure–activity relationship, reaction & deactivation mechanism and rational improving design of selective catalytic reduction deNO_x catalysts: Challenges and opportunities. *Fuel* **2023**, *343*, 127924. [CrossRef]
15. Shi, Z.; Peng, Q.; Jiaqiang, E.; Xie, B.; Wei, J.; Yin, R.; Fu, G. Mechanism, performance and modification methods for NH_3-SCR catalysts: A review. *Fuel* **2023**, *331*, 125885. [CrossRef]
16. Raja, S.A.M.S.; Alphin, M.S.; Sivachandiran, L. Promotional effects of modified TiO_2-and carbon-supported V_2O_5-and MnO_x-based catalysts for the selective catalytic reduction of NO_x: A review. *Catal. Sci. Technol.* **2020**, *10*, 7795–7813. [CrossRef]
17. Zhang, M.; Guan, Z.; Qiao, Y.; Zhou, S.; Chen, G.; Guo, R.; Pan, W.; Wu, J.; Li, F.; Ren, J. The impact of catalyst structure and morphology on the catalytic performance in NH_3-SCR reaction: A review. *Fuel* **2024**, *361*, 130541. [CrossRef]
18. Damma, D.; Ettireddy, P.R.; Reddy, B.M.; Smirniotis, P.G. A review of low temperature NH_3-SCR for removal of NO_x. *Catalysts* **2019**, *9*, 349. [CrossRef]
19. Wang, H.; Huang, B.; Yu, C.; Lu, M.; Huang, H.; Zhou, Y. Research progress, challenges and perspectives on the sulfur and water resistance of catalysts for low temperature selective catalytic reduction of NO_x by NH_3. *Appl. Catal. A Gen.* **2019**, *588*, 117207. [CrossRef]
20. Zhu, H.; Song, L.; Li, K.; Wu, R.; Qiu, W.; He, H. Low-temperature SCR catalyst development and industrial applications in China. *Catalysts* **2022**, *12*, 341. [CrossRef]
21. Liu, C.; Wang, H.; Zhang, Z.; Liu, Q. The latest research progress of NH_3-SCR in the SO_2 resistance of the catalyst in low temperatures for selective catalytic reduction of NO_x. *Catalysts* **2020**, *10*, 1034. [CrossRef]

22. Wu, T.; Guo, R.T.; Li, C.F.; You, Y.H.; Pan, W.G. Recent advances in core-shell structured catalysts for low-temperature NH_3-SCR of NO_x. *Chemosphere* **2023**, *333*, 138942. [CrossRef] [PubMed]
23. Li, H.; Schill, L.; Fehrmann, R.; Riisager, A. Recent developments of core–shell structured catalysts for the selective catalytic reduction of NO_x with ammonia. *Inorg. Chem. Front.* **2023**, *10*, 727–755. [CrossRef]
24. Liu, G.; Zhang, H.; Li, Y.; Wang, P.; Zhan, S. Selective catalytic reduction of NO_x with NH_3 over copper-based catalysts: Recent advances and future prospects. *EES Catal.* **2024**, *2*, 231–252. [CrossRef]
25. Zhang, K.; Luo, N.; Huang, Z.; Zhao, G.; Chu, F.; Yang, R.; Tang, X.; Wang, G.; Gao, F.; Huang, X. Recent advances in low-temperature NH_3-SCR of NO_x over Ce-based catalysts: Performance optimizations, reaction mechanisms and anti-poisoning countermeasures. *Chem. Eng. J.* **2023**, *476*, 146889. [CrossRef]
26. Zhou, J.; Guo, R.T.; Zhang, X.F.; Liu, Y.Z.; Duan, C.P.; Wu, G.L.; Pan, W.G. Cerium oxide-based catalysts for low-temperature selective catalytic reduction of NO_x with NH_3: A review. *Energy Fuels* **2021**, *35*, 2981–2998. [CrossRef]
27. Yao, X.J.; Gong, Y.T.; Li, H.L.; Yang, F.M. Research progress of ceria-based catalysts in the selective catalytic reduction of NO_x by NH_3. *Acta Phys. -Chim. Sin.* **2015**, *31*, 817–828. [CrossRef]
28. Xu, J.; Zhang, Y.; Zou, X.; Tang, T.; Zhang, Q.; Guo, F.; Liu, H. Recent advances and perspectives in the resistance of SO_2 and H_2O of cerium-based catalysts for NO_x selective catalytic reduction with ammonia. *New J. Chem.* **2022**, *46*, 2053–2067. [CrossRef]
29. Zhang, Z.; Li, J.; Tian, J.; Zhong, Y.; Zou, Z.; Dong, R.; Gao, S.; Xu, W.; Tan, D. The effects of Mn-based catalysts on the selective catalytic reduction of NO_x with NH_3 at low temperature: A review. *Fuel Process. Technol.* **2022**, *230*, 107213. [CrossRef]
30. Xu, G.; Guo, X.; Cheng, X.; Yu, J.; Fang, B. A review of Mn-based catalysts for low-temperature NH_3-SCR: NO x removal and H_2O/SO_2 resistance. *Nanoscale* **2021**, *13*, 7052–7080. [CrossRef]
31. Wei, L.G.; Guo, R.T.; Zhou, J.; Qin, B.; Chen, X.; Bi, Z.X.; Pan, W.G. Chemical deactivation and resistance of Mn-based SCR catalysts for NO_x removal from stationary sources. *Fuel* **2022**, *316*, 123438. [CrossRef]
32. Ogugua, P.C.; Wang, E.; Jinyang, Z.; Wang, Q.; Su, H. Advancements in low-temperature NH_3-SCR of NO_x using Ba-based catalysts: A critical review of preparation, mechanisms, and challenges. *Environ. Sci. Pollut. Res.* **2023**, *30*, 84972–84998. [CrossRef] [PubMed]
33. Wang, L.; Liu, M.; Ren, S.; Li, X.; Chen, Z.; Wang, M.; Chen, T.; Yang, J. Recent advance for NO_x removal with carbonaceous material for low-temperature NH_3-SCR reaction. *Catal. Today* **2023**, *418*, 114053. [CrossRef]
34. Huang, G.; Yang, J.; Lv, C.; Li, D.; Fang, D. Research progress of NH_3-SCR over carbon-based catalysts for NO_x removal. *J. Environ. Chem. Eng.* **2023**, *11*, 110966. [CrossRef]
35. Guo, K.; Ji, J.; Song, W.; Sun, J.; Tang, C.; Dong, L. Conquering ammonium bisulfate poison over low-temperature NH_3-SCR catalysts: A critical review. *Appl. Catal. B* **2021**, *297*, 120388. [CrossRef]
36. Arnarson, L.; Falsig, H.; Rasmussen, S.B.; Lauritsen, J.V.; Moses, P.G. A complete reaction mechanism for standard and fast selective catalytic reduction of nitrogen oxides on low coverage VO_x/TiO_2 (0 0 1) catalysts. *J. Catal.* **2017**, *346*, 188–197. [CrossRef]
37. Topsoe, N.Y.; Dumesic, J.A.; Topsoe, H. Vanadia-titania catalysts for selective catalytic reduction of nitric-oxide by ammonia: II Studies of active sites and formulation of catalytic cycles. *J. Catal.* **1995**, *151*, 241–252. [CrossRef]
38. He, G.; Lian, Z.; Yu, Y.; Yang, Y.; Liu, K.; Shi, X.; Yan, Z.; Shan, W.; He, H. Polymeric vanadyl species determine the low-temperature activity of V-based catalysts for the SCR of NO_x with NH_3. *Sci. Adv.* **2018**, *4*, eaau4637. [CrossRef]
39. Chen, X.; Yu, S.; Liu, W.; Zhang, S.; Liu, S.; Feng, Y.; Zhang, X. Recent advance on cobalt-based oxide catalyst for the catalytic removal of volatile organic compounds: A review. *Resour. Chem. Mater.* **2022**, *1*, 27–46. [CrossRef]
40. Jo, D.; Ryu, T.; Park, G.T.; Kim, P.S.; Kim, C.H.; Nam, I.S.; Hong, S.B. Synthesis of high-silica LTA and UFI zeolites and NH_3–SCR performance of their copper-exchanged form. *ACS Catal.* **2016**, *6*, 2443–2447. [CrossRef]
41. Ryu, T.; Kim, H.; Hong, S.B. Nature of active sites in Cu-LTA NH_3-SCR catalysts: A comparative study with Cu-SSZ-13. *Appl. Catal. B* **2019**, *245*, 513–521. [CrossRef]
42. Tarach, K.A.; Jabłońska, M.; Pyra, K.; Liebau, M.; Reiprich, B.; Gläser, R.; Góra-Marek, K. Effect of zeolite topology on NH_3-SCR activity and stability of Cu-exchanged zeolites. *Appl. Catal. B* **2021**, *284*, 119752. [CrossRef]
43. Zhang, T.; Shi, J.; Liu, J.; Wang, D.; Zhao, Z.; Cheng, K.; Li, J. Enhanced hydrothermal stability of Cu-ZSM-5 catalyst via surface modification in the selective catalytic reduction of NO with NH_3. *Appl. Surf. Sci.* **2016**, *375*, 186–195. [CrossRef]
44. Park, J.H.; Park, H.J.; Baik, J.H.; Nam, I.S.; Shin, C.H.; Lee, J.H.; CHO, B.K.; Oh, S.H. Hydrothermal stability of CuZSM5 catalyst in reducing NO by NH_3 for the urea selective catalytic reduction process. *J. Catal.* **2006**, *240*, 47–57. [CrossRef]
45. Wang, H.; Xu, R.; Jin, Y.; Zhang, R. Zeolite structure effects on Cu active center, SCR performance and stability of Cu-zeolite catalysts. *Catal. Today* **2019**, *327*, 295–307. [CrossRef]
46. Wilken, N.; Nedyalkova, R.; Kamasamudram, K.; Li, J.; Currier, N.W.; Vedaiyan, R.; Yezerets, A.; Olsson, L. Investigation of the effect of accelerated hydrothermal aging on the Cu sites in a Cu-BEA catalyst for NH_3-SCR applications. *Top. Catal.* **2013**, *56*, 317–322. [CrossRef]
47. Zhao, Z.; Yu, R.; Zhao, R.; Shi, C.; Gies, H.; Xiao, F.S.; Vos, D.D.; Yokoi, T.; Bao, X.; Kolb, U.; et al. Cu-exchanged Al-rich SSZ-13 zeolite from organotemplate-free synthesis as NH_3-SCR catalyst: Effects of Na^+ ions on the activity and hydrothermal stability. *Appl. Catal. B* **2017**, *217*, 421–428. [CrossRef]
48. Xie, L.; Liu, F.; Ren, L.; Shi, X.; Xiao, F.S.; He, H. Excellent performance of one-pot synthesized Cu-SSZ-13 catalyst for the selective catalytic reduction of NO_x with NH_3. *Environ. Sci. Technol.* **2014**, *48*, 566–572. [CrossRef]

49. Fickel, D.W.; D'Addio, E.; Lauterbach, J.A.; Lobo, R.F. The ammonia selective catalytic reduction activity of copper-exchanged small-pore zeolites. *Appl. Catal. B* **2011**, *102*, 441–448. [CrossRef]
50. Shan, Y.; Shan, W.; Shi, X.; Du, J.; Yu, Y.; He, H. A comparative study of the activity and hydrothermal stability of Al-rich Cu-SSZ-39 and Cu-SSZ-13. *Appl. Catal. B* **2020**, *264*, 118511. [CrossRef]
51. Li, R.; Zhu, Y.; Zhang, Z.; Zhang, C.; Fu, G.; Yi, X.; Huang, Q.; Yang, F.; Liang, W.; Zheng, A.; et al. Remarkable performance of selective catalytic reduction of NO_x by ammonia over copper-exchanged SSZ-52 catalysts. *Appl. Catal. B* **2021**, *283*, 119641. [CrossRef]
52. Cao, Y.; Fan, D.; Tian, P.; Cao, L.; Sun, T.; Xu, S.; Yang, M.; Liu, Z. The influence of low-temperature hydration methods on the stability of Cu-SAPO-34 SCR catalyst. *Chem. Eng. J.* **2018**, *354*, 85–92. [CrossRef]
53. Jo, D.; Lim, J.B.; Ryu, T.; Nam, I.S.; Camblor, M.A.; Hong, S.B. Unseeded hydroxide-mediated synthesis and CO_2 adsorption properties of an aluminosilicate zeolite with the RTH topology. *J. Mater. Chem. A Mater.* **2015**, *3*, 19322–19329. [CrossRef]
54. Zhu, J.; Liu, Z.; Xu, L.; Ohnishi, T.; Yanaba, Y.; Ogura, M.; Wakihara, T.; Okubo, T. Understanding the high hydrothermal stability and NH_3-SCR activity of the fast-synthesized ERI zeolite. *J. Catal.* **2020**, *391*, 346–356. [CrossRef]
55. Wei, X.; Ke, Q.; Cheng, H.; Guo, Y.; Yuan, Z.; Zhao, S.; Sun, T.; Wang, S. Seed-assisted synthesis of Cu-(Mn)-UZM-9 zeolite as excellent NO removal and N_2O inhibition catalysts in wider temperature window. *Chem. Eng. J.* **2020**, *391*, 123491. [CrossRef]
56. Lee, J.H.; Kim, Y.J.; Ryu, T.; Kim, P.S.; Kim, C.H.; Hong, S.B. Synthesis of zeolite UZM-35 and catalytic properties of copper-exchanged UZM-35 for ammonia selective catalytic reduction. *Appl. Catal. B* **2017**, *200*, 428–438. [CrossRef]
57. Wang, X.; Xu, Y.; Zhao, Z.; Liao, J.; Chen, C.; Li, Q. Recent progress of metal-exchanged zeolites for selective catalytic reduction of NO_x with NH_3 in diesel exhaust. *Fuel* **2021**, *305*, 121482. [CrossRef]
58. Chen, Z.; Fan, C.; Pang, L.; Ming, S.; Guo, W.; Liu, P.; Chen, H.; Li, T. One-pot synthesis of high performance Cu-SAPO-18 catalyst for NO reduction by NH_3-SCR: Influence of silicon content on the catalytic properties of Cu-SAPO-18. *Chem. Eng. J.* **2018**, *348*, 608–617. [CrossRef]
59. Gao, Q.; Han, S.; Ye, Q.; Cheng, S.; Kang, T.; Dai, H. Effects of lanthanide doping on the catalytic activity and hydrothermal stability of Cu-SAPO-18 for the catalytic removal of NO_x (NH_3-SCR) from diesel engines. *Catalysts* **2020**, *10*, 336. [CrossRef]
60. Zhou, T.; Yuan, Q.; Pan, X.; Bao, X. Growth of Cu/SSZ-13 on SiC for selective catalytic reduction of NO with NH_3. *Chin. J. Catal.* **2018**, *39*, 71–78. [CrossRef]
61. Lin, Q.; Feng, X.; Zhang, H.; Lin, C.; Liu, S.; Xu, H.; Chen, Y. Hydrothermal deactivation over CuFe/BEA for NH_3-SCR. *J. Ind. Eng. Chem.* **2018**, *65*, 40–50. [CrossRef]
62. Wan, J.; Chen, J.; Zhao, R.; Zhou, R. One-pot synthesis of Fe/Cu-SSZ-13 catalyst and its highly efficient performance for the selective catalytic reduction of nitrogen oxide with ammonia. *J. Environ. Sci.* **2021**, *100*, 306–316. [CrossRef] [PubMed]
63. Cao, Y.; Feng, X.; Xu, H.; Lan, L.; Gong, M.; Chen, Y. Novel promotional effect of yttrium on Cu–SAPO-34 monolith catalyst for selective catalytic reduction of NO_x by NH_3 (NH_3-SCR). *Catal. Commun.* **2016**, *76*, 33–36. [CrossRef]
64. Feng, X.; Lin, Q.; Cao, Y.; Zhang, H.; Li, Y.; Xu, H.; Lin, C.; Chen, Y. Neodymium promotion on the low-temperature hydrothermal stability of a Cu/SAPO-34 NH_3-SCR monolith catalyst. *J. Taiwan. Inst. Chem. Eng.* **2017**, *80*, 805–812. [CrossRef]
65. Chen, Z.; Guo, L.; Qu, H.; Liu, L.; Xie, H.; Zhong, Q. Controllable positions of Cu^{2+} to enhance low-temperature SCR activity on novel Cu-Ce-La-SSZ-13 by a simple one-pot method. *Chem. Commun.* **2020**, *56*, 2360–2363. [CrossRef]
66. Han, S.; Cheng, J.; Ye, Q.; Cheng, S.; Kang, T.; Dai, H. Ce doping to Cu-SAPO-18: Enhanced catalytic performance for the NH_3-SCR of NO in simulated diesel exhaust. *Microporous Mesoporous Mater.* **2019**, *276*, 133–146. [CrossRef]
67. Ma, Y.; Li, Z.; Zhao, N.; Teng, Y. One-pot synthesis of Cu–Ce co-doped SAPO-5/34 hybrid crystal structure catalysts for NH_3-SCR reaction with SO_2 resistance. *J. Rare Earth* **2021**, *39*, 1217–1223. [CrossRef]
68. Zhou, J.; Zhao, C.; Lin, J.; Yang, H.; Zhou, R. Promotional effects of cerium modification of Cu-USY catalysts on the low-temperature activity of NH_3-SCR. *Catal. Commun.* **2018**, *114*, 60–64. [CrossRef]
69. Chen, Y.; Li, J.; Teng, W.; Liu, W.; Ren, S.; Yang, J.; Liu, Q. Revealing the crystal-plane effects of CuO during the NH_3-SCR over CuO/TiO_2 catalysts. *J. Environ. Chem. Eng.* **2023**, *11*, 110787. [CrossRef]
70. Bjørkedal, O.H.; Regli, S.K.; Nuguid, R.J.G.; Vullum, P.E.; Kröcher, O.; Ferri, D.; Rønning, M. One-pot synthesis of highly dispersed mesoporous Cu/ZrO_2 catalysts for NH_3-SCR. *Catal. Today* **2022**, *384*, 113–121. [CrossRef]
71. Liu, J.; Zhou, S.; Cheng, H.; Li, H.; Zhu, W.; Liu, J. Unveiling the role of high-valent copper cations in the selective catalytic reduction of NO_x with NH_3 at low temperature. *Fuel* **2022**, *318*, 123607. [CrossRef]
72. Wu, X.; Meng, H.; Du, Y.; Liu, J.; Hou, B.; Xie, X. Insight into Cu_2O/CuO collaboration in the selective catalytic reduction of NO with NH_3: Enhanced activity and synergistic mechanism. *J. Catal.* **2020**, *384*, 72–87. [CrossRef]
73. Zhang, T.; Qiu, F.; Li, J. Design and synthesis of core-shell structured meso-Cu-SSZ-13@ mesoporous aluminosilicate catalyst for SCR of NO_x with NH_3: Enhancement of activity, hydrothermal stability and propene poisoning resistance. *Appl. Catal. B* **2016**, *195*, 48–58. [CrossRef]
74. Ting-Ting, X.; Gang-Gang, L.; Kai-Hua, Z.; Xin-Yan, Z.; Xin, Z.; Shao-Qing, Z. Effective reduction of nitric oxide over a core–shell Cu-SAPO-34@ Fe-MOR zeolite catalyst. *RSC Adv.* **2023**, *13*, 638–651. [CrossRef] [PubMed]
75. Jia, L.; Liu, J.; Huang, D.; Zhao, J.; Zhang, J.; Li, K.; Li, Z.; Zhu, W.; Zhao, Z.; Liu, J. Interface engineering of a bifunctional Cu-SSZ-13@ CZO core–shell catalyst for boosting potassium ion and SO_2 tolerance. *ACS Catal.* **2022**, *12*, 11281–11293. [CrossRef]

76. Deng, S.; Wang, Z.; Deng, D.; Chen, Z.; He, D.; He, H.; Ji, Y.; Hou, G.; Sun, W.; Liu, L. One-pot synthesis of hollow single crystal SSZ-13 zeolite by creating aluminum gradients with excellent activity for NH_3-SCR. *Microporous Mesoporous Mater.* **2021**, *314*, 110865. [CrossRef]
77. Jabłońska, M. Review of the application of Cu-containing SSZ-13 in NH_3-SCR-DeNO_x and NH_3-SCO. *RSC Adv.* **2022**, *12*, 25240–25261. [CrossRef]
78. Chen, J.; Huang, W.; Bao, S.; Zhang, W.; Liang, T.; Zheng, S.; Yi, L.; Guo, L.; Wu, X. A review on the characterization of metal active sites over Cu-based and Fe-based zeolites for NH_3-SCR. *RSC Adv.* **2022**, *12*, 27746–27765. [CrossRef]
79. Mohan, S.; Dinesha, P.; Kumar, S. NO_x reduction behaviour in copper zeolite catalysts for ammonia SCR systems: A review. *Chem. Eng. J.* **2020**, *384*, 123253. [CrossRef]
80. Chen, X.; Zhou, S.; Zhang, X.; Chen, S.; Wang, L.; Zhang, C.; Gao, S.; Yu, D.; Fan, X.; Cheng, Y.; et al. Research progress on the preparation of transition metal-modified zeolite catalysts and their catalytic performance for the purification of engine exhausts. *J. Mater. Chem. A Mater.* **2024**, *12*, 16293–16328. [CrossRef]
81. Guo, A.; Liu, H.; Li, Y.; Luo, Y.; Ye, D.; Jiang, J.; Chen, P. Recent progress in novel zeolite catalysts for selective catalytic reduction of nitrogen oxides. *Catal. Today* **2023**, *422*, 114212. [CrossRef]
82. Gao, F. Fe-exchanged small-pore zeolites as ammonia selective catalytic reduction (NH_3-SCR) catalysts. *Catalysts* **2020**, *10*, 1324. [CrossRef]
83. Wang, Y.; Li, J.; Liu, Z. Selective catalytic reduction of NO_x by NH_3 over Cu-AEI zeolite catalyst: Current status and future perspective. *Appl. Catal. B* **2023**, *343*, 123479. [CrossRef]
84. Leistner, K.; Mihai, O.; Wijayanti, K.; Kumar, A.; Kamasamudram, K.; Currier, N.W.; Yezerts, A.; Olsson, L. Comparison of Cu/BEA, Cu/SSZ-13 and Cu/SAPO-34 for ammonia-SCR reactions. *Catal. Today* **2015**, *258*, 49–55. [CrossRef]
85. Kamasamudram, K.; Currier, N.W.; Chen, X.; Yezerets, A. Overview of the practically important behaviors of zeolite-based urea-SCR catalysts, using compact experimental protocol. *Catal. Today* **2010**, *151*, 212–222. [CrossRef]
86. Gao, F.; Mei, D.; Wang, Y.; Szanyi, J.; Peden, C.H. Selective catalytic reduction over Cu/SSZ-13: Linking homo-and heterogeneous catalysis. *J. Am. Chem. Soc.* **2017**, *139*, 4935–4942. [CrossRef]
87. Gao, F.; Peden, C.H. Recent progress in atomic-level understanding of Cu/SSZ-13 selective catalytic reduction catalysts. *Catalysts* **2018**, *8*, 140. [CrossRef]
88. Chen, L.; Janssens, T.V.; Vennestrøm, P.N.; Jansson, J.; Skoglundh, M.; Gronbeck, H. A complete multisite reaction mechanism for low-temperature NH_3-SCR over Cu-CHA. *ACS Catal.* **2020**, *10*, 5646–5656. [CrossRef]
89. Hammershøi, P.S.; Jensen, A.D.; Janssens, T.V. Impact of SO_2-poisoning over the lifetime of a Cu-CHA catalyst for NH_3-SCR. *Appl. Catal. B* **2018**, *238*, 104–110. [CrossRef]
90. Hammershøi, P.S.; Jangjou, Y.; Epling, W.S.; Jensen, A.D.; Janssens, T.V. Reversible and irreversible deactivation of Cu-CHA NH_3-SCRcatalysts by SO_2 and SO_3. *Appl. Catal. B* **2018**, *226*, 38–45. [CrossRef]
91. Hammershøi, P.S.; Vennestrøm, P.N.; Falsig, H.; Jensen, A.D.; Janssens, T.V. Importance of the Cu oxidation state for the SO_2-poisoning of a Cu-SAPO-34 catalyst in the NH_3-SCR reaction. *Appl. Catal. B* **2018**, *236*, 377–383. [CrossRef]
92. Shan, Y.; Shi, X.; Yan, Z.; Liu, J.; Yu, Y.; He, H. Deactivation of Cu-SSZ-13 in the presence of SO_2 during hydrothermal aging. *Catal. Today* **2019**, *320*, 84–90. [CrossRef]
93. Shen, M.; Zhang, Y.; Wang, J.; Wang, C.; Wang, J. Nature of SO_3 poisoning on Cu/SAPO-34 SCR catalysts. *J. Catal.* **2018**, *358*, 277–286. [CrossRef]
94. Wijayanti, K.; Andonova, S.; Kumar, A.; Li, J.; Kamasamudram, K.; Currier, N.W.; Yezerets, A.; Olsson, L. Impact of sulfur oxide on NH_3-SCR over Cu-SAPO-34. *Appl. Catal. B* **2015**, *166*, 568–579. [CrossRef]
95. Wijayanti, K.; Xie, K.; Kumar, A.; Kamasamudram, K.; Olsson, L. Effect of gas compositions on SO_2 poisoning over Cu/SSZ-13 used for NH_3-SCR. *Appl. Catal. B* **2017**, *219*, 142–154. [CrossRef]
96. Wang, B.; Zhang, Y.; Fan, X. Deactivation of Cu SCR catalysts based on small-pore SSZ-13 zeolites: A review. *Chem. Phys.* **2023**, *6*, 100207. [CrossRef]
97. Han, S.; Ye, Q.; Gao, Q.; Dai, H. Improved SO_2 tolerance of Cu-SAPO-18 by Ce-doping in the selective catalytic reduction of NO with NH_3. *Catalysts* **2020**, *10*, 783. [CrossRef]
98. Yang, J.; Li, Z.; Cui, J.; Ma, Y.; Li, Y.; Zhang, Q.; Song, K.; Yang, C. Fabrication of wide temperature lanthanum and cerium doped Cu/TNU-9 catalyst with excellent NH3-SCR performance and outstanding SO^{2+} H_2O tolerance. *J. Rare Earth* **2023**, *41*, 1195–1202. [CrossRef]
99. Liu, Q.; Fu, Z.; Ma, L.; Niu, H.; Liu, C.; Li, J.; Zhang, Z. MnOx-CeO_2 supported on Cu-SSZ-13: A novel SCR catalyst in a wide temperature range. *Appl. Catal. A Gen.* **2017**, *547*, 146–154. [CrossRef]
100. Zhang, J.; Yan, Z.; Yu, Y.; Li, Y. Reasonably designed $CuSbTiO_x$ series catalysts with high NH_3-SCR activity and obviously improved SO_2 tolerance. *New J. Chem.* **2024**, *48*, 4335–4345. [CrossRef]
101. Yu, Y.; Chen, C.; He, C.; Miao, J.; Chen, J. In situ growth synthesis of CuO@Cu-MOFs core-shell materials as novel low-temperature NH_3-SCR catalysts. *ChemCatChem* **2019**, *11*, 979–984. [CrossRef]
102. Shi, J.W.; Wang, Y.; Duan, R.; Gao, C.; Wang, B.; He, C.; Niu, C. The synergistic effects between Ce and Cu in $Cu_yCe_{1-y}W_5O_x$ catalysts for enhanced NH_3-SCR of NO_x and SO_2 tolerance. *Catal. Sci. Technol.* **2019**, *9*, 718–730. [CrossRef]
103. Hao, Z.; Liu, G.; Ma, N.; Zhang, H.; Li, Y.; Xia, Y.; Zhang, D.; Zhan, S. Oxygen-vacancy mediated acidity and redox properties on WO_x/Cu-doped CeO_2 for the removal of NO_x. *J. Environ. Chem. Eng.* **2021**, *9*, 106024. [CrossRef]

104. Wang, X.; Liu, Y.; Ying, Q.; Yao, W.; Wu, Z. The superior performance of Nb-modified Cu-Ce-Ti mixed oxides for the selective catalytic reduction of NO with NH_3 at low temperature. *Appl. Catal. A Gen.* **2018**, *562*, 19–27. [CrossRef]
105. Qin, B.; Guo, R.T.; Zhou, J.; Wei, L.G.; Yin, T.Y.; Pan, W.G. Promotional role of Nb modification on $CuCeO_x$ catalyst for low temperature selective catalytic reduction of NO with NH_3: A mechanism investigation. *Fuel* **2022**, *329*, 125390. [CrossRef]
106. Jiang, J.; Zheng, R.; Jia, Y.; Guo, L.; Huang, M.; Hu, J.; Xia, Y. Investigation of SO_2 and H_2O poisoning over Cu-HPMo/TiO_2 catalyst for Low temperature SCR: An experimental and DFT study. *Mol. Catal.* **2020**, *493*, 111044. [CrossRef]
107. Chen, Z.; Liu, L.; Qu, H.; Zhou, B.; Xie, H.; Zhong, Q. Migration of cations and shell functionalization for Cu-Ce-La/SSZ-13@ ZSM-5: The contribution to activity and hydrothermal stability in the selective catalytic reduction reaction. *J. Catal.* **2020**, *392*, 217–230. [CrossRef]
108. Di, Z.; Wang, H.; Zhang, R.; Chen, H.; Wei, Y.; Jia, J. ZSM-5 core–shell structured catalyst for enhancing low-temperature NH_3-SCR efficiency and poisoning resistance. *Appl. Catal. A Gen.* **2022**, *630*, 118438. [CrossRef]
109. Chen, Z.; Wang, H.; Zhang, X.; Wu, M.; Qu, H. Construction of multifunctional interface engineering on Cu-SSZ-13@ Ce-MnO_x/Mesoporous-silica catalyst for boosting activity, SO_2 tolerance and hydrothermal stability. *J. Hazard. Mater.* **2024**, *477*, 135268. [CrossRef]
110. Jangjou, Y.; Do, Q.; Gu, Y.; Lim, L.G.; Sun, H.; Wang, D.; Kumar, A.; Li, J.; Grabow, L.C.; Epling, W.S. Nature of Cu active centers in Cu-SSZ-13 and their responses to SO_2 exposure. *ACS Catal.* **2018**, *8*, 1325–1337. [CrossRef]
111. Su, W.; Li, Z.; Zhang, Y.; Meng, C.; Li, J. Identification of sulfate species and their influence on SCR performance of Cu/CHA catalyst. *Catal. Sci. Technol.* **2017**, *7*, 1523–1528. [CrossRef]
112. Wijayanti, K.; Leistner, K.; Chand, S.; Kumar, A.; Kamasamudram, K.; Currier, N.W.; Yezerets, A.; Olsson, L. Deactivation of Cu-SSZ-13 by SO_2 exposure under SCR conditions. *Catal. Sci. Technol.* **2016**, *6*, 2565–2579. [CrossRef]
113. Bergman, S.L.; Dahlin, S.; Mesilov, V.V.; Xiao, Y.; Englund, J.; Xi, S.; Tang, C.; Skoglundh, M.; Pettersson, L.J.; Bernasek, S.L. In-situ studies of oxidation/reduction of copper in Cu-CHA SCR catalysts: Comparison of fresh and SO_2-poisoned catalysts. *Appl. Catal. B* **2020**, *269*, 118722. [CrossRef]
114. Shen, M.; Wen, H.; Hao, T.; Yu, T.; Fan, D.; Wang, J.; Li, W.; Wang, J. Deactivation mechanism of SO_2 on Cu/SAPO-34 NH_3-SCR catalysts: Structure and active Cu^{2+}. *Catal. Sci. Technol.* **2015**, *5*, 1741–1749. [CrossRef]
115. He, J.; Impeng, S.; Zhang, J.; Zhang, J.; Wang, P.; Zhang, D. SO_2-tolerant NO_x reduction over SO_4^{2-}-coordinated Cu-SAPO-34 catalysts via protecting the reduction and re-oxidation of Cu sites. *Chem. Eng. J.* **2022**, *448*, 137720. [CrossRef]
116. Li, P.; Xin, Y.; Zhang, H.; Yang, F.; Tang, A.; Han, D.; Jia, J.; Wang, J.; Li, Z.; Zhang, Z. Recent progress in performance optimization of Cu-SSZ-13 catalyst for selective catalytic reduction of NO_x. *Front. Chem.* **2022**, *10*, 1033255. [CrossRef]
117. Yu, Y.; Tan, W.; An, D.; Wang, X.; Liu, A.; Zou, W.; Tang, C.; Ge, C.; Tong, Q.; Sun, J.; et al. Insight into the SO_2 resistance mechanism on γ-Fe_2O_3 catalyst in NH_3-SCR reaction: A collaborated experimental and DFT study. *Appl. Catal. B* **2021**, *281*, 119544. [CrossRef]
118. Qin, G.; Zheng, J.; Li, Y.; Yang, Y.; Liu, X.; Han, X.; Huang, Z. Tailor the crystal planes of MIL-101 (Fe) derivatives to enhance the activity of SCR reaction at medium and low temperature. *J. Colloid Interface Sci.* **2022**, *615*, 432–444. [CrossRef]
119. Yang, W.; Zhou, B.; Zhang, Y.; Ren, J.; Wu, C.; Gates, I.D.; Liu, Y.; Gao, Z. A novel low-temperature Fe-Fe double-atom catalyst for a "fast SCR" reaction. *Mol. Catal.* **2022**, *533*, 112769. [CrossRef]
120. Zhang, N.; Wang, J.; Li, Q.; Xin, Y.; Zheng, L.; Wang, Y.; Zhang, Z. Enhanced selective catalytic reduction of NO_x with NH_3 over homoatomic dinuclear sites in defective α-Fe_2O_3. *Chem. Eng. J.* **2021**, *426*, 131845. [CrossRef]
121. Xu, Q.; Li, Z.; Wang, L.; Zhan, W.; Guo, Y.; Guo, Y. Understanding the role of redox properties and NO adsorption over $MnFeO_x$ for NH_3-SCR. *Catal. Sci. Technol.* **2022**, *12*, 2030–2041. [CrossRef]
122. Zhang, W.; Shi, X.; Yan, Z.; Shan, Y.; Zhu, Y.; Yu, Y.; He, H. Design of high-performance iron–niobium composite oxide catalysts for NH_3-SCR: Insights into the interaction between Fe and Nb. *ACS Catal.* **2021**, *11*, 9825–9836. [CrossRef]
123. Xin, Y.; Zhang, N.; Li, Q.; Zhang, Z.; Cao, X.; Zheng, L.; Zeng, Y.; Anderson, J.A. Active site identification and modification of electronic states by atomic-scale doping to enhance oxide catalyst innovation. *ACS Catal.* **2018**, *8*, 1399–1404. [CrossRef]
124. Chen, W.; Yang, S.; Liu, H.; Huang, F.; Shao, Q.; Liu, L.; Sun, J.; Sun, C.; Chen, D.; Dong, L. Single-atom Ce-modified α-Fe_2O_3 for selective catalytic reduction of NO with NH_3. *Environ. Sci. Technol.* **2022**, *56*, 10442–10453. [CrossRef] [PubMed]
125. Sun, P.; Jin, S.; Wang, J.; Wu, J.; Cai, L.; Zhou, Y.; Wang, X.; Zhang, R.; Ling, L.; Jin, M. Deep insights into the promotion role of Sm doping in the sulfur resistance of Fe_2O_3 catalyst for NH_3-SCR: A combined experimental and DFT study. *J. Phys. Chem. Solids* **2024**, *184*, 111666. [CrossRef]
126. Xin, Y.; Zhang, N.; Li, Q.; Zhang, Z.; Cao, X.; Zheng, L.; Zeng, Y.; Anderson, J.A. Selective catalytic reduction of NO_x with NH_3 over short-range ordered WOFe structures with high thermal stability. *Appl. Catal. B* **2018**, *229*, 81–87. [CrossRef]
127. Liu, Z.; Su, H.; Chen, B.; Li, J.; Woo, S.I. Activity enhancement of WO_3 modified Fe_2O_3 catalyst for the selective catalytic reduction of NO_x by NH_3. *Chem. Eng. J.* **2016**, *299*, 255–262. [CrossRef]
128. Liu, F.; Shan, W.; Lian, Z.; Liu, J.; He, H. The smart surface modification of Fe_2O_3 by WO_x for significantly promoting the selective catalytic reduction of NO_x with NH_3. *Appl. Catal. B* **2018**, *230*, 165–176. [CrossRef]
129. Shu, Y.; Sun, H.; Quan, X.; Chen, S. Enhancement of catalytic activity over the iron-modified Ce/TiO_2 catalyst for selective catalytic reduction of NO_x with ammonia. *J. Phys. Chem. C* **2012**, *116*, 25319–25327. [CrossRef]
130. Tang, X.; Shi, Y.; Gao, F.; Zhao, S.; Yi, H.; Xie, Z. Promotional role of Mo on $Ce_{0.3}FeO_x$ catalyst towards enhanced NH_3-SCR catalytic performance and SO_2 resistance. *Chem. Eng. J.* **2020**, *398*, 125619. [CrossRef]

131. Stahl, A.; Wang, Z.; Schwämmle, T.; Ke, J.; Li, X. Novel Fe-W-Ce mixed oxide for the selective catalytic reduction of NO_x with NH_3 at low temperatures. *Catalysts* **2017**, *7*, 71. [CrossRef]
132. Ren, Z.; Fan, H.; Wang, R. A novel ring-like Fe_2O_3-based catalyst: Tungstophosphoric acid modification, NH_3-SCR activity and tolerance to H_2O and SO_2. *Catal. Commun.* **2017**, *100*, 71–75. [CrossRef]
133. Yao, G.; Wei, Y.; Gui, K.; Ling, X. Catalytic performance and reaction mechanisms of NO removal with NH_3 at low and medium temperatures on Mn-W-Sb modified siderite catalysts. *J. Environ. Sci.* **2022**, *115*, 126–139. [CrossRef] [PubMed]
134. Kang, L.; Han, L.; He, J.; Li, H.; Yan, T.; Chen, G.; Zhang, J.; Shi, L.; Zhang, D. Improved NO_x reduction in the presence of SO_2 by using Fe_2O_3-promoted halloysite-supported CeO_2–WO_3 catalysts. *Environ. Sci. Technol.* **2018**, *53*, 938–945. [CrossRef] [PubMed]
135. Han, L.; Gao, M.; Feng, C.; Shi, L.; Zhang, D. Fe_2O_3–CeO_2@Al_2O_3 nanoarrays on Al-mesh as SO_2-tolerant monolith catalysts for NO_x reduction by NH_3. *Environ. Sci. Technol.* **2019**, *53*, 5946–5956. [CrossRef]
136. Chen, L.; Wang, X.; Cong, Q.; Ma, H.; Li, S.; Li, W. Design of a hierarchical Fe-ZSM-5@ CeO_2 catalyst and the enhanced performances for the selective catalytic reduction of NO with NH_3. *Chem. Eng. J.* **2019**, *369*, 957–967. [CrossRef]
137. Liu, J.; Liu, J.; Zhao, Z.; Wei, Y.; Song, W. Fe-Beta@ CeO_2 core-shell catalyst with tunable shell thickness for selective catalytic reduction of NO_x with NH_3. *AIChE J.* **2017**, *63*, 4430–4441. [CrossRef]
138. Jiang, M.; Yan, Z.; Zhang, Y.; Zhang, C.; Chang, C.; Xiao, M.; Ruan, L.; Yan, Y.; Yu, Y.; He, H. Simultaneous modification of redox and acidic properties of FeO_x catalysts derived from MIL-100 (Fe) via HPW incorporation for NH_3-SCR. *Appl. Catal. B* **2024**, *358*, 124416. [CrossRef]
139. Ren, Z.; Teng, Y.; Zhao, L.; Wang, R. Keggin-tungstophosphoric acid decorated Fe_2O_3 nanoring as a new catalyst for selective catalytic reduction of NO_x with ammonia. *Catal. Today* **2017**, *297*, 36–45. [CrossRef]
140. Tan, W.; Xie, S.; Shan, W.; Lian, Z.; Xie, L.; Liu, A.; Gao, F.; Dong, L.; He, H.; Liu, F. CeO_2 doping boosted low-temperature NH_3-SCR activity of $FeTiO_x$ catalyst: A microstructure analysis and reaction mechanistic study. *Front. Environ. Sci. Eng.* **2022**, *16*, 60. [CrossRef]
141. Ma, S.; Tan, H.; Li, Y.; Wang, P.; Zhao, C.; Niu, X.; Zhu, Y. Excellent low-temperature NH_3-SCR NO removal performance and enhanced H_2O resistance by Ce addition over the $Cu_{0.02}Fe_{0.2}Ce_yTi_{1-y}O_x$ (y= 0.1, 0.2, 0.3) catalysts. *Chemosphere* **2020**, *243*, 125309. [CrossRef] [PubMed]
142. Bai, Y.; Hou, Y.; Li, Q.; Han, X.; Wang, H.; Wu, Z.; Huang, Z. Amorphous FeO_x–$Mn_{0.1}O_y$ catalyst with rich oxygen vacancies for ammonia selective catalytic reduction of nitrogen oxide at low temperatures. *Fuel* **2023**, *349*, 128644. [CrossRef]
143. Wang, H.; Qu, Z.; Liu, L.; Dong, S.; Qiao, Y. Promotion of NH_3-SCR activity by sulfate-modification over mesoporous Fe doped CeO_2 catalyst: Structure and mechanism. *J. Hazard. Mater.* **2021**, *414*, 125565. [CrossRef] [PubMed]
144. Wang, Y.; Chen, L.; Wang, W.; Wang, X.; Li, B.; Zhang, S.; Li, W.; Li, S. Revealing the excellent low-temperature activity of the $Fe_{1-x}Ce_xO_\delta$-S catalyst for NH_3-SCR: Improvement of the lattice oxygen mobility. *ACS Appl. Mater. Interfaces* **2023**, *15*, 17834–17847. [CrossRef] [PubMed]
145. Liu, J.; Meeprasert, J.; Namuangruk, S.; Zha, K.; Li, H.; Huang, L.; Maitarad, P.; Shi, L.; Zhang, D. Facet–activity relationship of TiO_2 in Fe_2O_3/TiO_2 nanocatalysts for selective catalytic reduction of NO with NH_3: In situ DRIFTs and DFT studies. *J. Phys. Chem. C* **2017**, *121*, 4970–4979. [CrossRef]
146. Han, J.; Meeprasert, J.; Maitarad, P.; Nammuangruk, S.; Shi, L.; Zhang, D. Investigation of the facet-dependent catalytic performance of Fe_2O_3/CeO_2 for the selective catalytic reduction of NO with NH_3. *J. Phys. Chem C* **2016**, *120*, 1523–1533. [CrossRef]
147. Teng, W.; Li, J.; Dai, X.; Chen, Y.; Wu, H.; Liu, W.; Ren, S.; Yang, J.; Liu, Q. Promoting the NH_3-SCR performance of Fe_2O_3-TiO_2 catalyst through regulation of the exposed crystal facets of Fe_2O_3. *Appl. Surf. Sci.* **2024**, *647*, 158938. [CrossRef]
148. Zhang, S.; Zhang, B.; Liu, B.; Sun, S. A review of Mn-containing oxide catalysts for low temperature selective catalytic reduction of NO_x with NH_3: Reaction mechanism and catalyst deactivation. *RSC Adv.* **2017**, *7*, 26226–26242. [CrossRef]
149. Gao, F.; Tang, X.; Yi, H.; Zhao, S.; Li, C.; Li, J.; Shi, Y.; Meng, X. A review on selective catalytic reduction of NO_x by NH_3 over Mn–based catalysts at low temperatures: Catalysts, mechanisms, kinetics and DFT calculations. *Catalysts* **2017**, *7*, 199. [CrossRef]
150. Guo, R.T.; Qin, B.; Wei, L.G.; Yin, T.Y.; Zhou, J.; Pan, W.G. Recent progress of low-temperature selective catalytic reduction of NO_x with NH_3 over manganese oxide-based catalysts. *Phys. Chem. Chem. Phys.* **2022**, *24*, 6363–6382. [CrossRef]
151. Peña, D.A.; Uphade, B.S.; Smirniotis, P.G. TiO_2-supported metal oxide catalysts for low-temperature selective catalytic reduction of NO with NH_3: I. Evaluation and characterization of first row transition metals. *J. Catal.* **2004**, *221*, 421–431. [CrossRef]
152. He, G.; Gao, M.; Peng, Y.; Yu, Y.; Shan, W.; He, H. Superior oxidative dehydrogenation performance toward NH_3 determines the excellent low-temperature NH_3-SCR activity of Mn-based catalysts. *Environ. Sci. Technol.* **2021**, *55*, 6995–7003. [CrossRef] [PubMed]
153. Kapteijn, F.; Singoredjo, L.; Andreini, A.; Moulijn, J.A. Activity and selectivity of pure manganese oxides in the selective catalytic reduction of nitric oxide with ammonia. *Appl. Catal. B* **1994**, *3*, 173–189. [CrossRef]
154. Tang, X.; Hao, J.; Xu, W.; Li, J. Low temperature selective catalytic reduction of NO_x with NH_3 over amorphous MnO_x catalysts prepared by three methods. *Catal. Commun.* **2007**, *8*, 329–334. [CrossRef]
155. Kang, M.; Park, E.D.; Kim, J.M.; Yie, J.E. Manganese oxide catalysts for NO_x reduction with NH_3 at low temperatures. *Appl. Catal. A Gen.* **2007**, *327*, 261–269. [CrossRef]
156. Kang, M.; Yeon, T.H.; Park, E.D.; Yie, J.E.; Kim, J.M. Novel MnO_x catalysts for NO reduction at low temperature with ammonia. *Catal. Lett.* **2006**, *106*, 77–80. [CrossRef]

157. Tang, X.; Li, J.; Sun, L.; Hao, J. Origination of N_2O from NO reduction by NH_3 over β-MnO_2 and α-Mn_2O_3. *Appl. Catal. B* **2010**, *99*, 156–162. [CrossRef]
158. Fang, X.; Liu, Y.; Chen, L.; Cheng, Y. Influence of surface active groups on SO_2 resistance of birnessite for low-temperature NH_3-SCR. *Chem. Eng. J.* **2020**, *399*, 125798. [CrossRef]
159. Liu, J.; Wei, Y.; Li, P.Z.; Zhang, P.; Su, W.; Sun, Y.; Zou, R.; Zhao, Y. Experimental and theoretical investigation of mesoporous MnO_2 nanosheets with oxygen vacancies for high-efficiency catalytic DeNO_x. *ACS Catal.* **2018**, *8*, 3865–3874. [CrossRef]
160. Xu, S.; Chen, J.; Li, Z.; Liu, Z. Highly ordered mesoporous MnO_x catalyst for the NH_3-SCR of NO_x at low temperatures. *Appl. Catal. A Gen.* **2023**, *649*, 118966. [CrossRef]
161. Chen, R.; Fang, X.; Li, Z.; Liu, Z. Selective catalytic reduction of NO_x with NH_3 over a novel MOF-derived MnO_x catalyst. *Appl. Catal. A Gen.* **2022**, *643*, 118754. [CrossRef]
162. Zhang, Y.; Zhang, G.; Chen, G.; Leng, Z.; Xia, D.; Wang, Z. Enabling wide-temperature selective catalytic reduction of NO_X via modulating redox ability of Mn-based catalysts. *Energy Fuels* **2024**, *38*, 8960–8967. [CrossRef]
163. Zhou, X.; Wang, P.; Shen, Z.; Chen, S.; Wang, Q.; Cheng, D.; Zhang, D. Low-temperature NO_x reduction over hydrothermally stable SCR catalysts by engineering low-coordinated Mn active sites. *Chem. Eng. J.* **2022**, *442*, 136182. [CrossRef]
164. Li, X.; Li, Q.; Zhong, L.; Song, Z.; Yu, S.; Zhang, C.; Fang, Q.; Chen, G. DFT analysis of the reaction mechanism for NH_3-SCR of NO_x over Mn/γ-Al_2O_3 catalyst. *J. Phys. Chem. C* **2019**, *123*, 25185–25196. [CrossRef]
165. Zeng, Y.; Lyu, F.; Wang, Y.; Zhang, S.; Zhong, Q.; Zhong, Z. New insight on N_2O formation over MnO_x/TiO_2 catalysts for selective catalytic reduction of NO_x with NH_3. *Mol. Catal.* **2022**, *525*, 112356. [CrossRef]
166. Yang, S.; Xiong, S.; Liao, Y.; Xiao, X.; Qi, F.; Peng, Y.; Fu, Y.; Shan, W.; Li, J. Mechanism of N_2O formation during the low-temperature selective catalytic reduction of NO with NH_3 over Mn–Fe spinel. *Environ. Sci. Technol.* **2014**, *48*, 10354–10362. [CrossRef]
167. Guo, J.; Gan, F.; Zhao, Y.; He, J.; Wang, B.; Gao, T.; Jiang, X.; Ma, S. Revealing the crystal facet effect on N_2O formation during the NH_3-SCR over α-MnO_2 catalysts. *RSC Adv.* **2023**, *13*, 4032–4039. [CrossRef]
168. Zhang, Y.; Guan, B.; Zheng, C.; Zhou, J.; Su, T.; Guo, J.; Chen, J.; Chen, Y.; Zhang, J.; Dang, H.; et al. Research on the resistance of catalysts for selective catalytic reduction: Current progresses and future perspectives. *J. Clean. Prod.* **2023**, *434*, 139920. [CrossRef]
169. Hou, Q.; Liu, Y.; Hou, Y.; Han, X.; Huang, Z. Ordered mesoporous $MnAlO_x$ oxides dominated by calcination temperature for the selective catalytic reduction of NO_x with NH_3 at low temperature. *Catalysts* **2022**, *12*, 637. [CrossRef]
170. Li, Y.; Wan, Y.; Sun, R.; Qian, G.; Liu, Z.; Dan, J.; Yu, F. Novel 2D layered manganese silicate nanosheets with excellent performance for selective catalytic reduction of NO with ammonia. *ChemCatChem* **2022**, *14*, e202200909. [CrossRef]
171. Yao, X.; Chen, L.; Cao, J.; Chen, Y.; Tian, M.; Yang, F.; Sun, J.; Tang, C.; Dong, L. Enhancing the deNO_x performance of MnO_x/CeO_2-ZrO_2 nanorod catalyst for low-temperature NH_3-SCR by TiO_2 modification. *Chem. Eng. J.* **2019**, *369*, 46–56. [CrossRef]
172. Yang, R.; Gao, Z.; Sun, M.; Fu, G.; Cheng, G.; Liu, W.; Yang, X.; Zhao, X.; Yu, L. A highly active VO_x-MnO_x/CeO_2 for selective catalytic reduction of NO: The balance between redox property and surface acidity. *J. Rare Earth* **2021**, *39*, 1370–1381. [CrossRef]
173. Gao, F.; Tang, X.; Yi, H.; Zhao, S.; Wang, J.; Gu, T. Improvement of activity, selectivity and H_2O & SO_2-tolerance of micro-mesoporous $CrMn_2O_4$ spinel catalyst for low-temperature NH_3-SCR of NO_x. *Appl. Surf. Sci.* **2019**, *466*, 411–424. [CrossRef]
174. Fan, H.; Fan, J.; Chang, T.; Wang, X.; Wang, X.; Huang, Y.; Zhang, Y.; Shen, Z. Low-temperature Fe–MnO_2 nanotube catalysts for the selective catalytic reduction of NO_x with NH_3. *Catal. Sci. Technol.* **2021**, *11*, 6553–6563. [CrossRef]
175. Zhu, J.; Shao, Y.; Li, Z.; Li, K.; Ren, X.; Jia, L.; Li, H.; Cheng, H.; Liu, J.; Liu, J. Modulating the acidity and reducibility of FeMn/TiO_2 to boost the low-temperature selective catalytic reduction of NO_x. *Fuel* **2024**, *366*, 131316. [CrossRef]
176. Chen, Z.; Ren, S.; Xing, X.; Li, X.; Chen, L.; Wang, M. Unveiling the inductive strategy of different precipitants on $MnFeO_x$ catalyst for low-temperature NH_3-SCR reaction. *Fuel* **2023**, *335*, 126986. [CrossRef]
177. Wei, L.; Li, X.; Mu, J.; Wang, X.; Fan, S.; Yin, Z.; Tadé, M.O.; Liu, S. Rationally tailored redox properties of a mesoporous Mn–Fe spinel nanostructure for boosting low-temperature selective catalytic reduction of NO_x with NH_3. *ACS Sustain. Chem. Eng.* **2020**, *8*, 17727–17739. [CrossRef]
178. Gu, J.; Zhu, B.; Duan, R.; Chen, Y.; Wang, S.; Liu, L.; Wang, X. Highly dispersed MnO_x–FeO_x supported by silicalite-1 for the selective catalytic reduction of NO_x with NH_3 at low temperatures. *Catal. Sci. Technol.* **2020**, *10*, 5525–5534. [CrossRef]
179. Chen, C.; Feng, C.; Wang, Y.; Li, J.; Liu, Z.; Wang, W.; Pan, Y.; Liu, Y. Design of robust Co-doped Mn_3O_4 spinel catalysts for selective catalytic reduction of NO with NH_3 at low temperatures. *Appl. Surf. Sci.* **2022**, *602*, 154384. [CrossRef]
180. Wang, G.; Liang, Y.; Song, J.; Xu, K.; Pan, Y.; Xu, X.; Zhao, Y. Co-doped $MnCeO_x/ZrO_2$ catalysts for low temperature selective catalytic reduction of NO. *Res. Chem. Intermed.* **2022**, *48*, 2627–2640. [CrossRef]
181. Zhu, Y.; Xiao, X.; Wang, J.; Ma, C.; Jia, X.; Qiao, W.; Ling, L. Enhanced activity and water resistance of hierarchical flower-like Mn-Co binary oxides for ammonia-SCR reaction at low temperature. *Appl. Surf. Sci.* **2021**, *569*, 150989. [CrossRef]
182. Zhao, Q.; Chen, B.; Li, J.; Wang, X.; Crocker, M.; Shi, C. Insights into the structure-activity relationships of highly efficient CoMn oxides for the low temperature NH_3-SCR of NO_x. *Appl. Catal. B* **2020**, *277*, 119215. [CrossRef]
183. Perumal, S.K.; Yu, H.; Aghalayam, P.; Kim, H.S. Unravelling the role of Zr–Laponite supports in enhancing the activity of a MnNi catalyst for the low-temperature NH_3-selective catalytic reduction reaction. *Energy Fuels* **2024**, *38*, 4516–4525. [CrossRef]
184. Kang, M.; Park, E.D.; Kim, J.M.; Yie, J.E. Cu–Mn mixed oxides for low temperature NO reduction with NH_3. *Catal. Today* **2006**, *111*, 236–241. [CrossRef]

185. Luo, W.; Yang, L.; Zhang, Z.; Cao, G.; Li, J.; Liu, B. Flexible Ti mesh-supported MnO_x–CuO_x/TiO_2 nanosheet monolithic catalysts for low-temperature selective catalytic reduction of NO_x with NH_3. *ACS Appl. Nano Mater.* **2024**, *7*, 6262–6272. [CrossRef]
186. La Greca, E.; Kharlamova, T.S.; Grabchenko, M.V.; Svetlichnyi, V.A.; Pantaleo, G.; Consentino, L.; Stonkus, O.A.; Vodyankina, O.V.; Liotta, L.F. Influence of Y doping on catalytic activity of CeO_2, MnO_x, and $CeMnO_x$ catalysts for selective catalytic reduction of NO by NH_3. *Catalysts* **2023**, *13*, 901. [CrossRef]
187. Jiang, B.; Deng, B.; Zhang, Z.; Wu, Z.; Tang, X.; Yao, S.; Lu, H. Effect of Zr addition on the low-temperature SCR activity and SO_2 tolerance of Fe–Mn/Ti catalysts. *J. Phys. Chem. C* **2014**, *118*, 14866–14875. [CrossRef]
188. Zhou, Y.; Su, B.; Ren, S.; Chen, Z.; Su, Z.; Yang, J.; Chen, L.; Wang, M. Nb_2O_5-modified Mn-Ce/AC catalyst with high $ZnCl_2$ and SO_2 tolerance for low-temperature NH_3-SCR of NO. *J. Environ. Chem. Eng.* **2021**, *9*, 106323. [CrossRef]
189. Hu, X.; Shi, Q.; Zhang, H.; Wang, P.; Zhan, S.; Li, Y. NH_3-SCR performance improvement over Mo modified Mo (x)-MnO_x nanorods at low temperatures. *Catal. Today* **2017**, *297*, 17–26. [CrossRef]
190. Zhang, S.; Zhang, Q.; Hu, X.; Huang, Y. A Novel MnO_x–MoO_x Codoped Iron-Based Catalyst for NH_3-SCR with Superior Catalytic Activity over a Wide Temperature Range. *Ind. Eng. Chem. Res.* **2024**, *63*, 8163–8174. [CrossRef]
191. Dong, Y.; Ran, M.; Zhang, X.; Lin, S.; Li, W.; Yang, Y.; Song, H.; Wu, W.; Liu, S.; Zheng, C.; et al. Promoting effect of polyoxometallic acid modification on the NH_3-SCR performance of Mn-based catalysts. *J. Environ. Chem. Eng.* **2024**, *12*, 112823. [CrossRef]
192. Cao, F.; Xiang, J.; Su, S.; Wang, P.; Hu, S.; Sun, L. Ag modified Mn–Ce/γ-Al_2O_3 catalyst for selective catalytic reduction of NO with NH_3 at low-temperature. *Fuel Process Technol.* **2015**, *135*, 66–72. [CrossRef]
193. Wang, H.; Lin, M.; Murayama, T.; Feng, S.; Haruta, M.; Miura, H.; Shishido, T. Ag size/structure-dependent effect on low-temperature selective catalytic oxidation of NH_3 over Ag/MnO_2. *ACS Catal.* **2021**, *11*, 8576–8584. [CrossRef]
194. Chang, H.; Chen, X.; Li, J.; Ma, L.; Wang, C.; Liu, C.; Schwank, J.W.; Hao, J. Improvement of activity and SO_2 tolerance of Sn-modified MnO_x–CeO_2 catalysts for NH_3-SCR at low temperatures. *Environ. Sci. Technol.* **2013**, *47*, 5294–5301. [CrossRef] [PubMed]
195. Xie, H.; Chen, C.; He, P.; Mu, G.; Wang, K.; Yang, C.; Chai, S.; Wang, N.; Ge, C. Promoting H_2O/SO_2 resistance of Ce-Mn/TiO_2 nanostructures by Sb^{5+}/Sb^{3+} addition for Selective catalytic reduction of NO with NH_3. *Appl. Surf. Sci.* **2022**, *600*, 154146. [CrossRef]
196. Li, X.; Yin, Y.; Yao, C.; Zuo, S.; Lu, X.; Luo, S.; Ni, C. $La_{1-x}Ce_xMnO_3$/attapulgite nanocomposites as catalysts for NO reduction with NH_3 at low temperature. *Particuology* **2016**, *26*, 66–72. [CrossRef]
197. Fan, X.; Hao, L.; Gu, X.; Li, S. Low-temperature selective catalytic reduction of NO with NH_3 over a biochar-supported perovskite oxide catalyst. *Energy Fuels* **2023**, *37*, 7339–7352. [CrossRef]
198. Yao, X.; Ma, K.; Zou, W.; He, S.; An, J.; Yang, F.; Dong, L. Influence of preparation methods on the physicochemical properties and catalytic performance of MnO_x-CeO_2 catalysts for NH_3-SCR at low temperature. *Chin. J. Catal.* **2017**, *38*, 146–159. [CrossRef]
199. Chen, X.; Wang, P.; Fang, P.; Ren, T.; Liu, Y.; Cen, C.; Wang, H.; Wu, Z. Tuning the property of Mn-Ce composite oxides by titanate nanotubes to improve the activity, selectivity and SO_2/H_2O tolerance in middle temperature NH_3-SCR reaction. *Fuel Process Technol.* **2017**, *167*, 221–228. [CrossRef]
200. Shen, Q.; Zhang, L.; Sun, N.; Wang, H.; Zhong, L.; He, C.; Wei, W.; Sun, Y. Hollow MnO_x-CeO_2 mixed oxides as highly efficient catalysts in NO oxidation. *Chem. Eng. J.* **2017**, *322*, 46–55. [CrossRef]
201. Qi, G.; Yang, R.T.; Chang, R. MnO_x-CeO_2 mixed oxides prepared by co-precipitation for selective catalytic reduction of NO with NH_3 at low temperatures. *Appl. Catal. B* **2004**, *51*, 93–106. [CrossRef]
202. Li, S.; Zheng, Z.; Zhao, Z.; Wang, Y.; Yao, Y.; Liu, Y.; Zhang, J.; Zhang, Z. CeO_2 Nanoparticle-loaded MnO_2 nanoflowers for selective catalytic reduction of NO_x with NH_3 at low temperatures. *Molecules* **2022**, *27*, 4863. [CrossRef] [PubMed]
203. Zhao, S.; Shi, J.W.; Niu, C.; Wang, B.; He, C.; Liu, W.; Xiao, L.; Ma, D.; Wang, H.; Cheng, Y. $FeVO_4$-supported Mn–Ce oxides for the low-temperature selective catalytic reduction of NO_x by NH_3. *Catal. Sci. Technol.* **2021**, *11*, 6770–6781. [CrossRef]
204. Huang, X.; Dong, F.; Zhang, G.; Tang, Z. Constructing TiO_2@$CeMnO_x$ nanocages by self-sacrificial hydrolytic etching MIL-125 for efficient wide-temperature selective catalytic reduction of nitrogen oxides. *Chem. Eng. J.* **2022**, *432*, 134236. [CrossRef]
205. Wu, T.; Ren, S.; Guo, R.T.; Li, C.F.; You, Y.H.; Guo, S.Y.; Pan, W.G. The promotion effect of Pr doping on the catalytic performance of $MnCeO_x$ catalysts for low-temperature NH_3-SCR. *Fuel* **2024**, *357*, 129917. [CrossRef]
206. Rong, J.; Zhao, W.; Luo, W.; Kang, K.; Long, L.; Chen, Y.; Yao, X. Doping effect of rare earth metal ions Sm^{3+}, Nd^{3+} and Ce^{4+} on denitration performance of MnO_x catalyst in low temperature NH_3-SCR reaction. *J. Rare Earth* **2023**, *41*, 1323–1335. [CrossRef]
207. Ji, X.; Cai, Y.; Zhang, B.; Yu, H.; Liu, Q.; Wang, X.; Liu, A.; Qian, Q.; Tong, Q.; Tan, W.; et al. Optimization of robust $FeMnSmO_x$ catalyst for low-temperature (<150 °C) NH_3–SCR of NO_x. *Ind. Eng. Chem. Res.* **2024**, *63*, 2705–2716. [CrossRef]
208. He, X.; Zhu, F.; Dong, L.; Guo, H.; Liu, X.; Ren, G.; Ma, X. Sm-MnO_x/TiO_2-{001} with preferentially exposed anatase {001} facet for selective catalytic reduction of NO with NH_3. *Appl. Catal. A Gen.* **2023**, *664*, 119353. [CrossRef]
209. Wang, F.; Wang, P.; Lan, T.; Shen, Y.; Ren, W.; Zhang, D. Ultralow-temperature NO_x reduction over $SmMn_2O_5$ Mullite catalysts via modulating the superficial dual-functional active sites. *ACS Catal.* **2022**, *12*, 7622–7632. [CrossRef]
210. Wang, Q.; Wang, Y.; Wei, L.; Wang, K.; Liu, C.; Ma, D.; Liu, Q. Promotional mechanism of activity of $CeEuMnO_x$ ternary oxide for low temperature SCR of NO_x. *J. Rare Earth* **2023**, *41*, 965–974. [CrossRef]
211. Guan, J.; Zhou, L.; Li, W.; Hu, D.; Wen, J.; Huang, B. Improving the performance of Gd addition on catalytic activity and SO_2 resistance over MnO_x/ZSM-5 catalysts for low-temperature NH_3-SCR. *Catalysts* **2021**, *11*, 324. [CrossRef]

212. Gao, C.; Xiao, B.; Shi, J.W.; He, C.; Wang, B.; Ma, D.; Cheng, Y.; Niu, C. Comprehensive understanding the promoting effect of Dy-doping on $MnFeO_x$ nanowires for the low-temperature NH_3-SCR of NO_x: An experimental and theoretical study. *J. Catal.* **2019**, *380*, 55–67. [CrossRef]
213. Xu, B.; Wang, Z.; Hu, J.; Zhang, L.; Zhang, Z.; Liang, H.; Zhang, Y.; Fan, G. Dy-modified Mn/TiO_2 catalyst used for the selective catalytic reduction of NO in ammonia at low temperatures. *Molecules* **2024**, *29*, 277. [CrossRef] [PubMed]
214. Zhuang, K.; ZHANG, Y.P.; HUANG, T.J.; Bin, L.U.; Kai, S.H.E.N. Sulfur-poisoning and thermal reduction regeneration of holmium-modified Fe-Mn/TiO_2 catalyst for low-temperature SCR. *J. Fuel Chem. Technol.* **2017**, *45*, 1356–1364. [CrossRef]
215. Fang, Z.; Zhang, S.; Wang, A.; Guo, Y.; Guo, Y.; Wang, L.; Zhan, W. Er-modified MnO_x for selective catalytic reduction of NO_x with NH_3 at low temperature: Promoting effect of erbium on catalytic performance. *J. Rare Earth* **2023**, *41*, 917–925. [CrossRef]
216. Niu, C.; Wang, B.; Xing, Y.; Su, W.; He, C.; Xiao, L.; Xu, Y.; Zhao, S.; Cheng, Y.; Shi, J.W. Thulium modified MnO_x/TiO_2 catalyst for the low-temperature selective catalytic reduction of NO with ammonia. *J. Clean. Prod.* **2021**, *290*, 125858. [CrossRef]
217. Liu, J.; Lv, D.; Wang, Y.; Zhao, Y.; Li, G.; Zhang, G. Influence of catalyst structural remodelling on the performance of NH_3-SCR reactions: A Mini Review. *ChemCatChem* 2024, e202401076, *Early View*. [CrossRef]
218. Zha, K.; Cai, S.; Hu, H.; Li, H.; Yan, T.; Shi, L.; Zhang, D. In situ DRIFTs investigation of promotional effects of tungsten on MnO_x-CeO_2/meso-TiO_2 catalysts for NO_x reduction. *J. Phys. Chem. C* **2017**, *121*, 25243–25254. [CrossRef]
219. Xue, H.; Guo, X.; Mao, D.; Meng, T.; Yu, J.; Ma, Z. Phosphotungstic acid-modified MnO_x for selective catalytic reduction of NO_x with NH_3. *Catalysts* **2022**, *12*, 1248. [CrossRef]
220. Zhang, Y.; Wang, D.; Wang, J.; Chen, Q.; Zhang, Z.; Pan, X.; Miao, Z.; Zhan, B.; Wu, Z.; Yang, X. $BiMnO_3$ perovskite catalyst for selective catalytic reduction of NO with NH_3 at low temperature. *Chin. J. Catal.* **2012**, *33*, 1448–1454. [CrossRef]
221. Liang, Y.; Liu, W.; Wu, H.; Liu, Q.; Yao, L. Promoting effect of Si on MnO_x catalysts for low-temperature NH_3-SCR of NO: Enhanced N_2 selectivity and SO_2 resistance. *Fuel* **2024**, *355*, 129478. [CrossRef]
222. Zhu, Y.; Wang, J.; Ma, C.; Zhang, Y.; Qiao, W.; Ling, L. Development of highly active three-dimensional cross-linked structural manganese-titanium composite oxides for NO_x abatement: Insight into the resistance to sulfur and alkali metal poisoning mechanism. *Chem. Eng. J.* **2023**, *474*, 145573. [CrossRef]
223. Chen, Z.; Yang, Q.; Li, H.; Li, X.; Wang, L.; Tsang, S.C. Cr–MnO_x mixed-oxide catalysts for selective catalytic reduction of NO_x with NH_3 at low temperature. *J. Catal.* **2010**, *276*, 56–65. [CrossRef]
224. Chen, Z.; Wang, F.; Li, H.; Yang, Q.; Wang, L.; Li, X. Low-temperature selective catalytic reduction of NO_x with NH_3 over Fe–Mn mixed-oxide catalysts containing $Fe_3Mn_3O_8$ phase. *Ind. Eng. Chem. Res.* **2012**, *51*, 202–212. [CrossRef]
225. Zhou, X.; Yu, F.; Sun, R.; Tian, J.; Wang, Q.; Dai, B.; Dan, J.; Pfeiffer, H. Two-dimensional MnFeCo layered double oxide as catalyst for enhanced selective catalytic reduction of NO_x with NH_3 at low temperature (25–150 °C). *Appl. Catal. A Gen.* **2020**, *592*, 117432. [CrossRef]
226. Zhang, K.; Xu, L.; Niu, S.; Lu, C.; Wang, D.; Zhang, Q.; Li, J. Iron-manganese-magnesium mixed oxides catalysts for selective catalytic reduction of NO_x with NH_3. *Korean J. Chem. Eng.* **2017**, *34*, 1858–1866. [CrossRef]
227. Chen, S.; Yan, Q.; Zhang, C.; Wang, Q. A novel highly active and sulfur resistant catalyst from Mn-Fe-Al layered double hydroxide for low temperature NH_3-SCR. *Catal. Today* **2019**, *327*, 81–89. [CrossRef]
228. Zhou, Y.; Ren, S.; Wang, M.; Yang, J.; Chen, Z.; Chen, L. Mn and Fe oxides co-effect on nanopolyhedron CeO_2 catalyst for NH_3-SCR of NO. *J. Energy Inst.* **2021**, *99*, 97–104. [CrossRef]
229. Yu, J.; Guo, F.; Wang, Y.; Zhu, J.; Liu, Y.; Su, F.; Gao, S.; Xu, G. Sulfur poisoning resistant mesoporous Mn-base catalyst for low-temperature SCR of NO with NH_3. *Appl. Catal. B* **2010**, *95*, 160–168. [CrossRef]
230. Qiao, J.; Wang, N.; Wang, Z.; Sun, W.; Sun, K. Porous bimetallic $Mn_2Co_1O_x$ catalysts prepared by a one-step combustion method for the low temperature selective catalytic reduction of NO_x with NH_3. *Catal. Commun.* **2015**, *72*, 111–115. [CrossRef]
231. Hu, X.; Huang, L.; Zhang, J.; Li, H.; Zha, K.; Shi, L.; Zhang, D. Facile and template-free fabrication of mesoporous 3D nanosphere-like $Mn_xCo_{3-x}O_4$ as highly effective catalysts for low temperature SCR of NO_x with NH_3. *J. Mater. Chem. A* **2018**, *6*, 2952–2963. [CrossRef]
232. Jiang, H.; Kong, D.; Niu, Y.; Wang, S. Synthesis of Co-doped MnO_2 catalysts with the assistance of PVP for low-temperature SCR. *Catal. Sci. Technol.* **2020**, *10*, 8086–8093. [CrossRef]
233. Chen, R.; Fang, X.; Li, J.; Zhang, Y.; Liu, Z. Mechanistic investigation of the enhanced SO_2 resistance of Co-modified MnO_x catalyst for the selective catalytic reduction of NO_x by NH_3. *Chem. Eng. J* **2023**, *452*, 139207. [CrossRef]
234. Qiu, M.; Zhan, S.; Yu, H.; Zhu, D. Low-temperature selective catalytic reduction of NO with NH_3 over ordered mesoporous $Mn_xCo_{3-x}O_4$ catalyst. *Catal. Commun.* **2015**, *62*, 107–111. [CrossRef]
235. Gao, F.; Tang, X.; Yi, H.; Li, J.; Zhao, S.; Wang, J.; Chu, C.; Li, C. Promotional mechanisms of activity and SO_2 tolerance of Co-or Ni-doped MnO_x-CeO_2 catalysts for SCR of NO_x with NH_3 at low temperature. *Chem. Eng. J.* **2017**, *317*, 20–31. [CrossRef]
236. Li, Y.; Chen, H.; Chen, L.; Zhang, Y.; Mi, Y.; Liao, M.; Liu, W.; Wu, D.; Li, Z.; Peng, H. Ternary $MnCoVO_x$ catalysts with remarkable *de*NO_x performance: Dual acid-redox sites control strategy. *Appl. Catal. B* **2022**, *318*, 121779. [CrossRef]
237. Wan, Y.; Zhao, W.; Tang, Y.; Li, L.; Wang, H.; Cui, Y.; Gu, J.; Li, Y.; Shi, J. Ni-Mn bi-metal oxide catalysts for the low temperature SCR removal of NO with NH_3. *Appl. Catal. B* **2014**, *148*, 114–122. [CrossRef]
238. Gao, F.; Tang, X.; Sani, Z.; Yi, H.; Zhao, S.; Yu, Q.; Zhou, Y.; Shi, Y.; Ni, S. Spinel-structured Mn–Ni nanosheets for NH_3-SCR of NO with good H_2O and SO_2 resistance at low temperature. *Catal. Sci. Technol.* **2020**, *10*, 7486–7501. [CrossRef]

239. Han, Y.; Mu, J.; Li, X.; Gao, J.; Fan, S.; Tan, F.; Zhao, Q. Triple-shelled $NiMn_2O_4$ hollow spheres as an efficient catalyst for low-temperature selective catalytic reduction of NO_x with NH_3. *Chem. Commun.* **2018**, *54*, 9797–9800. [CrossRef]
240. Yan, Q.; Xiao, J.; Gui, R.; Chen, Z.; Wang, Y.; Li, Y.; Zhu, T.; Wang, Q.; Xin, Y. Insights into enhancement of NH_3-SCR activity and N_2 selectivity of LDHs-derived $NiMnAlO_x$ catalysts: Combination of experiments and DFT calculations. *Appl. Catal. B* **2024**, *343*, 123489. [CrossRef]
241. Hou, Q.; Liu, Y.; Hou, Y.; Han, X.; Huang, Z. Tunable highly dispersed $Ni_{a-x}Mn_xAlO_y$ catalysts derived from layered double oxide for low temperature NO_x removal. *Catal. Lett.* **2024**, *154*, 4389–4402. [CrossRef]
242. Liu, J.; Li, X.; Li, R.; Zhao, Q.; Ke, J.; Xiao, H.; Wang, L.; Liu, S.; Tade, M.; Wang, S. Facile synthesis of tube-shaped Mn-Ni-Ti solid solution and preferable Langmuir-Hinshelwood mechanism for selective catalytic reduction of NO_x by NH_3. *Appl. Catal. A Gen.* **2018**, *549*, 289–301. [CrossRef]
243. Chen, L.; Li, R.; Li, Z.; Yuan, F.; Niu, X.; Zhu, Y. Effect of Ni doping in $Ni_xMn_{1-x}Ti_{10}$ (x = 0.1–0.5) on activity and SO_2 resistance for NH_3-SCR of NO studied with in situ DRIFTS. *Catal. Sci. Technol.* **2017**, *7*, 3243–3257. [CrossRef]
244. Yan, Q.; Xiao, J.; Gui, R.; Chen, Z.; Li, Y.; Zhu, T.; Wang, Q.; Xin, Y. Mechanistic insight into the promotion of the low-temperature NH_3–SCR activity over $NiMnFeO_x$ LDO catalysts: A Combined Experimental and DFT Study. *Environ. Sci. Technol.* **2023**, *57*, 20708–20717. [CrossRef] [PubMed]
245. Zuo, J.; Chen, Z.; Wang, F.; Yu, Y.; Wang, L.; Li, X. Low-temperature selective catalytic reduction of NO_x with NH_3 over novel Mn–Zr mixed oxide catalysts. *Ind. Eng. Chem. Res.* **2014**, *53*, 2647–2655. [CrossRef]
246. Zhang, B.; Liebau, M.; Liu, B.; Li, L.; Zhang, S.; Gläser, R. Selective catalytic reduction of NO_x with NH_3 over Mn–Zr–Ti mixed oxide catalysts. *J. Mater. Sci.* **2019**, *54*, 6943–6960. [CrossRef]
247. Lian, Z.; Liu, F.; He, H.; Shi, X.; Mo, J.; Wu, Z. Manganese–niobium mixed oxide catalyst for the selective catalytic reduction of NO_x with NH_3 at low temperatures. *Chem. Eng. J.* **2014**, *250*, 390–398. [CrossRef]
248. Chang, H.; Li, J.; Chen, X.; Ma, L.; Yang, S.; Schwank, J.W.; Hao, J. Effect of Sn on MnO_x–CeO_2 catalyst for SCR of NO_x by ammonia: Enhancement of activity and remarkable resistance to SO_2. *Catal. Commun.* **2012**, *27*, 54–57. [CrossRef]
249. Wang, C.; Gao, F.; Ko, S.; Liu, H.; Yi, H.; Tang, X. Structural control for inhibiting SO_2 adsorption in porous MnCe nanowire aerogel catalysts for low-temperature NH_3-SCR. *Chem. Eng. J.* **2022**, *434*, 134729. [CrossRef]
250. Song, J.; Liu, S.; Ji, Y.; Xu, W.; Yu, J.; Liu, B.; Chen, W.; Zhang, J.; Jia, L.; Zhu, T.; et al. Dual single-atom Ce-Ti/MnO_2 catalyst enhances low-temperature NH_3-SCR performance with high H_2O and SO_2 resistance. *Nano Res.* **2023**, *16*, 299–308. [CrossRef]
251. Wei, Y.; Jin, S.; Zhang, R.; Li, W.; Wang, J.; Yang, S.; Wang, H.; Yang, M.; Liu, Y.; Qiao, W.; et al. Preparation of mesoporous Mn–Ce–Ti–O aerogels by a one-pot sol–gel method for selective catalytic reduction of NO with NH_3. *Materials* **2020**, *13*, 475. [CrossRef] [PubMed]
252. Liu, Z.; Zhu, J.; Li, J.; Ma, L.; Woo, S.I. Novel Mn–Ce–Ti mixed-oxide catalyst for the selective catalytic reduction of NO_x with NH3. *ACS Appl. Mater. Interfaces* **2014**, *6*, 14500–14508. [CrossRef] [PubMed]
253. Chen, L.; Yao, X.; Cao, J.; Yang, F.; Tang, C.; Dong, L. Effect of Ti^{4+} and Sn^{4+} co-incorporation on the catalytic performance of CeO_2-MnO_x catalyst for low temperature NH_3-SCR. *Appl. Surf. Sci.* **2019**, *476*, 283–292. [CrossRef]
254. Meng, D.; Zhan, W.; Guo, Y.; Guo, Y.; Wang, L.; Lu, G. A highly effective catalyst of Sm-MnO_x for the NH_3-SCR of NO_x at low temperature: Promotional role of Sm and its catalytic performance. *ACS Catal.* **2015**, *5*, 5973–5983. [CrossRef]
255. Gao, C.; Shi, J.W.; Fan, Z.; Wang, B.; Wang, Y.; He, C.; Wang, X.; Li, J.; Niu, C. "Fast SCR" reaction over Sm-modified MnO_x-TiO_2 for promoting reduction of NO_x with NH_3. *Appl. Catal. A Gen.* **2018**, *564*, 102–112. [CrossRef]
256. Xu, Q.; Fang, Z.; Chen, Y.; Guo, Y.; Guo, Y.; Wang, L.; Wang, Y.; Zhang, J.; Zhan, W. Titania–samarium–manganese composite oxide for the low-temperature selective catalytic reduction of NO with NH_3. *Environ. Sci. Technol.* **2020**, *54*, 2530–2538. [CrossRef]
257. Chen, Z.; Ren, S.; Wang, M.; Yang, J.; Chen, L.; Liu, W.; Liu, Q.; Su, B. Insights into samarium doping effects on catalytic activity and SO_2 tolerance of $MnFeO_x$ catalyst for low-temperature NH_3-SCR reaction. *Fuel* **2022**, *321*, 124113. [CrossRef]
258. Sun, C.; Liu, H.; Chen, W.; Chen, D.; Yu, S.; Liu, A.; Dong, L.; Feng, S. Insights into the Sm/Zr co-doping effects on N_2 selectivity and SO_2 resistance of a MnO_x-TiO_2 catalyst for the NH_3-SCR reaction. *Chem. Eng. J.* **2018**, *347*, 27–40. [CrossRef]
259. Wang, B.; Wang, M.; Han, L.; Hou, Y.; Bao, W.; Zhang, C.; Feng, G.; Chang, L.; Huang, Z.; Wang, J. Improved activity and SO_2 resistance by Sm-modulated redox of $MnCeSmTiO_x$ mesoporous amorphous oxides for low-temperature NH_3-SCR of NO. *ACS Catal.* **2020**, *10*, 9034–9045. [CrossRef]
260. Sun, P.; Guo, R.T.; Liu, S.M.; Wang, S.X.; Pan, W.G.; Li, M.Y. The enhanced performance of MnO_x catalyst for NH_3-SCR reaction by the modification with Eu. *Appl. Catal. A Gen.* **2017**, *531*, 129–138. [CrossRef]
261. Fan, Z.; Shi, J.W.; Gao, C.; Gao, G.; Wang, B.; Wang, Y.; He, C.; Niu, C. Gd-modified MnO_x for the selective catalytic reduction of NO by NH_3: The promoting effect of Gd on the catalytic performance and sulfur resistance. *Chem. Eng. J.* **2018**, *348*, 820–830. [CrossRef]
262. Ma, Z.; Wu, X.; Feng, Y.; Si, Z.; Weng, D. Effects of WO_3 doping on stability and N_2O escape of MnO_x–CeO_2 mixed oxides as a low-temperature SCR catalyst. *Catal. Commun.* **2015**, *69*, 188–192. [CrossRef]
263. Yang, S.; Qi, F.; Xiong, S.; Dang, H.; Liao, Y.; Wong, P.K.; Li, J. MnO_x supported on Fe–Ti spinel: A novel Mn based low temperature SCR catalyst with a high N_2 selectivity. *Appl. Catal. B* **2016**, *181*, 570–580. [CrossRef]
264. Jia, B.; Guo, J.; Shu, S.; Fang, N.; Li, J.; Chu, Y. Effects of different Zr/Ti ratios on NH_3–SCR over $MnO_x/Zr_yTi_{1-y}O_2$: Characterization and reaction mechanism. *Mol. Catal.* **2017**, *443*, 25–37. [CrossRef]

265. Lee, S.M.; Park, K.H.; Hong, S.C. MnO_x/CeO_2–TiO_2 mixed oxide catalysts for the selective catalytic reduction of NO with NH_3 at low temperature. *Chem. Eng. J.* **2012**, *195*, 323–331. [CrossRef]
266. Shen, B.; Zhang, X.; Ma, H.; Yao, Y.; Liu, T. A comparative study of Mn/CeO_2, Mn/ZrO_2 and Mn/Ce-ZrO_2 for low temperature selective catalytic reduction of NO with NH_3 in the presence of SO_2 and H_2O. *J. Environ. Sci.* **2013**, *25*, 791–800. [CrossRef]
267. Zhang, Q.; Qiu, C.; Xu, H.; Lin, T.; Lin, Z.; Gong, M.; Chen, Y. Low-temperature selective catalytic reduction of NO with NH_3 over monolith catalyst of MnO_x/CeO_2–ZrO_2–Al_2O_3. *Catal. Today* **2011**, *175*, 171–176. [CrossRef]
268. Wang, H.; Chen, W.; Jin, W.; Liu, Y. Mn mixed oxide catalysts supported on Sn-doped CoAl-LDO for low-temperature NH_3-SCR. *Catal. Sci. Technol.* **2023**, *13*, 3147–3157. [CrossRef]
269. Xie, A.; Tang, Y.; Huang, X.; Jin, X.; Gu, P.; Luo, S.; Yao, C.; Li, X. Three-dimensional nanoflower $MnCrO_x$/Sepiolite catalyst with increased SO_2 resistance for NH_3-SCR at low temperature. *Chem. Eng. J.* **2019**, *370*, 897–905. [CrossRef]
270. Mu, J.; Li, X.; Sun, W.; Fan, S.; Wang, X.; Wang, L.; Qin, M.; Gan, G.; Yin, Z.; Zhang, D. Enhancement of low-temperature catalytic activity over a highly dispersed Fe–Mn/Ti catalyst for selective catalytic reduction of NO_x with NH_3. *Ind. Eng. Chem. Res.* **2018**, *57*, 10159–10169. [CrossRef]
271. Shen, B.; Liu, T.; Zhao, N.; Yang, X.; Deng, L. Iron-doped Mn-Ce/TiO_2 catalyst for low temperature selective catalytic reduction of NO with NH_3. *J. Environ. Sci.* **2010**, *22*, 1447–1454. [CrossRef] [PubMed]
272. Thirupathi, B.; Smirniotis, P.G. Nickel-doped Mn/TiO_2 as an efficient catalyst for the low-temperature SCR of NO with NH_3: Catalytic evaluation and characterizations. *J. Catal.* **2012**, *288*, 74–83. [CrossRef]
273. Xiao, F.; Gu, Y.; Tang, Z.; Han, F.; Shao, J.; Xu, Q.; Zhu, H. ZrO_2 modified MnO_x/attapulgite catalysts for NH_3-SCR of NO at low temperature. *J. Chem. Eng. Jpn.* **2015**, *48*, 481–487. [CrossRef]
274. Zhao, Q.; Huang, X.; Zhao, T.; Cui, R.; Zhang, J.; Tang, Z. Rationally designed confined structure Ce-Mn-TNTs catalyst for low-temperature NH_3-SCR reaction with superior activity and H_2O/SO_2 tolerance. *ACS Sustain. Chem. Eng.* **2024**, *12*, 9987–10001. [CrossRef]
275. Jin, R.; Liu, Y.; Wang, Y.; Cen, W.; Wu, Z.; Wang, H.; Weng, X. The role of cerium in the improved SO_2 tolerance for NO reduction with NH_3 over Mn-Ce/TiO_2 catalyst at low temperature. *Appl. Catal. B* **2014**, *148*, 582–588. [CrossRef]
276. Li, F.; Xie, J.; Fang, D.; He, F.; Qi, K.; Gong, P. Mechanistic study of Ce-modified MnO_x/TiO_2 catalysts with high NH_3-SCR performance and SO_2 resistance at low temperatures. *Res. Chem. Intermediat.* **2017**, *43*, 5413–5432. [CrossRef]
277. Zhao, X.; Mao, L.; Dong, G. Mn-Ce-V-WO_x/TiO_2 SCR catalysts: Catalytic activity, stability and interaction among catalytic oxides. *Catalysts* **2018**, *8*, 76. [CrossRef]
278. Huang, J.; Huang, H.; Jiang, H.; Liu, L. The promotional role of Nd on Mn/TiO_2 catalyst for the low-temperature NH_3-SCR of NO_x. *Catal. Today* **2019**, *332*, 49–58. [CrossRef]
279. Liu, J.; Guo, R.T.; Li, M.Y.; Sun, P.; Liu, S.M.; Pan, W.G.; Liu, S.W.; Sun, X. Enhancement of the SO_2 resistance of Mn/TiO_2 SCR catalyst by Eu modification: A mechanism study. *Fuel* **2018**, *223*, 385–393. [CrossRef]
280. Li, W.; Zhang, C.; Li, X.; Tan, P.; Zhou, A.; Fang, Q.; Chen, G. Ho-modified Mn-Ce/TiO_2 for low-temperature SCR of NO_x with NH_3: Evaluation and characterization. *Chin. J. Catal.* **2018**, *39*, 1653–1663. [CrossRef]
281. Zhang, X.; Yan, Q.; Wang, Q. Design of practical Ce/CoMnAl-LDO catalyst for low-temperature NH_3-SCR. *Catal. Commun.* **2020**, *142*, 106037. [CrossRef]
282. Jiang, L.; Liu, Q.; Ran, G.; Kong, M.; Ren, S.; Yang, J.; Li, J. V_2O_5-modified Mn-Ce/AC catalyst with high SO_2 tolerance for low-temperature NH_3-SCR of NO. *Chem. Eng. J.* **2019**, *370*, 810–821. [CrossRef]
283. Wang, C.; Sani, Z.; Tang, X.; Wang, Y.; Yi, H.; Gao, F. Novel Ni-Mn bi-oxides doped active coke catalysts for NH_3-SCR De-NO_x at low temperature. *ChemistrySelect* **2020**, *5*, 6494–6503. [CrossRef]
284. Li, R.; Yue, T.; Zheng, Y.; Li, G.; Gao, J.; Tong, Y.; Wang, J.; Ma, M.; Su, W. Promotional mechanism of La-Mn-Fe modification on activated coke for NH_3-SCR of NO_x at low temperatures. *Fuel* **2024**, *371*, 132016. [CrossRef]
285. Yang, J.; Zhou, J.; Tong, W.; Zhang, T.; Kong, M.; Ren, S. Low-temperature flue gas denitration with transition metal oxides supported on biomass char. *J. Energy Inst.* **2019**, *92*, 1158–1166. [CrossRef]
286. Chen, L.; Ren, S.; Liu, W.; Yang, J.; Chen, Z.; Wang, M.; Liu, Q. Low-temperature NH_3-SCR activity of M (M= Zr, Ni and Co) doped MnO_x supported biochar catalysts. *J. Environ. Chem. Eng.* **2021**, *9*, 106504. [CrossRef]
287. Fang, C.; Zhang, D.; Cai, S.; Zhang, L.; Huang, L.; Li, H.; Maitarad, P.; Shi, L.; Gao, R.; Zhang, J. Low-temperature selective catalytic reduction of NO with NH_3 over nanoflaky MnO_x on carbon nanotubes in situ prepared via a chemical bath deposition route. *Nanoscale* **2013**, *5*, 9199–9207. [CrossRef]
288. Pourkhalil, M.; Moghaddam, A.Z.; Rashidi, A.; Towfighi, J.; Mortazavi, Y. Preparation of highly active manganese oxides supported on functionalized MWNTs for low temperature NO_x reduction with NH_3. *Appl. Surf. Sci.* **2013**, *279*, 250–259. [CrossRef]
289. Zhang, D.; Zhang, L.; Fang, C.; Gao, R.; Qian, Y.; Shi, L.; Zhang, J. MnO_x–CeO_x/CNTs pyridine-thermally prepared via a novel in situ deposition strategy for selective catalytic reduction of NO with NH_3. *RSC Adv.* **2013**, *3*, 8811–8819. [CrossRef]
290. Zhang, D.; Zhang, L.; Shi, L.; Fang, C.; Li, H.; Gao, R.; Huang, L.; Zhang, J. In situ supported MnO_x–CeO_x on carbon nanotubes for the low-temperature selective catalytic reduction of NO with NH_3. *Nanoscale* **2013**, *5*, 1127–1136. [CrossRef]
291. Xu, Y.; Wang, P.; Pu, Y.; Jiang, L.; Yang, L.; Jiang, W.; Yao, L. MnCe/GAC-CNTs catalyst with high activity, SO_2 and H_2O tolerance for low-temperature NH_3-SCR. *Sep. Purif. Technol.* **2023**, *305*, 122498. [CrossRef]

292. You, X.; Sheng, Z.; Yu, D.; Yang, L.; Xiao, X.; Wang, S. Influence of Mn/Ce ratio on the physicochemical properties and catalytic performance of graphene supported MnO_x-CeO_2 oxides for NH_3-SCR at low temperature. *Appl. Surf. Sci.* **2017**, *423*, 845–854. [CrossRef]
293. Sheng, Z.; Ma, D.; Yu, D.; Xiao, X.; Huang, B.; Yang, L.; Wang, S. Synthesis of novel MnO_x@ TiO_2 core-shell nanorod catalyst for low-temperature NH_3-selective catalytic reduction of NO_x with enhanced SO_2 tolerance. *Chin. J. Catal.* **2018**, *39*, 821–830. [CrossRef]
294. Fu, Z.; Zhang, G.; Han, W.; Tang, Z. The water resistance enhanced strategy of Mn based SCR catalyst by construction of TiO_2 shell and superhydrophobic coating. *Chem. Eng. J.* **2021**, *426*, 131334. [CrossRef]
295. Ma, D.; Yang, L.; Huang, B.; Wang, L.; Wang, X.; Sheng, Z.; Dong, F. MnO_x–CeO_2@TiO_2 core–shell composites for low temperature SCR of NO_x. *New J. Chem.* **2019**, *43*, 15161–15168. [CrossRef]
296. Cheng, S.; Shao, J.; Huang, B.; Guan, J.; Zhou, L. Promotion effect of urchin-like MnO_x@PrO_x hollow core–shell structure catalysts for the low-temperature selective catalytic reduction of NO with NH_3. *RSC Adv.* **2020**, *10*, 13855–13865. [CrossRef]
297. Li, S.; Huang, B.; Yu, C. A CeO_2-MnO_x core-shell catalyst for low-temperature NH_3-SCR of NO. *Catal. Commun.* **2017**, *98*, 47–51. [CrossRef]
298. Gan, L.; Li, K.; Yang, W.; Chen, J.; Peng, Y.; Li, J. Core-shell-like structured α-MnO_2@CeO_2 catalyst for selective catalytic reduction of NO: Promoted activity and SO_2 tolerance. *Chem. Eng. J.* **2020**, *391*, 123473. [CrossRef]
299. Cai, Z.; Zhang, G.; Tang, Z.; Zhang, J. MnFe@ CeO_x core–shell nanocages for the selective catalytic reduction of NO with NH_3 at low temperature. *ACS Appl. Nano Mater.* **2022**, *5*, 3619–3631. [CrossRef]
300. Yu, C.; Hou, D.; Huang, B.; Lu, M.; Peng, R.; Zhong, Z. A MnO_x@Eu-CeO_x nanorod catalyst with multiple protective effects: Strong SO_2-tolerance for low temperature $DeNO_x$ processes. *J. Hazard. Mater.* **2020**, *399*, 123011. [CrossRef]
301. Li, Y.; Hou, Y.; Zhang, Y.; Yang, Y.; Huang, Z. Confinement of MnO_x@Fe_2O_3 core-shell catalyst with titania nanotubes: Enhanced N_2 selectivity and SO_2 tolerance in NH_3-SCR process. *J. Colloid Interface Sci.* **2022**, *608*, 2224–2234. [CrossRef] [PubMed]
302. Zhao, T.; Huang, X.; Cui, R.; Zhang, G.; Tang, Z. Unveiling a remarkable enhancement role by designing a confined structure Ho-TNTs@Mn catalyst for low-temperature NH_3-SCR reaction. *Nanoscale* **2023**, *15*, 12540–12557. [CrossRef] [PubMed]
303. Zhao, T.; Huang, X.; Cui, R.; Song, X.; Tang, Z. Design the confinement structure Mn-TNTs@Ce catalyst for selective catalytic reduction of nitrogen oxides with superior SO_2 resistance over a wider operation window. *Appl. Catal. B* **2024**, *358*, 124353. [CrossRef]
304. Huang, X.; Dong, F.; Zhang, G.; Guo, Y.; Tang, Z. A strategy for constructing highly efficient yolk-shell Ce@Mn@TiO_x catalyst with dual active sites for low-temperature selective catalytic reduction of NO with NH_3. *Chem. Eng. J.* **2021**, *419*, 129572. [CrossRef]
305. Yan, R.; Lin, S.; Li, Y.; Liu, W.; Mi, Y.; Tang, C.; Wang, L.; Peng, H. Novel shielding and synergy effects of Mn-Ce oxides confined in mesoporous zeolite for low temperature selective catalytic reduction of NO_x with enhanced SO_2/H_2O tolerance. *J. Hazard Mater.* **2020**, *396*, 122592. [CrossRef]
306. Cai, S.; Hu, H.; Li, H.; Shi, L.; Zhang, D. Design of multi-shell Fe_2O_3@ MnO_x@CNTs for the selective catalytic reduction of NO with NH_3: Improvement of catalytic activity and SO_2 tolerance. *Nanoscale* **2016**, *8*, 3588–3598. [CrossRef]
307. Zhang, L.; Zhang, D.; Zhang, J.; Cai, S.; Fang, C.; Huang, L.; Li, H.; Gao, R.; Shi, L. Design of meso-TiO_2@MnO_x–CeO_x/CNTs with a core–shell structure as $DeNO_x$ catalysts: Promotion of activity, stability and SO_2-tolerance. *Nanoscale* **2013**, *5*, 9821–9829. [CrossRef]
308. Qi, Z.; Gao, F.; Ko, S.; Tang, X.; Yi, H.; Liu, H.; Luo, N.; Du, Y. Synthesis of novel $Co_{(3-x)}$ Mn_xO_4@TiO_2 core-shell catalyst for low-temperature NH_3-SCR of NO_x with enhanced SO_2 tolerance. *Chem. Phys.* **2022**, *5*, 100120. [CrossRef]
309. Wang, X.; Zhao, Z.; Xu, Y.; Li, Q. Promoting effect of Ti addition on three-dimensionally ordered macroporous Mn-Ce catalysts for NH_3-SCR reaction: Enhanced N_2 selectivity and remarkable water resistance. *Appl. Surf. Sci.* **2021**, *569*, 151047. [CrossRef]
310. Liu, Y.; Zhu, B.; Chen, J.; Sun, Y.; Xu, M. Effect of Fe doping on NH_3 adsorption and resistance to sulfur poisoning on the surface of β-MnO_2 (110): A DFT-D study. *J. Mater. Sci.* **2022**, *57*, 18468–18485. [CrossRef]
311. Tian, B.; Ma, S.; Guo, J.; Zhao, Y.; Gao, T.; Jiang, X. Superior indicative and regulative function of Fe doping amount for MnO_2 catalyst with an oxygen vacancy in NH_3-SCR reaction: A DFT+ U study. *Appl. Surf. Sci.* **2022**, *601*, 154162. [CrossRef]
312. Wu, Z.; Jiang, B.; Liu, Y. Effect of transition metals addition on the catalyst of manganese/titania for low-temperature selective catalytic reduction of nitric oxide with ammonia. *Appl. Catal. B* **2008**, *79*, 347–355. [CrossRef]
313. Lin, Q.; Li, J.; Ma, L.; Hao, J. Selective catalytic reduction of NO with NH_3 over Mn–Fe/USY under lean burn conditions. *Catal. Today* **2010**, *151*, 251–256. [CrossRef]
314. Feng, X.; Wang, B.; Gao, G.; Gao, S.; Xie, C.; Shi, J.W. $Mn_yCo_{3-y}O_x$ bimetallic oxide prepared by ultrasonic technology for significantly improved catalytic performance in the reduction of NO_x with NH_3. *Fuel* **2023**, *352*, 129159. [CrossRef]
315. Kang, H.; Wang, J.; Zheng, J.; Chu, W.; Tang, C.; Ji, J.; Ren, R.; Wu, M.; Jing, F. Solvent-free elaboration of Ni-doped MnO_x catalysts with high performance for NH_3-SCR in low and medium temperature zones. *Mol. Catal.* **2021**, *501*, 111376. [CrossRef]
316. Liu, J.; Wu, X.; Hou, B.; Du, Y.; Liu, L.; Yang, B. $NiMn_2O_4$ sphere catalyst for the selective catalytic reduction of NO by NH_3: Insight into the enhanced activity via solvothermal method. *J. Environ. Chem. Eng.* **2021**, *9*, 105152. [CrossRef]
317. Che, Y.; Liu, X.; Shen, Z.; Zhang, K.; Hu, X.; Chen, A.; Zhang, D. Improved N_2 selectivity of MnO_x catalysts for NO_x reduction by engineering bridged Mn^{3+} sites. *Langmuir* **2023**, *39*, 7434–7443. [CrossRef]
318. Li, Y.; Li, G.; Zou, Y.; Liu, W.; Zhang, H.; Lu, S.; Li, Z.; Zhang, S.; Peng, H. Unveiling the remarkable $deNO_x$ performance of $MnMoVO_x$ catalysts via dual regulation of the redox and acid sites. *Appl. Catal. B* **2024**, *344*, 123612. [CrossRef]

319. Li, M.; Gao, M.; He, G.; Yu, Y.; He, H. Mechanistic insight into the promotion of the low-temperature NH_3-selective catalytic reduction activity over $Mn_xCe_{1-x}O_y$ catalysts: A combined experimental and density functional theory study. *Environ. Sci. Technol.* **2023**, *57*, 3875–3882. [CrossRef]
320. Fang, X.; Liu, Y.; Cheng, Y.; Cen, W. Mechanism of Ce-modified birnessite-MnO_2 in promoting SO_2 poisoning resistance for low-temperature NH_3-SCR. *ACS Catal.* **2021**, *11*, 4125–4135. [CrossRef]
321. Cheng, L.; Sin, S.; Ji, J.; Yang, S.; Tan, C.; Gu, Z.; Song, W.; Huang, C.; Sun, C.; Tang, C.; et al. Selective catalytic reduction of NO with NH_3 over MnO_x-CeO_2 catalysts: The great synergy between CeO_2 and crystalline phase of Mn_3O_4. *Fuel* **2023**, *342*, 127772. [CrossRef]
322. Zhu, Q.; Wang, A.; Zhang, J.; Guo, Y.; Guo, Y.; Wang, L.; Zhan, W. Low-temperature NH_3-SCR on Ce_x-Mn-Ti_y mixed oxide catalysts: Improved performance by the mutual effect between Ce and Ti. *Catalysts* **2022**, *12*, 471. [CrossRef]
323. Teng, Y.; Guo, X.; Xue, H.; Meng, T.; Han, L. Activity improvement of Mn/Al_2O_3 for NH_3-SCR reaction via the rare-earth (Ce, La, Nd and Y) oxides modification. *Catal. Lett.* **2024**, *154*, 3645–3653. [CrossRef]
324. Gevers, L.E.; Enakonda, L.R.; Shahid, A.; Ould-Chikh, S.; Silva, C.I.; Paalanen, P.P.; Aguilar-Tapia, A.; Jean-Louis, H.; Nejib Hedhili, M.; Wen, F.; et al. Unraveling the structure and role of Mn and Ce for NO_x reduction in application-relevant catalysts. *Nat. Commun.* **2022**, *13*, 2960. [CrossRef] [PubMed]
325. Liu, Y.; Gu, T.; Weng, X.; Wang, Y.; Wu, Z.; Wang, H. DRIFT studies on the selectivity promotion mechanism of Ca-modified Ce-Mn/TiO_2 catalysts for low-temperature NO reduction with NH_3. *J. Phys. Chem. C* **2012**, *116*, 16582–16592. [CrossRef]
326. Kim, D.H.; Park, Y.J.; Lee, K.Y.; Ha, H.P.; Kwon, D.W. Surface insights into MnO_x-based catalysts containing metal oxides for the selective catalytic reduction of NO_x with NH_3. *Appl. Catal. A Gen.* **2022**, *643*, 118770. [CrossRef]
327. Liu, Y.; Gao, F.; Ko, S.; Wang, C.; Liu, H.; Tang, X.; Yi, H.; Zhou, Y. Superior catalytic performance within H_2O vapor of W-modified $CoMn_2O_4/TiO_2$ catalyst for selective catalytic reduction of NO_x with NH_3. *Chem. Eng. J.* **2022**, *434*, 134770. [CrossRef]
328. Cai, Z.; Zhang, G.; Tang, Z.; Zhang, J. Engineering yolk–shell MnFe@CeO_x@TiO_x nanocages as a highly efficient catalyst for selective catalytic reduction of NO with NH_3 at low temperatures. *Nanoscale* **2022**, *14*, 12281–12296. [CrossRef]
329. Qiao, T.; Liu, Z.; Liu, C.; Meng, W.; Sun, H.; Lu, Y. MnO_x location on MnO_x-ZSM-5 to influence the catalytic activity for selective catalytic reduction of NO_x by NH_3. *Appl. Catal. A Gen.* **2021**, *617*, 118128. [CrossRef]
330. Ran, X.; Li, M.; Wang, K.; Qian, X.; Fan, J.; Sun, Y.; Luo, W.; Teng, W.; Zhang, W.; Yang, J. Spatially confined tuning the interfacial synergistic catalysis in mesochannels toward selective catalytic reduction. *ACS Appl. Mater. Interfaces* **2019**, *11*, 19242–19251. [CrossRef]
331. Guo, K.; Fan, G.; Gu, D.; Yu, S.; Ma, K.; Liu, A.; Tan, W.; Wang, J.; Du, X.; Zou, W.; et al. Pore size expansion accelerates ammonium bisulfate decomposition for improved sulfur resistance in low-temperature NH_3-SCR. *ACS Appl. Mater. Interfaces* **2019**, *11*, 4900–4907. [CrossRef] [PubMed]
332. Ito, E.; Hultermans, R.J.; Lugt, P.M.; Burgers, M.H.W.; Rigutto, M.S.; Van Bekkum, H.; Van den Bleek, C.M. Selective reduction of NO_x with ammonia over cerium-exchanged mordenite. *Appl. Catal. B* **1994**, *4*, 95–104. [CrossRef]
333. Liu, J.; Shi, X.; Lv, Z.; Yu, Y.; He, H. Ceria–tungsten–tin oxide catalysts with superior regeneration capacity after sulfur poisoning for NH_3-SCR process. *Catal. Sci. Technol.* **2022**, *12*, 2471–2481. [CrossRef]
334. Li, P.; Xin, Y.; Li, Q.; Wang, Z.; Zhang, Z.; Zheng, L. Ce–Ti amorphous oxides for selective catalytic reduction of NO with NH_3: Confirmation of Ce–O–Ti active sites. *Environ. Sci. Technol.* **2012**, *46*, 9600–9605. [CrossRef] [PubMed]
335. Liu, B.; Liu, J.; Xin, L.; Zhang, T.; Xu, Y.; Jiang, F.; Liu, X. Unraveling reactivity descriptors and structure sensitivity in low-temperature NH_3-SCR reaction over $CeTiO_x$ catalysts: A combined computational and experimental study. *ACS Catal.* **2021**, *11*, 7613–7636. [CrossRef]
336. Tang, C.; Zhang, H.; Dong, L. Ceria-based catalysts for low-temperature selective catalytic reduction of NO with NH_3. *Catal. Sci. Technol.* **2016**, *6*, 1248–1264. [CrossRef]
337. Ma, L.; Seo, C.Y.; Nahata, M.; Chen, X.; Li, J.; Schwank, J.W. Shape dependence and sulfate promotion of CeO_2 for selective catalytic reduction of NO_x with NH_3. *Appl. Catal. B* **2018**, *232*, 246–259. [CrossRef]
338. Zhang, P.; Guo, R.T.; Wu, L.J.; Pan, W.G. The enhancement of NH_3-SCR performance for CeO_2 catalyst by CO pretreatment. *Environ. Sci. Pollut. Res.* **2020**, *27*, 13617–13636. [CrossRef]
339. Yao, X.; Wang, Z.; Yu, S.; Yang, F.; Dong, L. Acid pretreatment effect on the physicochemical property and catalytic performance of CeO_2 for NH_3-SCR. *Appl. Catal. A Gen.* **2017**, *542*, 282–288. [CrossRef]
340. Chen, L.; Wang, Q.; Wang, X.; Cong, Q.; Ma, H.; Guo, T.; Li, S.; Li, W. High-performance CeO_2/halloysite hierarchical catalysts with promotional redox property and acidity for the selective catalytic reduction of NO with NH_3. *Chem. Eng. J.* **2020**, *390*, 124251. [CrossRef]
341. Zhang, L.; Li, L.; Cao, Y.; Yao, X.; Ge, C.; Gao, F.; Deng, Y.; Tang, C.; Dong, L. Getting insight into the influence of SO_2 on TiO_2/CeO_2 for the selective catalytic reduction of NO by NH_3. *Appl. Catal. B* **2015**, *165*, 589–598. [CrossRef]
342. Zhang, Z.; Li, R.; Wang, M.; Li, Y.; Tong, Y.; Yang, P.; Zhu, Y. Two steps synthesis of $CeTiO_x$ oxides nanotube catalyst: Enhanced activity, resistance of SO_2 and H_2O for low temperature NH_3-SCR of NO_x. *Appl. Catal. B* **2021**, *282*, 119542. [CrossRef]
343. Yao, X.; Kang, K.; Cao, J.; Chen, L.; Luo, W.; Zhao, W.; Rong, J.; Chen, Y. Enhancing the denitration performance and anti-K poisoning ability of CeO_2-TiO_2/P25 catalyst by H_2SO_4 pretreatment: Structure-activity relationship and mechanism study. *Appl. Catal. B* **2020**, *269*, 118808. [CrossRef]

344. Zhou, Q.; He, K.; Wang, X.; Lim, K.H.; Liu, P.; Wang, W.; Wang, Q. Investigation on the redox/acidic features of bimetallic MOF-derived $CeMO_x$ catalysts for low-temperature NH_3-SCR of NO_x. *Appl. Catal. A Gen.* **2022**, *643*, 118796. [CrossRef]
345. Zhang, R.; Zhong, Q.; Zhao, W.; Yu, L.; Qu, H. Promotional effect of fluorine on the selective catalytic reduction of NO with NH3 over CeO_2-TiO_2 catalyst at low temperature. *Appl. Surf. Sci.* **2014**, *289*, 237–244. [CrossRef]
346. Zeng, Y.; Wang, Y.; Hongmanorom, P.; Wang, Z.; Zhang, S.; Chen, J.; Zhong, Q.; Kawi, S. Active sites adjustable phosphorus promoted CeO_2/TiO_2 catalysts for selective catalytic reduction of NO_x by NH_3. *Chem. Eng. J.* **2021**, *409*, 128242. [CrossRef]
347. Zhao, W.; Tang, Y.; Wan, Y.; Li, L.; Yao, S.; Li, X.; Gu, J.; Li, Y.; Shi, J. Promotion effects of SiO_2 or/and Al_2O_3 doped CeO_2/TiO_2 catalysts for selective catalytic reduction of NO by NH_3. *J. Hazard. Mater.* **2014**, *278*, 350–359. [CrossRef]
348. Liu, C.; Chen, L.; Li, J.; Ma, L.; Arandiyan, H.; Du, Y.; Xu, J.; Hao, J. Enhancement of activity and sulfur resistance of CeO_2 supported on TiO_2–SiO_2 for the selective catalytic reduction of NO by NH_3. *Environ. Sci. Technol.* **2012**, *46*, 6182–6189. [CrossRef]
349. Li, L.; Tan, W.; Wei, X.; Fan, Z.; Liu, A.; Guo, K.; Ma, K.; Yu, S.; Ge, C.; Tang, C.; et al. Mo doping as an effective strategy to boost low temperature NH_3-SCR performance of CeO_2/TiO_2 catalysts. *Catal. Commun.* **2018**, *114*, 10–14. [CrossRef]
350. Wang, D.; Peng, Y.; Yang, Q.; Hu, F.; Li, J.; Crittenden, J. NH_3-SCR performance of WO_3 blanketed CeO_2 with different morphology: Balance of surface reducibility and acidity. *Catal. Today* **2019**, *332*, 42–48. [CrossRef]
351. Wang, F.; Wang, C.; Zhao, K.; Shan, Y.; Ma, Y.; Wang, C.; Li, Z.; Sun, X.; Li, K.; He, H.; et al. The design of the highly active NH_3-SCR catalyst Ce-W/UiO-66: Close coupling of active sites and acidic sites. *Sep. Purif. Technol.* **2022**, *300*, 121864. [CrossRef]
352. Yang, B.; Shen, Y.; Zeng, Y.; Li, B.; Shen, S.; Zhu, S. Effects of tin doping level on structure, acidity and catalytic performance of Ti-Ce-O_x catalyst for selective catalytic reduction of NO by ammonia. *J. Mol. Catal. A Chem.* **2016**, *418*, 138–145. [CrossRef]
353. Guo, R.T.; Li, M.Y.; Sun, P.; Pan, W.G.; Liu, S.M.; Liu, J.; Sun, X.; Liu, S.W. Mechanistic investigation of the promotion effect of bi modification on the NH_3–SCR performance of Ce/TiO_2 catalyst. *J. Phys. Chem. C* **2017**, *121*, 27535–27545. [CrossRef]
354. Mu, Y.; Huang, X.; Tang, Z.; Wang, Q. Ordered mesoporous TiO_2 framework confined CeSn catalyst exhibiting excellent high activity for selective catalytic reduction of NO with NH_3 at low temperature. *Chem. Eng. J.* **2023**, *454*, 140181. [CrossRef]
355. Zhang, G.; Han, W.; Zhao, H.; Zong, L.; Tang, Z. Solvothermal synthesis of well-designed ceria-tin-titanium catalysts with enhanced catalytic performance for wide temperature NH_3-SCR reaction. *Appl. Catal. B* **2018**, *226*, 117–126. [CrossRef]
356. Mu, Y.; Huang, X.; Tang, Z.; Wang, Q. Facile strategy to promote SO_2-resistance ability for NH_3-SCR catalyst $CeSnTiO_x$ via copper sulfate-modified: Boost from a double reaction site. *Sep. Purif. Technol.* **2025**, *353*, 128490. [CrossRef]
357. Liu, J.; Li, X.; Zhao, Q.; Ke, J.; Xiao, H.; Lv, X.; Liu, S.; Tade, M.; Wang, S. Mechanistic investigation of the enhanced NH_3-SCR on cobalt-decorated Ce-Ti mixed oxide: In situ FTIR analysis for structure-activity correlation. *Appl. Catal. B* **2017**, *200*, 297–308. [CrossRef]
358. Chang, H.; Li, J.; Yuan, J.; Chen, L.; Dai, Y.; Arandiyan, H.; Xu, J.; Hao, J. Ge, Mn-doped CeO_2–WO_3 catalysts for NH_3–SCR of NO_x: Effects of SO_2 and H_2 regeneration. *Catal. Today* **2013**, *201*, 139–144. [CrossRef]
359. Zhang, B.; Deng, L.; Liebau, M.; Ren, Y.; Luo, C.; Liu, B.; Zhang, S.; Gläser, R. Promotion effect of niobium on ceria catalyst for selective catalytic reduction of NO with NH_3. *J. Rare Earth* **2022**, *40*, 1535–1545. [CrossRef]
360. Zhu, H.; Wang, R. Rational design of porous Ce_xNb_{1-x} oxide hollow nanospheres as a novel NH_3-SCR catalyst. *J. Mater. Chem. A Mater.* **2022**, *10*, 12269–12277. [CrossRef]
361. Ma, S.; Gao, W.; Yang, Z.; Lin, R.; Wang, X.; Zhu, X.; Jiang, Y. Superior Ce–Nb–Ti oxide catalysts for selective catalytic reduction of NO with NH_3. *J. Energy Inst.* **2021**, *94*, 73–84. [CrossRef]
362. Jiang, Y.; Gao, W.; Bao, C.; Yang, Z.; Lin, R.; Wang, X. Comparative study of Ce-Nb-Ti oxide catalysts prepared by different methods for selective catalytic reduction of NO with NH_3. *Mol. Catal.* **2020**, *496*, 111161. [CrossRef]
363. Ding, L.; Zhang, S.; Liu, Q.; Yang, P.; Cai, Y.; Tan, W.; Song, W.; Gao, F.; Dong, L. The enhancement effect of Nb over $CeSi_2$ catalyst for the low-temperature NH_3-SCR performance. *Chem. Phys.* **2023**, *6*, 100205. [CrossRef]
364. Zhang, L.; Qu, H.; Du, T.; Ma, W.; Zhong, Q. H_2O and SO_2 tolerance, activity and reaction mechanism of sulfated Ni–Ce–La composite oxide nanocrystals in NH_3-SCR. *Chem. Eng. J.* **2016**, *296*, 122–131. [CrossRef]
365. Liu, Z.; Zhu, J.; Zhang, S.; Ma, L.; Woo, S.I. Selective catalytic reduction of NO_x by NH_3 over MoO_3-promoted CeO_2/TiO_2 catalyst. *Catal. Commun.* **2014**, *46*, 90–93. [CrossRef]
366. Tan, W.; Wang, J.; Cai, Y.; Li, L.; Xie, S.; Gao, F.; Liu, F.; Dong, L. Molybdenum oxide as an efficient promoter to enhance the NH_3-SCR performance of CeO_2-SiO_2 catalyst for NO_x removal. *Catal. Today* **2022**, *397*, 475–483. [CrossRef]
367. Liu, W.; Gao, Z.; Zhao, X.; Gao, J.; Yang, R.; Yu, L. Promotion effect of chromium on the activity and SO_2 resistance of CeO_2–TiO_2 catalysts for the NH3-SCR reaction. *Ind. Eng. Chem. Res.* **2021**, *60*, 11676–11688. [CrossRef]
368. Wang, Z.Y.; Guo, R.T.; Guan, Z.Z.; Shi, X.; Pan, W.G.; Fu, Z.G.; Qin, H.; Liu, X.Y. The promotion effect of Cr additive on $CeZr_2O_x$ catalyst for the low-temperature selective catalytic reduction of NO_x with NH_3. *Appl. Surf. Sci.* **2019**, *485*, 133–140. [CrossRef]
369. Wei, X.; Zhao, R.; Chu, B.; Xie, S.; Chen, K.; Li, L.; Zhao, S.; Li, B.; Dong, L. Significantly enhanced activity and SO_2 resistance of Zr-modified $CeTiO_x$ catalyst for low-temperature NH_3-SCR by H_2 reduction treatment. *Mol. Catal.* **2022**, *518*, 112069. [CrossRef]
370. Gong, P.; Xie, J.; Fang, D.; He, F.; Li, F.; Qi, K. Enhancement of the NH_3-SCR property of Ce-Zr-Ti by surface and structure modification with P. *Appl. Surf. Sci.* **2020**, *505*, 144641. [CrossRef]
371. Jin, Q.; Chen, M.; Tao, X.; Lu, B.; Shen, J.; Shen, Y.; Zeng, Y. Component synergistic catalysis of Ce-Sn-W-Ba-O_x/TiO_2 in selective catalytic reduction of NO with ammonia. *Appl. Surf. Sci.* **2020**, *512*, 145757. [CrossRef]
372. Xie, W.; Zhang, G.; Mu, B.; Tang, Z.; Zhang, J. The promoting effect of palygorskite on CeO_2-WO_3-TiO_2 catalyst for the selective catalytic reduction of NO_x with NH_3. *Appl. Clay Sci.* **2020**, *192*, 105641. [CrossRef]

373. Chen, J.; Zhao, W.; Wu, Q.; Mi, J.; Wang, X.; Ma, L.; Jiang, L.; Au, C.; Li, J. Effects of anaerobic SO_2 treatment on nano-CeO_2 of different morphologies for selective catalytic reduction of NO_x with NH_3. *Chem. Eng. J.* **2020**, *382*, 122910. [CrossRef]
374. Tan, W.; Wang, J.; Li, L.; Liu, A.; Song, G.; Guo, K.; Luo, Y.; Liu, F.; Gao, F.; Dong, L. Gas phase sulfation of ceria-zirconia solid solutions for generating highly efficient and SO_2 resistant NH_3-SCR catalysts for NO removal. *J. Hazard. Mater.* **2020**, *388*, 121729. [CrossRef] [PubMed]
375. Huang, B.; Yu, D.; Sheng, Z.; Yang, L. Novel CeO_2@TiO_2 core–shell nanostructure catalyst for selective catalytic reduction of NO_x with NH_3. *J. Environ. Sci.* **2017**, *55*, 129–136. [CrossRef] [PubMed]
376. Zhao, H.; Luo, J.; Tang, W.; Li, B.; Li, A.; Zhou, D.; Ou, Y.; Hou, C. A superior CeO_2@TiO_2 catalyst with high dispersion of CeO_2 for selective catalytic reduction of NO_x with NH_3. *Appl. Catal. A Gen.* **2023**, *661*, 119168. [CrossRef]
377. Liu, J.; Huo, Y.; Shi, X.; Liu, Z.; Shan, Y.; Yu, Y.; Shan, W.; He, H. Insight into the remarkable enhancement of NH_3-SCR performance of Ce-Sn oxide catalyst by tungsten modification. *Catal. Today* **2023**, *410*, 36–44. [CrossRef]
378. Liu, C.; Bi, Y.; Wang, H.; Zhang, Z.; Wang, J.; Guo, M.; Liu, Q. Promotional effects on NH_3-SCR performance of CeO_2–SnO_2 catalysts doped by TiO_2: A mechanism study. *Cataly. Surv. Asia* **2021**, *25*, 48–57. [CrossRef]
379. Yang, S.; Zhu, X.; Chen, S.; Zhu, X.; Liu, H.; Chen, J.; Chen, D.; Sun, C.; Li, J. Hexavalent metal cations doped into ceria inducing the formation of binuclear sites Ce^{3+}–O–Ce^{3+} to boost the NH_3-SCR reaction. *ACS Catal.* **2024**, *14*, 7277–7288. [CrossRef]
380. Liu, H.; Gao, C.; Chen, J.; Mi, J.; Yang, S.; Chen, D.; Si, W.; Peng, Y.; Sun, C.; Li, J. Optimized local geometry and electronic structure of MoO_3/CeO_2 catalyst by adding copper cations for boosted nitrogen oxide reduction performance. *Appl. Catal. B* **2023**, *332*, 122742. [CrossRef]
381. Chen, W.; Gu, J.; He, B.; Duan, R.; Liu, L.; Wang, X. Computational screening and synthesis of M(M= Mo and Cu)-doped CeO_2/silicalite-1 for medium-/low-temperature NH_3–SCR. *Ind. Eng. Chem. Res.* **2022**, *61*, 10091–10105. [CrossRef]
382. He, J.F.; Xiong, Z.B.; Du, Y.P.; Lu, W. Morphology effect of tungsten oxide on Ce/W catalyst for selective catalytic reduction of NO with NH_3: Influence of structure-directing agents. *J. Energy Inst.* **2021**, *94*, 85–95. [CrossRef]
383. Fang, X.; Qu, W.; Qin, T.; Hu, X.; Chen, L.; Ma, Z.; Liu, X.; Tang, X. Abatement of nitrogen oxides via selective catalytic reduction over Ce^1–W_1 atom-pair sites. *Environ. Sci. Technol.* **2022**, *56*, 6631–6638. [CrossRef] [PubMed]
384. Inomata, Y.; Hata, S.; Mino, M.; Kiyonaga, E.; Morita, K.; Hikino, K.; Yoshida, K.; Kubota, H.; Toyao, T.; Shimizu, K.; et al. Bulk vanadium oxide versus conventional V_2O_5/TiO_2: NH_3–SCR catalysts working at a low temperature below 150 °C. *ACS Catal.* **2019**, *9*, 9327–9331. [CrossRef]
385. Lian, Z.; Wei, J.; Shan, W.; Yu, Y.; Radjenovic, P.M.; Zhang, H.; He, G.; Liu, F.; Li, J.-F.; Tian, Z.-Q.; et al. Adsorption-induced active vanadium species facilitate excellent performance in low-temperature catalytic NO_x abatement. *J. Am. Chem. Soc.* **2021**, *143*, 10454–10461. [CrossRef]
386. Yin, Y.; Luo, B.; Li, K.; Moskowitz, B.M.; Mosevizky Lis, B.; Wachs, I.E.; Zhu, M.; Sun, Y.; Zhu, T.; Li, X. Plasma-assisted manipulation of vanadia nanoclusters for efficient selective catalytic reduction of NO_x. *Nat. Commun.* **2024**, *15*, 3592. [CrossRef]
387. Lin, L.Y.; Wang, Y.C.; Liu, Z.L. Highly active and stable VO_x/TiO_2 nanosheets for low-temperature NH_3-SCR of NO: Structure-directing role of support. *Chem. Eng. J.* **2024**, *484*, 149637. [CrossRef]
388. Hwang, K.H.; Park, N.; Lee, H.; Lee, K.M.; Jeon, S.W.; Kim, H.S.; Lee, Y.; Kim, T.J.; Lee, W.B.; Kim, D.H. Mechanochemical localization of vanadia on titania to prepare a highly sulfur-resistant catalyst for low-temperature NH_3-SCR. *Appl. Catal. B* **2023**, *324*, 122290. [CrossRef]
389. Inomata, Y.; Kubota, H.; Honmatsu, Y.; Takamitsu, H.; Sakotani, S.; Yoshida, K.; Toyao, T.; Shimizu, K.; Murayama, T. Sodium ion intercalation in vanadium oxide promotes low-temperature NH_3-SCR activity: Sodium vanadium bronzes ($Na_{0.33}V_2O_5$) for NO_x removal. *Appl. Catal. B* **2023**, *328*, 122536. [CrossRef]
390. Inomata, Y.; Kubota, H.; Hata, S.; Kiyonaga, E.; Morita, K.; Yoshida, K.; Sakaguchi, N.; Toyao, T.; Shimizu, K.; Ishikawa, S.; et al. Bulk tungsten-substituted vanadium oxide for low-temperature NO_x removal in the presence of water. *Nat. Commun.* **2021**, *12*, 557. [CrossRef]
391. Zhao, X.; Huang, L.; Li, H.; Hu, H.; Hu, X.; Shi, L.; Zhang, D. Promotional effects of zirconium doped $CeVO_4$ for the low-temperature selective catalytic reduction of NO_x with NH_3. *Appl. Catal. B* **2016**, *183*, 269–281. [CrossRef]
392. Zhao, X.; Huang, L.; Namuangruk, S.; Hu, H.; Hu, X.; Shi, L.; Zhang, D. Morphology-dependent performance of Zr–$CeVO_4$/TiO_2 for selective catalytic reduction of NO with NH_3. *Catal. Sci. Technol.* **2016**, *6*, 5543–5553. [CrossRef]
393. Liu, F.; He, H.; Lian, Z.; Shan, W.; Xie, L.; Asakura, K.; Yang, W.; Deng, H. Highly dispersed iron vanadate catalyst supported on TiO_2 for the selective catalytic reduction of NO_x with NH_3. *J. Catal.* **2013**, *307*, 340. [CrossRef]
394. Kim, J.; Kim, D.H.; Kwon, D.W.; Lee, K.Y.; Ha, H.P. Unveiling the traits of rare earth metal (RM)-substituted bimetallic $Ce_{0.5}RM_{0.5}V_1O_4$ phases to activate selective NH_3 oxidation and NO_x reduction. *Appl. Surf. Sci.* **2020**, *518*, 146238. [CrossRef]
395. Liu, Z.; Zhao, X.; Li, Y.; Niu, X.; Zhu, Y. Improving NH_3-SCR denitrification performance over $WaC_{0.4}TiO_x$ catalysts: Effect of surface acidity due to W addition on low-temperature and high-temperature activity. *Appl. Catal. A Gen.* **2022**, *643*, 118705. [CrossRef]
396. Zeng, Y.; Wang, Y.; Zhang, S.; Zhong, Q.; Rong, W.; Li, X. One-pot synthesis of ceria and cerium phosphate (CeO_2-$CePO_4$) nanorod composites for selective catalytic reduction of NO with NH_3: Active sites and reaction mechanism. *J. Colloid Interface Sci.* **2018**, *524*, 8–15. [CrossRef]
397. Yao, W.; Liu, Y.; Wang, X.; Weng, X.; Wang, H.; Wu, Z. The superior performance of sol–gel made Ce–O–P catalyst for selective catalytic reduction of NO with NH_3. *J. Phys. Chem. C* **2016**, *120*, 221–229. [CrossRef]

398. Zhao, C.; Li, Y.; Zhang, Z.; Tan, H.; Yuan, F.; Zhu, Y. Influence of $CePO_4$ with different crystalline phase on selective catalytic reduction of NO_x with ammonia. *J. Rare Earth* **2022**, *40*, 1219–1231. [CrossRef]
399. Lin, C.H.; Qin, R.C.; Cao, N.; Wang, D.; Liu, C.G. Synergistic effects of Keggin-type phosphotungstic acid-supported single-atom catalysts in a fast NH_3-SCR reaction. *Inorg. Chem.* **2022**, *61*, 19156–19171. [CrossRef]
400. Xie, R.; Ma, L.; Sun, K.; Zhou, G.; Qu, Z.; Yan, N. Catalytic performance and mechanistic evaluation of sulfated CeO_2 cubes for selective catalytic reduction of NO_x with ammonia. *J. Hazard. Mater.* **2021**, *420*, 126545. [CrossRef]
401. Yu, Y.; Zhang, J.; Chen, C.; Ma, M.; He, C.; Miao, J.; Li, H.; Chen, J. Selective catalytic reduction of NO_x with NH_3 over TiO_2 supported metal sulfate catalysts prepared via a sol–gel protocol. *New J. Chem.* **2020**, *44*, 13598–13605. [CrossRef]
402. Koebel, M.; Madia, G.; Elsener, M. Selective catalytic reduction of NO and NO_2 at low temperatures. *Catal. Today* **2002**, *73*, 239–247. [CrossRef]
403. Koebel, M.; Elsener, M.; Madia, G. Reaction pathways in the selective catalytic reduction process with NO and NO_2 at low temperatures. *Ind. Eng. Chem. Res.* **2001**, *40*, 52–59. [CrossRef]
404. Wei, Z.; Kang, X.; Yunhao, T.; Chuan, Q.; Shan, C.; Ying, M. Application of transition metal based MOF materials in selective catalytic reduction of nitrogen oxides. *Prog. Chem.* **2022**, *34*, 2638. [CrossRef]
405. Adil, K.; Świrk, K.; Zaki, A.; Assen, A.H.; Delahay, G.; Belmabkhout, Y.; Cadiau, A. Perspectives in adsorptive and catalytic mitigations of NO_x using metal–organic frameworks. *Energy Fuels* **2022**, *36*, 3347–3371. [CrossRef]
406. Gao, Y.; Gong, S.Y.; Chen, B.; Xing, W.H.; Fei, Y.F.; Hu, Z.T.; Pan, Z. Progress in metal-organic framework catalysts for selective catalytic reduction of NO_x: A mini-review. *Atmosphere* **2022**, *13*, 793. [CrossRef]
407. Szymaszek, A.; Motak, M.; Samojeden, B. The application of modified layered double hydroxides in selective catalytic reduction of nitrogen oxides by ammonia (NH-SCR). *Pol. J. Chem. Technol.* **2020**, *22*, 61–67. [CrossRef]
408. Yan, Q.; Hou, X.; Liu, G.; Li, Y.; Zhu, T.; Xin, Y.; Wang, Q. Recent advances in layered double hydroxides (LDHs) derived catalysts for selective catalytic reduction of NO_x with NH_3. *J. Hazard. Mater.* **2020**, *400*, 123260. [CrossRef]
409. Tan, Y.; Yi, H.; Tang, X.; Yu, Q.; Gao, F.; Liu, J.; Wang, Y.; Zhou, Y.; Kang, D.; Zhao, S. Layered double hydroxides for air pollution control: Applications, mechanisms and trends. *J. Clean. Prod.* **2024**, *436*, 140635. [CrossRef]
410. Gui, R.; Yan, Q.; Xue, T.; Gao, Y.; Li, Y.; Zhu, T.; Wang, Q. The promoting/inhibiting effect of water vapor on the selective catalytic reduction of NO_x. *J. Hazard. Mater.* **2022**, *439*, 129665. [CrossRef]
411. Zhang, Z.; Zhao, Z.; Tan, D.; Ye, Y.; Zhang, B.; Huang, B.; Zhong, W.; Hu, J. Overview of mechanisms of promotion and inhibition by H_2O for selective catalytic reduction denitrification. *Fuel Process. Technol.* **2023**, *252*, 107956. [CrossRef]
412. Zhang, N.; He, H.; Wang, D.; Li, Y. Challenges and opportunities for manganese oxides in low-temperature selective catalytic reduction of NO_x with NH_3: H_2O resistance ability. *J. Solid State Chem.* **2020**, *289*, 121464. [CrossRef]
413. Shen, Z.; Ren, S.; Zhang, B.; Bian, W.; Xing, X.; Zheng, Z. Sulfur and water resistance of carbon-based catalysts for low-temperature selective catalytic reduction of NO_x: A review. *Catalysts* **2023**, *13*, 1434. [CrossRef]
414. He, Z.; Wang, Y.; Liu, Y.; Lian, L.; Kong, D.; Zhao, Y. Recent advances in sulfur poisoning of selective catalytic reduction (SCR) denitration catalysts. *Fuel* **2024**, *365*, 131126. [CrossRef]
415. Szymaszek, A.; Samojeden, B.; Motak, M. The deactivation of industrial SCR catalysts—A short review. *Energies* **2020**, *13*, 3870. [CrossRef]
416. Song, I.; Lee, H.; Jeon, S.W.; Ibrahim, I.A.; Kim, J.; Byun, Y.; Jun, D.K.; Han, J.W.; Kim, D.H. Simple physical mixing of zeolite prevents sulfur deactivation of vanadia catalysts for NO_x removal. *Nat. Commun.* **2021**, *12*, 901. [CrossRef]
417. Song, J.; Sun, X.; Zhang, G.; Cheng, S.; Xu, Y.; Jiang, Y. Recent advances in improving SO_2 resistance of Ce-based catalysts for NH_3-SCR: Mechanisms and strategies. *Mol. Catal.* **2024**, *564*, 114347. [CrossRef]
418. Cai, Q.; Wang, F.; Hou, Y.; Jia, Y.; Liao, B.; Shen, B.; Zhang, D. Core-shell materials for selective catalytic reducing of NO_x with ammonia: Synthesis, anti-poisoning performance, and remaining challenges. *Fuel Process. Technol.* **2023**, *243*, 107675. [CrossRef]
419. Li, M.; Guo, Y.; Yang, J. Spatially nanoconfined architectures: A promising design for selective catalytic reduction of NO_x. *ChemCatChem* **2020**, *12*, 5599–5610. [CrossRef]
420. Chen, J.; Fang, X.; Ren, Z.; Qu, W.; Hu, X.; Ma, Z.; Chen, L.; Liu, X.; Chen, Y.; Tang, X. Single Mo atoms paired with neighbouring Ti atoms catalytically decompose ammonium bisulfate formed in low-temperature SCR. *J. Mater. Chem. A Mater.* **2022**, *10*, 6065–6072. [CrossRef]
421. Guan, B.; Jiang, H.; Wei, Y.; Liu, Z.; Wu, X.; Lin, H.; Huang, Z. Density functional theory researches for atomic structure, properties prediction, and rational design of selective catalytic reduction catalysts: Current progresses and future perspectives. *Mol. Catal.* **2021**, *510*, 111704. [CrossRef]
422. Dong, Y.; Ran, M.; Zhang, X.; Lin, S.; Zhao, H.; Yang, Y.; Liu, S.; Zheng, C.; Gao, X. Machine learning-accelerated disentanglement of activity–selectivity trade-off of multielement oxide denitration catalysts. *ACS ES T Eng.* **2024**, *4*, 1312–1320. [CrossRef]
423. Lu, M.; Gao, F.; Tan, Y.; Yi, H.; Gui, Y.; Xu, Y.; Wang, Y.; Zhou, Y.; Tang, X.; Chen, L. Knowledge-driven experimental discovery of Ce-based metal oxide composites for selective catalytic reduction of NO_x with NH_3 through interpretable machine learning. *ACS Appl. Mater. Interfaces* **2024**, *16*, 3593–3604. [CrossRef] [PubMed]